Lydd Ranges Sea Defence Scheme

Palaeoenvironmental Assessment

Ref:
241533.01
May 2023

wessexarchaeology

Portway House
Old Sarum Park
Salisbury
Wiltshire
SP4 6EB

www.wessexarch.co.uk

Wessex Archaeology Ltd is a Registered Charity no. 287786 (England & Wales) and SC042630 (Scotland)

Document Information

Document title	Lydd Ranges Sea Defence Scheme
Document subtitle	Palaeoenvironmental Assessment
Document reference	241532.01
Client name	Mackley Construction
Address	Bankside House Henfield Road Small Dole Henfield West Sussex BN5 9QX
Site location	South Brookes Lydd Ranges Lydd Camp Tourney Road Lydd
County	Kent and East Sussex
National grid reference	Jury's Gap NGR TR031174 Denge Marsh Sewer NGR TR065167
Statutory designations	
Planning authority	Folkstone and Hythe District Council; Rother District Council
Planning reference	18/1601/FH; RR/2018/3099/P
Museum name	
WA project name	241532
Project management by	Dr Alex Brown
Document compiled by	Dr Alex Brown, Hayley Hawkins

Quality Assurance

Issue	Date	Author	Approved by
1	28/02/2023	AB, HH	DSY
2	14/03/2023		
3	23/05/2023	AB, HH	

Contents

List of tables

List of Figures

Summary
Wessex Archaeology (WA) was commissioned by Mackley Construction to undertake a program of palaeoenvironmental assessment in support of the Lydd Ranges Sea Defence Scheme. A staged program of assessment and scientific dating was agreed, involving XRF core scanning, pollen and microfaunal assessment, followed by Optically Stimulated Luminescence (OSL) and radiocarbon dating of suitable deposits.

XRF core scanning focused on the fine-grained above-gravel stratigraphy (defined as those deposits forming following emplacement of the gravel barrier) from across Zones C, E and G, including three rotary cores (C01/WA-S03, E01/WA-S02 and G01/WA-S01), deposits from the marsh preserved behind the current Green Wall (HHWS-107) and a monolith recovered from clay exposures on the foreshore (monolith 111, TP11). The results of core scanning were used to identify potential zones of sediment mixing to refine the scope of the OSL dating. Targeted assessment of diatoms, foraminifera and ostracods was undertaken on HHWS-107 and TP11, with pollen assessment of peat from HHWS-107.

The program of works is designed to address a series of principal objectives, including dating of sediment infilling tidal inlets in the barrier system and investigation land-ocean interactions. This report assesses the preservation and quality of data to meet those research aims.

OSL dates from borehole C01/WA-S03 extended from the Bronze Age to the post-medieval, while those from GO1/WA-S01 extended from the Iron Age to the Romano-British period. The OSL dates were in poor agreement with radiocarbon dates from closely associated peat deposits which dated to the Romano-British/early medieval period. The dates reflect the very low concentrations of datable fine sandy quartz grains present in the samples. Partial resetting of grains is also likely to have resulted in over-estimation of the dates, resulting in older ages that would otherwise be expected.

Preservation of microfauna was uniformly poor in the samples, although one sample from clay exposures on the foreshore (monolith 111, TP 11) was suggestive of a marine-brackish environment.

Pollen preservation and concentration from the peat in HHWS-107 was variable, though generally poor. There is some suggestion of mixed oak-hazel woodland in the early Romano-British period and a subsequent reduction in woodland and expansion in tall herb swamp. Local vegetation may be filtering out pollen from the extra-local environment, but in general surviving woodland is likely to be patchy and locally abundant, cleared on a large scale since the Bronze Age. Large (Cereal-type) pollen grains may represent pollen grains of wetland grass taxa or cereal pollen deposited via animal vectors (e.g. contained in faeces).

Preservation of the peat is consistent with evidence for formation of organic beds of Romano-British date across Walland and Romney Marsh, attesting to a spatially and temporally dynamic relationship between marine, semi-terrestrial and dry land environments.

The results of XRF core scanning provided data on the relative abundance of different elements down-core. This data is presented in counts per second (cps) rather than concentrations, which can be difficult to interpret without calibration using bulk chemistry and can also be impacted by changes in grain size and composition, water content and organic matter content.

The results are variable, with considerable scattering in E01/WA-S02 and a high mean square error in monolith 111. HHWS-107, C01/WA-S03 and G01/WA-S01 produced reliable results, and are affected in the latter sequence by large voids in the sequence. The results suggest variations in elements indicative of shifts in marine and terrestrial inputs over time.

Owing to variable preservation of environmental proxies and datable deposits, no further analysis is recommended.

Acknowledgments
Wessex Archaeology are grateful to Mackley Construction for commissioning the work and to Mark Glennerster (Glennerster Consulting), Andrew Rintoul (Mackleys) Paul Fish (Jacobs), Paul Falcini and Carol Peirce (Environment Agency) for their help and assistance during the course of the project and Professor Andy Plater (University of Liverpool) for advice and support. The report was compiled by Dr Alex Brown with contributions from Hayley Hawkins with specialist assessment of samples by Dr John Athersuch (foraminifera and ostracod), Dr Nigel Cameron (diatoms), Dr Alex Brown (pollen), Professor Phil Toms (OSL dating), ^{14}CHRONO Centre, Queens University Belfast (radiocarbon dating) and BOSCORF (XRF core scanning). The report was reviewed by Dr Daniel Young. The project was managed on behalf of Wessex Archaeology by Alex Brown.

Lydd Ranges Sea Defence Scheme

Palaeoenvironmental Assessment

1 INTRODUCTION

1.1 Project background

1.1.1 Wessex Archaeology (WA) was commissioned by Mackley Construction (hereafter referred to as 'the Client') to undertake a program of palaeoenvironmental assessment works in support of the Lydd Ranges Sea Defence Scheme.

1.1.2 The Lydd Ranges Sea Defence Scheme comprises coastal defence improvement works designed to manage flood and erosion risk along the coastline of Romney Marsh over the next 25 years. The proposed improvement works extend for approximately 7.4 km west to east from Jury's Gap to Denge Marsh outfall, part of the Romney Marsh and Rye Bay SSSI and including the MOD firing range at Lydd, Kent (**Figure 1**).

1.1.3 The scheme has been divided into a series of Zones (A – K), corresponding to an alternating series of gravel ridges and inter-ridge marshes. Geoarchaeological fieldwork was targeted within three of the inter-ridge marshes located at Midrips (Zones C and E) and South Brooks (Zone G), with recommendations made for a program of targeted palaeoenvironmental assessment and scientific dating on retained samples.

1.2 Summary of previous phases of work

1.2.1 To offset the impact of coastal defence improvement works on deposits of geoarchaeological interest in the Dungeness, Romney Marsh and Rye Bay SSSI, a programme of palaeoenvironmental assessment and scientific dating was undertaken on samples retained following fieldwork (Wessex Archaeology 2022).

1.2.2 The scope of works followed a staged approach, as outlined in Jacobs (2020) and WA (2021a) and were revised as works progressed to comprise the following components:

Inter-ridge marsh hand auger survey (Nov 2020)

1.2.3 The works initially comprised plans for a grid of approximately 50 hand auger holes across zones C, E and G in marshland landward of the Green Wall. However, ground and weather conditions presented significant challenges to the work and in no case was the target depth of 2 metres below ground level (mbgl) reached. The marsh surface was flooded, preventing UXO (unexploded ordnance) clearance. Hand auger locations were restricted to transects along the base of the Green Wall, comprising a series of auger holes in Zone C (HA1–HA16), Zone E (HA17–HA33) and Zone G (HA34–HA43).

1.2.4 Most auger holes were not advanced beyond ~0.3-0.5 m due to the increasingly stiff silts and clays with no location extending beyond 1.0 mbgl. The decision was taken to wait until the summer of 2021 when the marshes may dry out before undertaking a second phase of work to investigate the marsh deposits using hand-held (powered) window sampling equipment.

Green Wall rotary coring (March 2021)

1.2.5 Three rotary cores were drilled on the Green Wall, one in each of Zones C, E and G, with the aim of investigating the full sequence of Holocene sediments to the basal sands at anticipated depths up to 15 mbgl. However, in all three cases the rotary cores refused on gravel deposits at depths of 9 mbgl (C01, Zone C), 6 mbgl (E01, Zone E) and 10.5 mbgl (G01, Zone G) respectively, requiring a subsequent phase of fieldwork using a Sonic drilling rig.

Beach survey (July 2021)

1.2.6 Monitoring of beach works was undertaken during July 2021 in parallel with the construction of groynes, involving machine excavated scrapes to expose clay deposits sealed below beach gravels. In total 14 scrapes were monitored across Zones C (TP1), E (TP2, 3, 13-14) and G (TP4-12) with elevations taken on the surface of the clay deposits. Although the scrapes were stepped, the degree of water ingress made them unsafe to enter and only one monolith sample was recovered through the clays in TP 11 (Zone G).

Green Wall sonic coring (August 2021)

1.2.7 An additional phase of coring on the Green Wall using a Sonic drill was undertaken during August 2021 with the aim of recording and sampling the remaining sequences following on from the depths reached at each of the rotary core locations. Each sonic core successfully penetrated the gravels with samples retained from the underlying stratigraphy to depths of 13.5 mbgl (Zones C, WA-S03) and 15 mbgl (Zones E, WA-S02 and G, WA-S01).

1.2.8 The combined rotary/sonic logs are referred to as C01/WA-S03 (Zone C), E01/WA-S02 (Zone E) and G01/WA-S01 (Zone G).

Inter-ridge marsh hand held window sampling (September 2021)

1.2.9 The final phase of fieldwork was undertaken in September 2021, involving 30 hand-held window samples (HHWS), ten in each Zone along three transects (Zone C, HHWS 121 to HHWS 130; Zone E, HHWS 111 to HHWS120; Zone G, HHWS101 to HHWS110. Four cores were retained (HHWS104, 107, 114 and 125) each containing alluvium and a fourth comprising peat from Zone G (HHWS107).

1.3 Scope of report

1.3.1 Following a stakeholder engagement meeting in December 2021, a program for palaeoenvironmental assessment and scientific dating was agreed which would follow a staged approach as detailed below and in **Table 1**.

1.3.2 This staged approach allowed for targeted sampling for scientific dating, with additional pollen and microfauna work (diatoms, foraminifera and ostracods) to investigate past environments and land-ocean interactions.

- Stage 1 – XRF core scanning, pollen and microfauna assessment
- Stage 2 – OSL and radiocarbon dating

Stage 1

1.3.3 XRF core scanning focused on scanning of the fine-grained above-gravel stratigraphy (defined as those sediments formed following the emplacement of the gravel barrier across the site) in all three rotary cores from the Green Wall, in addition to XRF scanning of fine-

grained marsh deposits in HHWS 107 (inter-ridge marsh) and monolith 11, TP11 (foreshore).

1.3.4 In addition to producing high-resolution geochemical data, the results of XRF core scanning from the Green Wall will be used to determine the level of mixing apparent in fine-grained sediment, with the aim of distinguishing between sediment redeposited during construction of the sea wall and naturally deposited silty clays. The interface between these deposits is not visually apparent in the deposits. Using XRF core scanning is considered a cost and time-effective means of refining the subsequent OSL dating at Stage 2.

1.3.5 Targeted assessment of microfauna (diatoms, foraminifera and ostracods) is undertaken on fine-grained marsh deposits above and below peat deposits in HHWS-107 and from clays sampled from the foreshore (TP11). The data will provide an environmental context for these deposits in support of the sediment provenance and land-ocean interaction research objective.

1.3.6 Pollen assessment of peat in HHWS-107 will produce data on the concentration and preservation of palynomorphs, and potentially address concerns surrounding the possibility that the peat is eroded and redeposited. Radiocarbon dating will be of little value In the event data suggests the peat is eroded and redeposited.

Stage 2

1.3.7 The results of XRF core scanning and pollen analysis were utilised to determine the scope of and need for targeted OSL dating and radiocarbon dating.

Table 1 Recommendations for assessment and scientific dating

Technique	Zone C	Zone E	Zone G
XRF core scanning	(C01/WA-S03) 2–7.4 mbgl	(E01/WA-S02) 2–5.3 mbgl	(G01/WA-S01) 2–6.5 mbgl (HHWS 207) 0.1–0.59 mbgl (TP 11) 0.8-1.30 mbgl
Pollen *Peat, inter-ridge marsh*	-	-	(HHWS-107) 4 samples
Diatoms, Foraminifera and Ostracods *Peat, inter-ridge marsh*	-	-	(HHWS-107) 4 samples (TP 11) 4 samples
OSL dating *Above-gravel marsh deposits*	(C01/WA-S03) 4 samples	-	(G01/WA-S01) 4 samples
Radiocarbon dating *Peat, inter-ridge marsh*	(C01/WA-S03) 1 sample	-	(HHWS-107) 2 samples

1.3.8 The program of works outlined above are designed to address and contribute to a series of Principal Objectives, developed in consultation with Professor Andrew Plater, Natural England's specialist advisor for the site (detailed in Jacobs 2020, Table 4-1).

1.3.9 The potential to contribute to these overarching objectives is considered in the discussion (**Section 6**), focused on Principal Objectives 3 and 4 below. Items 1, 2 and 5 were considered in the preceding fieldwork report (Wessex Archaeology 2022) and are not considered further:

1. Investigation of the topography of the bedrock and early Holocene depositional environment;

2. Developing relative sea-level curves using basal peats overlying bedrock;

3. OSL dating of sediments infilling tidal inlets;

4. Sediment provenance and land-ocean interaction;

5. Origins and archaeology of the Green Wall.

2 GEOARCHAEOLOGICAL BACKGROUND

2.1 Introduction

2.1.1 The following section provides a summary of the known geoarchaeological record for the Site and surrounding landscape. An archaeological background to the Scheme is contained in the accompanying archaeological watching brief WSI (Wessex Archaeology 2021) and is not repeated here.

2.1.2 Where age estimates are available for deposits, these are expressed in millions of years (Mya), thousands of years (Kya) and within the Holocene epoch as years Before Present (BP) with the corresponding Anno Domini (AD) date for historic periods. Where radiocarbon dates are included, the uncalibrated date (BP) is quoted followed by the calibrated date (cal. BP or cal. AD) following the above format date. These dates are supplemented where relevant with the comparable Marine Isotope Stage (MIS) where odd numbers indicate an interglacial period and even numbers a glacial period.

2.1.3 All depths are provided as metres below ground level (mbgl) and metres above ordnance datum (m aOD)

2.2 Bedrock Geology

2.2.1 The underlying bedrock is mapped by the British Geological Survey (BGS) as sandstones, siltstones and mudstones of the Hastings Beds formed 134–145 Mya during the Cretaceous Period.

2.3 Quaternary Geology

2.3.1 The Site is part of the Dungeness Foreland barrier running along the southern shores of Romney Marsh. The site has been designated as a Site of Specialist Scientific Interest (SSSI) owing to its ecological and geomorphological value. The sedimentary sequence across the Scheme comprises nearshore sands overlain by gravels of the prograding barrier of the Dungeness Foreland. The barrier is interrupted by a series of natural depressions infilled with Holocene fine-grained and locally organic sediment representing tidal inlets and brackish lagoons.

2.3.2 Lydd Ranges has been well studied are part of a significant body of investigation on the Holocene evolution of Romney Marsh and the Dungeness Foreland, including an ALSF (Aggregate Levy Sustainability Fund) study focusing on barrier dynamics and marshland evolution (Long et al 2007).

2.3.3 The results of this research provide an important geomorphological context for the proposed geoarchaeological works, drawing on a geoarchaeological desk-based review and study of

the palaeoenvironmental potential of the Lydd Ranges (Wessex Archaeology 2018). The current shingle barrier of the Dungeness Foreland overlies a series of older beach ridges that formed part of a more extensive coastal barrier extending from Farlight Head in the west (19km south-west of Lydd) to Hythe in the east (18km north-east of Lydd).

Pre-barrier development

2.3.4 The gravel barrier of the Dungeness Foreland is underlain by a sequence of nearshore sands that are >10 m thick at Jury's Gap and with a surface elevation of around -2 m aOD (Long et al 2006). OSL (Optically Stimulated Luminescence) dating of these nearshore sands demonstrates that they are of a progressively more recent date from west to east as the barrier developed under the influence of eastward longshore drift. The formation of these nearshore sands has been dated in the west at Broomhill to about 5000 years ago and at the eastern end of the scheme to 500 years ago, with an increase in the eastward rate of progradation during the last 2000 years (Long et al 2007, Roberts and Plater 2007).

Gravel barrier development

2.3.5 Development of the Dungeness Foreland occurred as a result of sea-level rise during the Holocene, reworking beach and seedbed gravels and accelerating erosion of the chalk cliffs and shore platforms. These processes resulted in an increased supply of sediment which was transported to the east along the coastline through a process of longshore drift (Long and Hughes 1995). OSL dates establish the early formation of the barrier to approximately 5000 BP (Long et al 2007).

2.3.6 Early Holocene sea-level rise also resulted in the drowning, breakdown and retreat of the former barrier systems, with the sediment recycled into the subsequent barrier systems including the Dungeness Foreland (Mellett et al 2012).

2.3.7 The gravel barrier currently has a surface relief of +3 to +4 m aOD between Jury's Gap and South Brooks, with a depth of gravels of up to 6+ m. The gravel barrier gradually prograded eastward, creating a huge tidal lagoon to landward and leading to the establishment of tidal mudflats and saltmarsh across Romney Marsh; these were subsequently replaced by freshwater peats which had begun to form within the valley of the River Rother from 6800 cal. BP.

2.3.8 Marine influence gradually increased from 3000 cal. BP with the development of large tidal inlets at Rye, Romney and Hythe, with freshwater peats succeeded by marine-dominated tidal flats and saltmarsh across Romney Marsh, punctuated by localised survival of raised mire (e.g., Walland Mire) into the medieval period.

Inter-ridge depressions

2.3.9 The last two-thousand years are marked by a close interaction between the barrier development and back barrier environment within Romney Marsh. The opening of a series of tidal inlets through the barrier led to phases of increased flooding and supply of fine-grained sediment into the marsh, followed by subsequent narrowing and closure of these inlets.

2.3.10 These former inlets through the barrier are apparent today as a series of inter-ridge depressions. The connection between these depressions (gravel lows) and the sea is still open to debate. Palaeoenvironmental assessment and deposit modelling will assist in establishing whether marshes were located behind to gravel foreland, were open to the east, or were infilling inter-ridge lows open directly to the tidal ingress from the south.

2.3.11 The chronology of these post-gravel deposits is unclear due to a lack of radiocarbon dating, although palaeomagnetic dating (Plater et al 2006) suggests that these deposits accumulated between 1050-550 BP (AD 900–1400). Recent GI works at the Midrips did identify a 1.1 m thick organic silt (Opus 2014) that has the potential to produce suitable material for radiocarbon dating.

2.3.12 The deposits encountered at the South Brooks are likely to be later than those to the west, reflecting the rapid eastward progradation of the gravel barrier from 2000 years ago. Palaeomagnetic dating of deposits from South Brooks suggests sediment deposition around 925–575 BP (AD 1025–1375), with foraminiferal analysis showing a sequence of tidal and brackish environments (Plater et al 2006).

2.4 Summary of geoarchaeological fieldwork

2.4.1 A programme of geoarchaeological works was undertaken in Zones C, E and G along the foreshore, Green Wall and marshland landward of the Green Wall over the course of 2020 and 2021 (**Figure 1**). The scope of works followed a staged approach, detailed in **Section 1.3** and Jacobs (2020).

2.4.2 The results of the geoarchaeological works and all retained samples are detailed in the borehole survey report (Wessex Archaeology 2022, Appendix 1) and summarised below in **Table 2**.

Table 2 Survey works at Lydd Ranges

Area / method		Dates	Zone C	Zone E	Zone G
Marsh	**HHWS**	Sept 2021	121-130	111-120	101-110
	HA	Nov 2020	HA1-HA16	HA17-HA33	HA34-HA43
Green Wall	**RC**	March 2021	C01	E01	G01
	SC	Aug 2021	WA-SC03	WA-SC02	WA-SC01
Beach	**TP**	July 2021	1	2, 3, 13, 14	4 – 12

HHWS = hand held window sample; HA = hand auger; RC = rotary core; SC = sonic core; TP = trial pit

2.4.3 Work within the marshland landward of the Green Wall involved 30 hand-held window samples, 10 within each zone. This was accompanied by three rotary and sonic cores on the Green Wall to maximum depths of 15m to sample and record the full sequence of Holocene sediments to the surface of the basal sands. Exposures of silty clay were monitored on the foreshore in 14 test pits (scrapes), recording the elevation and retrieving samples where appropriate.

2.4.4 Boreholes through the Green Wall identified a consistent sequence of deposits across Zones C, E and G comprising a basal sand (representing shoreface and intertidal deposits) overlain sands and gravels interpreted as evidence for the development of a spit and barrier complex.

Basal sands

2.4.5 Sonic cores encountered sands sealed beneath sands and gravels at 12.72 mbgl (-6.26 m aOD, Zone C), 13.11 mbgl (-6.58 m aOD, Zone E) and 12.11 mbgl (-6.35 m aOD, Zone G). The deposits variously comprise fine to medium-coarse poorly sorted sands, with bands of silty clay. The full thickness of the basal sands was not determined as the deposit will not be impacted by design elements of the scheme.

Sands and gravels

2.4.6 Sands and gravels were recorded in the sonic boreholes advanced through the Green Wall, overlying basal sands and overlain by storm beach gravels. The sands and gravels comprise firm grey medium to coarse sands with sub-angular to sub-rounded flint gravels. The full thickness of the sands and gravels was established in Zone E at 2.89 m (10.5–13.11 mbgl; -3.97– -6.58 m aOD), directly overlain by storm beach gravels.

Gravels

2.4.7 The overlying gravels represent contemporary storm beach deposits recorded in all three rotary and sonic boreholes advanced through the Green Wall. They comprise clast supported subrounded to rounded flint gravels and cobbles with a surface elevation of 7.4 mbgl (-0.94 m aOD; Zone C), 5.3 mbgl (1.23 m aOD; Zone E) and 6.65 mbgl (-0.15 m aOD; Zone G) reaching a maximum thickness of 5.2m in zone (5.30–10.5 mbgl; 1.23– -3.97 m aOD).

Inter-ridge marsh deposits

2.4.8 The intervening inter-ridge depressions within the gravel barrier variously contain sequences of fine-grained sediment along with sands, clayey-gravels and localised peats deposited within former tidal inlets. The formation of these marshland sediments reflects a period of significant coastal change under the influence of the eastward progradation of the gravel barrier, together with rapid sedimentation of the intervening inter-gravel lows.

2.4.9 The fine-grained sediment comprised both structureless silty clays overlying laminated silty clays, with surface elevations between 2.05–1.52 m aOD (Zone C), 2.07–1.37 m aOD (Zone E) and 1.90–1.56 m aOD (Zone G). A 0.38 m thick peat deposit was recorded in Zone G at -0.72– -0.94 m aOD, stratified in silty-clays.

2.4.10 Hand-held window samples also consistently record deposits flint gravels, in cases in rich clay deposits. It was not possible in most cases to determine how deep the upper gravel unit extends or whether they seal marsh deposits. In most, although not all cases, the gravel deposits recorded from c. 0–1mbgl occur along or near the edges of the inter-ridge zones or towards the base of the Green Wall. It seems probable therefore that these shallow gravel deposits may represent more recent periodic erosion (e.g., during storms and barrier breaches/overtopping) or progradation of the gravel barrier.

2.4.11 Corresponding silt and clay deposits were also recorded on the foreshore, varying in elevation beneath contemporary beach shingle from 1.02 m aOD (Zone C), 0.69– -0.85 m aOD (Zone E) and 0.37–0m aOD (Zone G). The silty clay deposits only crop out on the foreshore in relation to the corresponding inter-ridge depressions, extending out from the adjacent marshes landward of the Green Wall where they have been subject to variable erosion.

3 AIMS AND OBJECTIVES

3.1 Overarching aims and objectives

3.1.1 The overarching aims and objectives of the works include:

- Determine the level of preservation and concentration of palaeoenvironmental remains (pollen, foraminifera, ostracods and diatoms) within the deposits;

- Interpret the results to inform reconstructions of past environment and landscape change;
- Assess the geoarchaeological and archaeological significance of the deposits;
- Make suitable and proportionate recommendations for further work

3.2 Aims and objectives

3.2.1 The aims and objectives of the works address two of the specific research objectives of the project, as outlined in Jacobs 2020:

- OSL dating of sediments infilling tidal inlets;
- Sediment provenance and land-ocean interaction.

3.2.2 The aims and objectives were achieved through the following:

- OSL dating of fine-grained marsh sediments in boreholes C01/WA-S03, G01/WA-S03 and radiocarbon dating of organic deposits in C01/WA-S03 and HHWS-107;
- XRF core scanning of fine-grained sediment in boreholes C01/WA-S03, E01/WA-S02, G01/WA-S03, HHWS-107 and monolith 111 (TP11);
- Assessment of pollen from HHWS-107;
- Assessment of diatom, foraminifera and ostracods from HHWS-107 and monolith 111.

4 METHODS

4.1 Luminescence dating

4.1.1 Eight samples were submitted to the University of Gloucester Luminescence dating laboratory for luminescence dating and analysed using conventional Optically Stimulated Luminescence (OSL) dating of quartz grains.

4.1.2 Four samples were submitted from each of cores C01/WA-S03 and G01 WA-S01 recovered in opaque liners, and derived from marsh deposits preserved below the Green Wall (**Table 3**)

4.1.3 The full methodological details for the OSL dating are provided in the specialist report (**Appendix 1**).

4.2 Radiocarbon dating

4.2.1 Three small bulk subsamples were taken, processed and assessed from core samples C01/WA-S03 (one sample) and HHWS-107 (two samples). The subsamples were processed for plant macrofossils to recover material suitable for radiocarbon dating (itemised in **Appendix 1**).

4.2.2 The sub-samples were processed by standard wet-sieving methods for the recovery of waterlogged plant remains; the organic fraction was retained on a 0.25 mm mesh. Flots were stored in sealed containers with deionised water. The flots were scanned under a x10–

x40 stereo-binocular microscope and the preservation and nature of the macroremains recorded. Nomenclature follows Stace (1997).

4.2.3 Suitable material was identified under a binocular microscope, stored in glass tubes, and sent to the ^{14}CHRONO Centre at Queens University Belfast for radiocarbon dating. The macrofossil samples were treated with acid, and the measurement corrected using AMS $\delta^{13}C$ values; further detail on the laboratory methods is given in 14Chrono (2019). The age ranges were calculated with OxCal 4.4 (Bronk-Ramsey 2008, 2009) using the IntCal20 curve (Reimer *et al*. 2020). Radiocarbon dates are quoted as uncalibrated years before present (BP), followed by the lab code and date ranges at 95% confidence with the end points rounded out to the nearest 10 years (calibrated) or 5 years (modelled, in italics, see Bayliss and Marshall 2020).

4.3 XRF core scanning

4.3.1 X-ray fluorescence (XRF) scanning was undertaken on inter-ridge sediments at five locations (C01/WA-S03, E01/WA-S02, G01/WA-S02, HHWS-107 and Monolith 111), with the aim of producing high-resolution, non-destructive geochemical data to investigate the sediment provenance and land-ocean interactions of the above-gravel stratigraphy.

4.3.2 The selected sediment cores were delivered to the British Ocean Sediment Core Research Facility (BOSCORF) where measurements were carried out using an Itrax XRF scanner. As X-rays produced by the scanner have the potential to irradiate sediments and manipulate any luminescence dates produced, the cores were split in two halves with one half retained for potential luminescence dating. Measurements on the working half of each core were undertaken at <1 cm resolution intervals. High-resolution optically adjusted images were also produced to support the geochemical results.

4.3.3 The raw geochemical data was cleaned, with specific major elements and outliers (i.e. where the validity exceeded or dropped below the value of 1) removed. The elements Calcium (Ca) and Strontium (Sr) were removed to account for seasonal fluctuations in the water table and the impact of this on post-depositional decalcification. The data was normalised to create log ratios and presented alongside elemental concentrations (**Figures 3-11**) to identify any relationships between the geochemistry and environmental variables. To aid interpretation, lithozones were subdivided based on notable trends in the geochemistry and compared against the lithostratigraphy.

4.3.4 The data is presented as cps (counts per second) rather than ppm (parts per million). Results presented as cps can be difficult to interpret without calibration using bulk chemistry; this has not been undertaken at this stage. The results do however provide an indication of broad changes in sediment source (see paragraph 6.3.6 for a discussion of variables affecting interpretation of geochemical results).

4.4 Pollen

4.4.1 A total of four sub-samples of 1 ml volume were processed using standard pollen extraction methods (Moore et al 1991) from borehole HHWS-107.

4.4.2 Pollen was identified and counted using a Meiji ML5970 Phase Contrast Microscope. A minimum of one-hundred total land pollen (TLP) grains were counted in each sample in addition to aquatics and fern spores, and where 100 counts were not possible, all pollen and spores were counted from four transects. One Lycopodium tablet was added to enable calculation of pollen concentrations. Pollen and spores were identified to the lowest possible

taxonomic level. Plant nomenclature followed Stace (1997) and Bennett et al. (1994). Identification of indeterminable grains was according to Cushing (1967).

4.4.3 At assessment stage the results are not presented as pollen diagrams but are presented in tabular form as raw data.

4.5 Diatoms

4.5.1 A total of eight sub-samples were prepared for diatom assessment, four from borehole HHWS-107 and four from monolith 111.

4.5.2 Diatom preparation followed standard techniques (Battarbee et al. 2001). Two coverslips were made from each sample and fixed in Naphrax for diatom microscopy. A large area of the coverslips on each slide was scanned for diatoms at magnifications of x400 and x1000 under phase contrast illumination.

4.5.3 Diatom floras and taxonomic publications were consulted to assist with diatom identification; these include Hendey (1964), Van der Werff & Huls (1957-1974), Hartley et al. (1996), Krammer & Lange-Bertalot (1986-1991) and Witkowski et al. (2000). Diatom species' salinity preferences are indicated using the halobian groups of Hustedt (1953, 1957), these salinity groups are summarised as follows:

- Polyhalobian: marine >30 gl-1 salinity
- Mesohalobian: brackish 0.2-30 gl-1 salinity
- Oligohalobian - Halophilous: optimum in slightly brackish water
- Oligohalobian - Indifferent: optimum in freshwater but tolerant of slightly brackish water
- Halophobous: exclusively freshwater
- Unknown: taxa of unknown salinity preference

4.6 Foraminifera and ostracods

4.6.1 A total of eight sub-samples were prepared for foraminifera and ostracod assessment, four each from borehole HHWS-107 and monolith 111.

4.6.2 The sub-samples were weighed, then broken into small pieces by hand, placed into ceramic bowls, and dried in an oven. Boiling-hot water was then poured over them and a small amount of sodium carbonate added to help disaggregate the clay fraction. Each sub-sample was left to soak overnight. Washing was with hand-hot water through a 75 micron sieve, with the remaining residue being returned to the ceramic bowl for final drying in the oven. The residues were then stored in labelled plastic bags.

4.6.3 For examination, each sample was placed in a nest of sieves (>50, >250, >150µm, and base pan) and thoroughly shaken. Each grade was then sprinkled onto a picking tray, a little at a time, and viewed under a binocular microscope. ‘Contained material’ were logged on a presence(x)/absence basis as shown in accompanying tables.

4.6.4 In only one core (VC-T15) was there a sufficient sequence in which the 'contained material' (which would contribute to the environmental reconstruction) could be logged and this is shown in A.

4.6.5 The abundance of each foraminifera and ostracod species was estimated semi-quantitatively (one specimen, several specimens, common and abundant/superabundant) by experience and by eye. Species identification comes from Murray (2006) for the foraminifera, Athersuch et al. (1989) for the brackish and marine ostracods, and Meisch (2000) for the freshwater ostracods, in addition to expert judgement.

5 RESULTS

5.1 Introduction

5.1.1 This section provides a detailed synthesis of the results of each analytical technique, with discussion of the results presented in **Section 6**. The full specialist reports and raw data are provided in **Appendix 1**.

5.2 Luminescence and radiocarbon dating

Luminescence dating

5.2.1 All eight samples produced age estimates (see **Table 3**). The four samples from borehole C01/WA-S03 dated from the Bronze/Iron Age to post-medieval, displaying evidence for an inversion between sample GL22006 (7.02–7.12 mbgl) and GL22005 (6.85–6.95 mblg).

5.2.2 Moreover, there is a disagreement in results between the OSL date from 6.10–6.20 mbgl (GL22004, 1200–740 BC) and the radiocarbon date from 5.83–5.85 mbgl (UBA-49060, cal. AD 70–210). The OSL dates from borehole G01/WA-S01 extend from the Iron Age to early Romano-British period, with closely matching date ranges for samples GL22010 to 22008, with a late Iron Age/early Romano-British date derived from sample GL22007.

Radiocarbon dating

5.2.3 The macrofossil evidence found in the sediment subsamples (**Appendix 1; Table 3**) was dominated by the remains of aquatic/wetland and eutrophic plants. Invertebrate remains were also present. Short-lived terrestrial plant material suitable for radiocarbon dating was present in the samples. The radiocarbon dating samples were successfully measured, providing results in the Romano-British to Early medieval period.

Table 3 Integrated radiocarbon and luminescence dating results.

Sample ID	Depth (mbgl)	Dating method	Lab Code	Age estimate	Date range	Period
C01	4.92-5.02	OSL	GL22003	460 ± 40	AD 1520–1600	Post-medieval
	5.83-5.85	AMS 14C	UBA-49060	1905 ± 25	cal. AD 70–210	Romano-British
	6.10-6.20	OSL	GL22004	2990 ± 230	1200–740 BC	Bronze Age
	6.85-6.95	OSL	GL22005	3370 ± 240	1580–1100 BC	Bronze Age
	7.02-7.12	OSL	GL22006	2880 ± 200	1060–660 BC	Bronze /Iron Age
G01	4.65-4.75	OSL	GL22007	2110 ± 170	260 BC – AD 80	Iron Age/Romano-British
	5.20-5.30	OSL	GL22008	2520 ± 160	660–340 BC	Iron Age
	5.80-5.90	OSL	GL22009	2480 ± 200	650–260 BC	Iron Age
	6.45-6.55	OSL	GL22010	2400 ± 160	540–220 BC	Iron Age
HHWS-107	0.62-0.64	AMS 14C	UBA-49061	1701 ± 25	cal. AD 255–415	Romano-British
	0.77-0.79	AMS 14C	UBA-49062	1868 ± 21	cal. AD 120–235	Romano-British

5.3 XRF core scanning

5.3.1 **Figures 3 to 11** summarise the results of the XRF core scanning for the selected elements (Al, Si, S, K, Ti, Cr, Mn, Fe, Ni, Cu, Zn, Br, Rb, and Zr), along with specific log ratios targeted as proxies for redox (Fe/Al and Mn/Fe), grain size (Zr/Rb and Zr/Fe), and marine (Br/Cl and Si/Rb) and terrestrial provenance (Fe/Ti and Zr/K).

C01/WA-S03

5.3.2 The XRF results for borehole C01/WA-S03 demonstrate greater cyclicity (cyclical fluctuation in relative abundance of marine and terrestrial indicators) below depths of 4.80 m (**Figures 3 and 4**) with elemental ratios Zr/Rb, Zr/K and Zr/Fe illustrating relatively simultaneous high and low peak values in association with *in situ* and laminated marsh deposits.

5.3.3 Visible trends in these log ratios are less pronounced within the reworked sediments recorded between depths of 1.20 and 4.80 m, with greater scattering illustrated for elemental ratios Fe/Ti, Fe/Al, Si/Rb, Zr/Rb, Zr/K and Zr/Fe. The complexity in values produced for the uppermost sequence of borehole C01/WA-S03 suggest increased reworking of deposits. The high concentrations in both Fe/Ti and Br/Cl above 4.80 m also confirms these deposits are intertidal in nature, with input of both terrestrial and marine derived material.

E01/WA-S02

5.3.4 The XRF results presented for borehole E01/WA-S02 illustrate considerable scattering likely associated with the lithostratigraphic sequence which solely comprises reworked sediments. No cyclic trends were identified from the geochemistry and therefore no lithozones were recorded (**Figures 5 and 6**).

G01/WA-S02

5.3.5 Borehole G01/S0-02 demonstrates very low values for all elemental ratios (**Figures 7 and 8)** between 6.34 and 5.95 m. Despite this, selected elements Fe, Rb, K, Ti and K show a positive correlation with relatively high values at this depth. These elements are often associated with terrigenous input and thus may suggest a decrease in marine influence. An abrupt increase in values for ratios Zr/Rb, Zr/K, Zr/Fe and Mn/Fe is however recorded between 5.50 m and 5.95 m. Furthermore, the ratio Zr/Rb illustrates very high values and is often inferred as a proxy of both grain size, and physical erosion and wave action. This coupled with a spike in Si, may indicate increasing in-wash of marine sediments. Si is not a marine proxy, but may be linked to sand of possible, though not exclusively marine origin.

5.3.6 Values for ratios Zr/Rb, Zr/K, Zr/Fe and Mn/Fe decline consistently in the overlying sediments, with very low and stable values recorded for all elemental ratios between 3.00 and 5.15 m. The exception is a short-lived increase in values for Si/Rb associated with gravelly silty clays recorded between 3.60 and 3.80 m. In addition, terrigenous proxies negatively correlate with marine indicators at this depth, with low values for Al, K, Ti, Fe, Rb, and Zr. This may suggest a reduction in terrigenous input.

5.3.7 Due to voids in the borehole G01, a result of poor retention/core loss, there is uncertainty in the geochemistry for depths between 1.60 and 3.00 m. Values for all elements and log ratios between 1.20 and 1.60 m are scattered due to their association with contemporary sands and gravels.

HHWS-107

5.3.8 The XRF results for HHWS-107 show greater cyclicity associated with *in situ* marsh and organic deposits (**Figures 9 and 10**). Between depths of 0.96 and 0.82 m, the values for terrigenous proxies Zr, Rb, Ti, K, Al are high relative to values recorded for elements interpreted as marine indicators (i.e. Si).

5.3.9 Between 0.82 and 0.71 m high values for terrestrial proxies Fe/Ti and Zr/K associated with peat development are recorded. Low values for marine indicators additionally suggest relatively stable conditions at time of deposition. High values for Br, a proxy for organic matter, are also documented for the uppermost section of peat between 0.59 m and 0.71 m. A dramatic increase in both marine and terrestrial proxies correspond with the reinstatement of *in situ* silty clay above the peat unit and supports a return to intertidal conditions. The topsoil is associated with very high values recorded for Br, typically associated with an increase in organic content.

Monolith 111

5.3.10 No cyclic trends were identified from the XRF results presented for Monolith 111, as illustrated in **Figure 11**. The selected elements appear to correspond with the mean square error (MSE), and therefore fail to accurately represent prevailing environmental conditions.

5.4 Pollen

5.4.1 Four samples were assessed for pollen from HHWS-107 through the peat deposits (0.60, 0.72, 0.82 and 0.96 m bgl, detailed below and in **Table 4**.

5.4.2 Although full assessment counts of 100 TLP were achieved in all four samples, pollen concentrations and preservation were found to be variable (see **Table 4**); either poor or moderate in all but the top sample (0.60 m) which produced excellent concentrations and good preservation of pollen.

5.4.3 There is significant variation in pollen assemblages through the peat. The basal and top sample are dominated by trees and shrubs (approx. 70%). The basal sample is composed of a mix of *Quercus* (oak), *Corlyus avellana*-type (hazel), *Betula* (birch) and *Pinus sylvestris* (pine), with smaller quantities of *Alnus glutinosa* (alder) and single grains for a range of other trees. The top sample by contrast is dominated primarily by *Alnus glutinosa* with smaller quantities of other trees.

5.4.4 The quantity of trees at 0.82 and 0.72 m is much smaller (26 and 9% respectively) and the assemblages are instead dominated by open ground herbaceous species. At 0.82 m pollen comprises a high quantity of Poaceae (grasses) with smaller quantities of a range of other plants including *Rumex acetosa* (common sorrel), Cyperaceae (sedges), Ranunculaceae (buttercups), *Plantago lanceolata* (ribwort plantain) and Asteraceae (daisies). Of interest at 0.82 m is the large number of cereal-type pollen grains (approx. 12% of assemblage).

5.4.5 The assemblage at 0.72 m is dominated by pollen of two main taxonomic families: Poaceae (40%) and Cyperaceae (34%), with a similar range of other herbaceous taxa in small quantities, and an increase in aquatic pollen, including *Potamogeton natans*-type (pondweed) and *Sparganium emersum*-type (unbranched bur-reed).

5.4.6 In addition to a dominance of tree pollen in the top sample (0.6 m), the pollen assemblage includes pollen of Cyperaceae, Poaceae and small quantities of a range of herbaceous

pollen similar to those recorded in the other three samples and including a single cereal-type pollen grain.

5.4.7 No microscopic charcoal was recorded in any of the samples. Interpretation of the pollen sequence is considered in **Section 6.2**.

Table 4 Pollen assessment, HHWS-107.

Depth (m)	**0.6**	**0.72**	**0.82**	**0.96**
Trees and Shrubs				
Betula (birch)	2	-	4	12
Pinus sylvestris (pine)	1	4	1	11
Corylus avellana type (hazel)	6	-	3	14
Ulmus (elm)	-	-	-	1
Quercus (oak)	3	2	9	20
Tilia (lime)	-	1	-	2
Alnus glutinosa (alder)	57	1	2	7
Fagus sylvatica (beech)	-	1	6	1
Salix (willow)	1	-	-	1
Ilex aquifolium (holly)	-	-	1	-
Hedera helix (ivy)	1	-	-	-
Dwarf Shrubs				
Calluna vulgaris (common heather)	1	-	2	-
Cultivated				
Cerealia type (cereal undiff.)	1	-	12	-
Herbaceous				
Rumex acetosa (common sorrel)	-	3	5	-
Chenopodiaceae (goosefoot family)	-	1	1	9
Brassicaceae (cabbage family)	1	-	-	-
Poaceae (grass family)	8	40	32	11
Cyperaceae (sedge family)	18	34	5	6
Ranunuculaceae (buttercup family)	-	2	4	-
Caryophyllaceae (pink family)	2	1	-	1
Rosaceae (rose family)	1	2	1	2
Lamiaceae (mint family)	-	-	2	-
Plantago lanceolata (ribwort plantain)	2	1	3	1
Rubiaceae (bedstraw family)	-	-	1	-
Cirsium (thistle)	1	1	-	-
Lactuceae (lettice family)	1	4	3	3
Asteraceae (daisies)	1	2	3	-
Fern Spores				
Pteropsida undiff. (undifferentiated fern spore)	19	-	1	-
Dryopteris filix-mas (male fern)	-	1	-	-
Aquatics				
Myriophyllum (alternate water-milfoil)	-	-	2	-
Potamogeton natans type (pondweed)	2	13	2	2
Sparganium emersum type (unbranched bur-reed)	-	10	3	-
Typha latifolia (bulrush)	1	-	-	-
TLP (Total Pollen Count)	**108**	**100**	**100**	**102**
Trees and Shrubs	71	9	26	69
Dwarf Shrubs	2	0	14	0
Herbs	35	91	60	33
Pollen concentration	**1**	**4**	**3**	**4**
Pollen preservation	**2**	**3**	**4**	**4**
Microcharcoal	**5**	**5**	**5**	**5**

Key: preservation and concentration. 1 = excellent, 2 = good, 3 = moderate, 4 = poor, 5 = absent

5.5 Diatoms

HHWS-107

5.5.1 Four samples were assessed for diatoms from HHWS-107 (0.34, 0.46, 0.58 and 0.98 m) from silty clay over and underlying the peat (0.59–0.97 m) (**Table 5**). Diatoms are present in all four samples, with moderately high quantities at 0.98 m, with the samples from above the peat containing low (0.58 m) or extremely low (0.46 and 0.34 m) quantities of diatoms.

5.5.2 The sample from 0.98 m has a moderately high number of diatoms that are moderately to well-preserved, and the assemblage is of moderate diversity. The diatom assemblage is composed entirely of marine, marine-brackish and brackish water diatoms that indicate a tidal depositional environment. The dominant marine taxa include *Cymatosira belgica, Paralia sulcata, Rhaphoneis minutissima, Rhaphoneis surirella, Thalassionema nitzschiodes* and *Trachyneis aspera*. Marine-brackish and brackish water diatoms include *Actinoptychus undulatus*, *Thalassiosira decipiens*, *Diploneis aestuari*, *Melosira* moniliforms and *Actinocyclus normanii*. No freshwater diatoms were recorded in this sample.

5.5.3 The diatom taxa from 0.58m has very low quantities and very poor preservation. However, except for a fragment of the marine planktonic species *Paralia sulcata*, the diatom assemblage is composed of non-planktonic freshwater taxa. These diatoms include *Craticula cuspidata*, *Epithemia adnata*, *Pinnularia divergens* and *Synedra* ulna. The *Epithemia* spp. present suggest the presence of aquatic macrophytes. Freshwater aerophilous diatoms include *Hantzschia amphioxys* and *Pinnularia major*. *Chrysophyte stomatocysts* are also relatively common. The presence of both aerophilous diatoms and *chrysophyte* cysts suggest an ephemeral freshwater aquatic habitat subject to lower water levels or drying out.

5.5.4 Samples from 0.46 and 0.34 m exhibit extremely poor diatom preservation and concentrations and are indeterminate at best.

Monolith 111

5.5.5 Four samples were assessed from monolith 111 (0.81, 0.98, 1.07 and 1.19 m). Diatoms are present in extremely low numbers and poorly preserved at 1.19 m and in moderately high numbers, variable preservation and moderate diversity in the top three samples.

5.5.6 From the top three samples the most common species is the marine planktonic diatom *Paralia sulcate*. Other marine taxa that are common in one or more of these samples are *Cymatosira belgica, Rhaphoneis surirella and Rhaphoneis amphiceros*. Polyhalobous diatoms that are present these samples are *Anorthoneis* sp., *Grammatophora* sp., *Nitzschia panduriformis, Rhaphoneis minutissima, Thalassionema nitzschiodes, Trachyneis aspera* and *Surirella comis.*

5.5.7 Marine-brackish and brackish-marine diatoms include *Actinoptychus undulatus, Cocconeis scutellum, Pseudopodosira westii, Thalassiosira decipiens, Diploneis aestuari, Diploneis didyma* and *Melosira moniliformis*. Freshwater diatoms are absent from all three samples with the assemblages representing coastal marine habitats.

Table 5 Diatom assessment, HHWS-107 and Monolith 111.

Sample depth (m)	Diatoms	Diatom Numbers	Quality of Preservation	Diversity	Assemblage type	Potential for % count
HHWS-107						
0.34	present	ex low	ex poor	-	indet fragments	none
0.46	present	ex low	ex poor	-	? fw	none
0.58	present	v low	v poor	low	fw non-pk, aero	v low
0.98	present	mod	mod	mod	mar, mar-bk	good
Monolith 111						
0.81	present	mod	mod	mod	mar, mar-bk	good
0.98	present	mod	mod to poor	mod	mar, mar-bk	good
1.07	present	mod	poor to mod	mod	mar, mar-bk	good
1.19	trace	ex low	ex poor	centric sp.	unknown	none

Key: (fw – freshwater; bk – brackish; mar – marine; mar-bk – marine-brackish; aero – aerophilous; mod – moderate; ex – extremely; indet – indeterminate diatom; non-pk – non-planktonic)

5.6 Foraminifera and ostracods

5.6.1 Eight samples were assessed for foraminifera and ostracods, four from HHWS-107 and four from Monolith 111.

HHWS-107

5.6.2 Preservation of foraminifera and ostracods was uniformly poor in all samples with no microfauna present. Single charophyte oogonium were recovered at 0.46 and 0.98 m suggesting possible freshwater or low salinity environments.

Monolith 111

5.6.3 Low numbers of ostracods were recorded at 0.81-0.83, 0.95-0.98 and 1.16-1.19 and absent entirely from 1.04-1.07 m. A high species richness of foraminifera were recorded in the sample at 0.81-0.83 m but were otherwise infrequent in the remaining three samples.

5.6.4 The sample at 0.81-0.83 included the following ostracods: *Palmoconcha laevata* (3v), *Propontocypris trigonella* (2v), *Aurila convexa* (3v) are all shallow marine species. *Pontocythere elongata* (3v) is often found in outer estuaries. *Hirschmannia viridis* (3v) is a marine to brackish indicator while *Cytherura gibba* is prefers brackish environments. All of these species prefer a weed rich environment. Other taxa recovered include *Leptocythere* sp. (1v), two species of *Semicytherura* sp. (3v) and an indeterminate form.

5.6.5 The following foraminifera were recorded, including miliolids (13), *Ammonia ?tepida* (5), *Haynesina germanica* (5) and *Elphidium williamsoni* (2), indicative of a marine to brackish environment.

5.6.6 Foraminifera and ostracods were infrequent in the remaining samples but included taxa indicative of a strongly marine brackish water environment (0.95 – 0.98 m) and a marginal marine environment (1.04-1.07 and 1.16-1.19 m).

6 DISCUSSION

6.1 Introduction

6.1.1 A program of palaeoenvironmental assessment was undertaken on retained samples, targeted to address the aims and objectives as outlined in **Section 3**. These investigations comprised XRF core scanning, OSL and radiocarbon dating and assessment of pollen and microfauna (diatoms, foraminifera and ostracods).

6.2 Chronology

6.2.1 The results of radiocarbon and OSL dating from organic and fine-grained marsh deposits are illustrated in **Figure 12** and **Table 3**. Comparison of results from each method highlights the generally earlier dates on samples dated using OSL when compared to radiocarbon ages on organic deposits.

6.2.2 In C01/WA-S03, a sample from an organic layer at 5.83-5.85 mbgl produced a date of cal. AD 70-120 (Romano-British), with an OSL sample at 6.10-6.20 mbgl producing a date of 1200-740 BC (Late Bronze Age). Samples from G01/WA-S01 produced OSL dates covering the Romano-British period through to the Iron Age, including evidence for some inversion in dates, with radiocarbon dates from peat preserved in marsh deposits behind the Green Wall at Zone G extending from cal. AD 120-235 to 255-415.

6.2.3 Radiocarbon dates on organic deposits separated by approximately 900m have therefore produced broadly comparable dates in the Romano-British period, several centuries later than closely associated OSL dates.

6.2.4 Despite the evidence for decalcification of the sediments apparent from the geochemical record, this is not considered to impact the radiocarbon results as all dates were derived on short-lived plant macrofossils. These fix carbon prior to burial while any fluctuation in depositional carbon is removed as part of the laboratory pre-treatment process. However, issues of decalcification might impact samples derived on bulk sediment, bone or mollusca.

6.2.5 Existing OSL dates from basal sands along the Dungeness Foreland show a decrease in age in deposits from west to east as the Foreland expanded under longshore drift. The sands are overlain by sands and gravels, gravels of the Dungeness Foreland and in turn marsh deposits in-filling inter-ridge depressions between the gravel ridges. OSL dates nearest to the top of the sand unit, from boreholes located close to the present study, suggest the sands were deposits between 3000-2000 years ago (Plater et al 2007, Roberts and Plater 2007) with current OSL dates from the marsh deposits producing a broadly similar date range. Moreover, the OSL dates are significantly older than palaeomagnetic dates derived on back barrier marsh deposits by Plater et al (2009), dating to between c. 1000-1500 AD.

6.2.6 The OSL dates from C01/WA-S03 and G01/WA-S01 are derived from a multi-grain assessment that acts as initial range-finders, but also in situations where there is limited datable material. This was the case with the samples from Lydd, that have very limited datable find sand-sized quartz grains and which likely include some partial resetting of grains and an over-estimation of their ages (Phil Toms, Paul Fish pers comm).

6.2.7 OSL dates may also be impacted by variability in the moisture content of the sediment over time. Roberts and Plater (2005, 2007) highlight that variations in water content can affect does rates to sediment grains, potentially leading to over-estimation of resulting ages.

Roberts and Plater (2005) modelled water history based on factors including measured field water content, pore water content, interstitial drainage characteristics of sediment in the contemporary inter to supratidal zone, together with an estimation of altitudinal changes in sea-level, with moisture content set at between 50 – 90%.

6.2.8 Although consideration of the impact of water history on OSL dates is valuable, similar modelling of the Lydd samples has not been undertaken at this stage in the absence of sufficiently precise data to accurate guide and model past water history. Although a coarse model of water content has been applied to the Lydd dates (0-100%), applying a value similar to Roberts and Plater (2005) is unlikely to resolve the inconsistencies arising from the young age and partial bleaching is considered to be the more dominant factor impacting the results. Variability in De values should not be taken as an indicator of the absence/presence of partial bleaching, particularly from the Lydd samples where fine silt grained aliquots were used in all but one of the samples.

6.2.9 Radiocarbon dates from cores between South Brooks and Wickmaryholm Pit indicate peat development at these locations between 1690-1420 cal. BP (cal. AD 260 – 530) (Waller at al 2007); the radiocarbon dates from C01/WAS-03 and HHWS-107 do not appear anomalous in this context, suggesting barrier emplacement across zones C and G by the early Romano-British period.

6.3 Sediment provenance and land-ocean interactions

6.3.1 Evidence for sediment provenance and land-ocean interactions is provided by the results of XRF core scanning (**Figures 3-11**), and diatom, foraminifera and ostracod assessment (**Table 5**). The various samples are derived from marsh sediments preserved behind (HHWS-107), below (C01-WA/S03, E01/WA-S02 and G01/WA-S01) and seaward of the current Green Wall (monolith 111, TP11).

Microfauna

6.3.2 Preservation of foraminifera and ostracods was almost uniformly poor, with no microfauna preserved in HHWS-107. Preservation of a single charophyte oogonium in two samples suggest possible freshwater or low salinity environments but should be interpreted with caution given the paucity/absence of corroboratory microfaunal evidence.

6.3.3 From clay exposures on the foreshore (monolith 111, TP11), only one sample produced a rich assemblage of foraminifera that along with preserved ostracods are indicative of a marine-brackish environment.

XRF core scanning

6.3.4 Data from XRF core scanning provides a measure of down-core changes in elements in fine-grained marsh sediments recovered in boreholes through the Green Wall (CO1/WA-S03, E01/WA-S02 and G01/WA-S01), marsh (HHWS-107) and foreshore (monolith 111, TP11).

6.3.5 Interpretation of XRF data considers the relative abundance of different elements down-core, presented as counts/second (cps) rather than as concentrations such as ‘parts per million’ (ppm).

6.3.6 As the results are presented as cps rather than concentrations, they can be difficult to interpret without calibration using bulk chemistry, although the results do provide an indication of broad changes in sediment source. The results can be impacted by variables

such as the surface of the measured sample where cracks or fissures in the sediment return null values. A range of other factors can affect the counts for elements, including changes in grain size, water content and organic matter content and changes in the source of sediment.

6.3.7 Both Calcium and Strontium were removed from the plots as both elements are linked to a process of post-depositional decalcification of deposits that can occur through the variable dissolution of carbonate matter present within the deposits.

6.3.8 Zr/Rb ratios are primarily a function of variation in grain size, while clays are generally enriched in Al and Sands in Si. Fe/Ti ratios are often indicative of a terrestrial input, and both Fe and Ti separately can be taken as indications of weathering of terrestrial material, or in the case of Fe and Mn/Fe ratios as evidence for redox processes (e.g. Gebregiorgis 2020).

6.3.9 Any discussion here is largely focused on the quality of data recovery and suitability for further study. Detailed discussion of the results in terms of sediment provenance would require conversion of the data into concentrations though some general observations are presented here.

6.3.10 The results of XRF core scanning were variable, with considerable scattering recorded in E01/WA-S02 (**Figures 5 and 6**) and a high mean square error in monolith 111 (TP11) (**Figure 11**) making the results problematic to interpret.

6.3.11 HHWS-107 (**Figures 9 and 10**) produced good results with evidence for cyclicity (cyclical fluctuation in relative abundance of marine and terrestrial indicators) in grain size and increasing counts for Rb in the peat. The high water and organic matter content of peat can be problematic for XRF core scanning, as both can dilute the signal from the minerogenic fraction of the sediment. However, in HHWS-107 there are peaks in Fe/Ti and Zr/K which may be indicative of some terrigenous input into the peat, perhaps due to erosion or periodic in-wash of sediment during high tides or storm surges. Additional organic matter content analysis may be useful in this context to highlight increasing minerogenic input into the peat. There is a subsequent increase in marine and terrestrial indicators in element ratios with a return to intertidal conditions.

6.3.12 Boreholes C01/WA-S03 (**Figures 4 and 5**) and G01/WA-S01 (**Figures 7 and 8**) produced good results, though values between 3.0 and 1.6 mbgl in G01/WA-S01 are negatively affected by voids in the core due to poor retention of sediment in the field. The results from the fine-grained sediments in both cores recorded low values for all elements but with variations in elements suggestive of shifts between marine and terrestrial inputs over time.

6.3.13 The results emphasise that the quality of core recovery and sediment type will impact the results, and that sections of cores may benefit from additional work in the form of bulk chemistry to calibrate the cps values and loss-on-ignition analysis to quantify the organic matter content of the peat.

6.4 Palaeoenvironments

6.4.1 The results of the diatom, foraminifera and ostracod assessments provided limited evidence for local environments. Evidence for the palaeoenvironment of the site is provided by pollen preserved in HHWS-107 (**Table 4**), considered against the palaeogeographic background of the Dungeness Foreland, Walland Marsh and associated wetlands.

6.4.2 Peat deposits were identified in core HHWS-107, interbedded in silty clay marsh deposits within Zone G (see **Figure 1 and 12** for context and dating). Radiocarbon dating indicated that this deposit formed during the Romano-British period, broadly comparable in date to organic deposits identified from borehole C01, located approximately 900 m to the west in Zone C.

6.4.3 Palaeogeographic models of Romney Marsh and the Dungeness Foreland include the development of tidal channels separating the site from Walland Marsh by at least the Stratigraphic and dating evidence indicates that breaches through the barrier in the late Roman period (around cal. AD 300-400) resulted in the formation of a tidal channel further to the north of the site, dominated by the Midley Channel and which persisted until reclamation in the 13th century (Long et al 2006).

6.4.4 Peat deposits are widely recorded across Romney Marsh and Walland Marsh and associated wetlands and provide a detailed history of a complex relationship between marine and semi-terrestrial wetland environments over the last several thousand years. The peatland environments include extensive alder carr swamps and raised bogs which began forming after around 4000 cal. BC, reaching their maximum extent around 1200 cal. BC and that with Walland Marsh were completed inundated by around 200 AD (Long et al 1998; Waller and Long 2003). Roman dates on peat have been produced from several locations (see Long et al 2006, Table 1).

6.4.5 In addition to the main marsh peat mapped to the north across Walland Marsh, thin (< 1m) freshwater reed peats have been recorded preserved within the inter-ridge depressions (Waller et al 1998, Kirby et al 2010, Spencer et al 1998, Long and Hughes 1995). Peat deposits recorded in Scotney Marsh to the north of the Site reflect multiple phases of peat formation within the undulating gravel topography, punctuated by phases of inundation. The second phase of peat development was dated to between approximately 100 cal. BC to cal. AD 400 (Spencer and Woodland 2002).

6.4.6 A cessation in peat formation in the late Romano-British period is consistent with evidence from across the UK for rising sea-levels following the Roman Warm Period leading to widespread inundation of coastal areas and abandonment of settlements (e.g. Van de Noort and Ellis 2000, Rippon 2021).

6.4.7 The preservation of a thin peat within HHWS-107 is therefore consistent with the evidence for formation of organic beds in the Roman period within the western reaches of Walland and associated marshes (synthesised in Waller et al 2010). The peat in HHWS-107 has a gradual contact at its base with the underlying marsh deposits, strongly indicating that the deposit formed in-situ, rather than through erosion and redeposition. Peat deposits have been recorded to the north of the site at Lydd, similarly developing within a gravel low, though dating earlier to the Bronze/Iron Age (Kirby et al 2010).

6.4.8 Preservation and concentration of pollen in HHWS-107 was found to be variable though largely moderate to poor. Variable preservation can result in biased pollen assemblages, favouring those taxa more resistant to decay processes (Havinga 1984). For example, pollen taxa such as alder, lime and birch are particularly resistant to decay, whereas taxa such as oak, grasses and sedges are particularly susceptible to decay.

6.4.9 Three of the four samples in HHWS-107 recorded either poor or moderate preservation (0.72, 0.82 and 0.96 m). In the basal sample (0.96 m) dominated by tree pollen, this may have resulted in under-estimation of herbaceous taxa susceptible to decay processes such

as grasses and sedges. However, the preservation of large quantities of oak, a taxon susceptible to decay, may suggest a limited bias in preservation or an abundance of oak in the local environment.

6.4.10 Poor preservation in samples at 0.82 and 0.72 m both include large numbers of grass and grasses/sedges respectively which were clearly identifiable though often crumpled, suggesting these taxa are likely to be an important component of the local environment.

6.4.11 The pollen sequence suggests the presence in the early Romano-British period of mixed oak-hazel woodland, with birch and alder likely on wetter soils and pine pollen representing a long-distance component. Pine is not considered to be growing locally unless percentages exceed 20% (Bennett 1984). Trees typically produce more pollen than herbaceous taxa, which is more widely dispersed by wind, thus biasing pollen sequences in favour of closed versus open environments. It is therefore possible that the tree pollen present in the basal sample may reflect a general abundance of trees in the extra-local environment, but not necessarily representative of extensive closed-canopy woodland.

6.4.12 This is followed by a significant reduction in woodland taxa and an abundance of herbaceous species indicative of tall herb fen environments, including stands of reed and sedges. An expansion of tall herb swamp at the sampling location could have resulting in some degree of filtering out of pollen from the extra-local environment, though the overall impression is one of a locally open wetland environment.

6.4.13 Pollen data from Southern Walland Marsh demonstrates the presence of nutrient-rich fen habitats and the development of wet alder carr woodland. Areas of dry ground are located c. 10 km west of the site and may be the source of a proportion of the tree pollen, or at least dryland taxa. The indication from the broader pollen data is that widespread woodland clearance had occurred by the Bronze Age (Waller and Schofield 2007). Trees such as alder, birch and willow are likely to have been more prevalent on wet soils within and along the margins of the wetland.

6.4.14 The large quantity of cereal-type pollen grains at 0.82 m could be taken for evidence for agricultural activity. However, cereal pollen grains are self-pollinated and tend to be dispersed only short distances from source unless transported further by other vectors (e.g. by animals on their fur or in their dung). Large cereal-type pollen grains may also represent large grass grains of species such as *Glyceria fluitans* (floating manna grass) growing within the wetland. Glycerol jelly used as a mounting medium can also result in swelling of pollen grains, though there was no evidence for a similar effect on other taxa preserved in this sample.

6.4.15 Although there is evidence for arable activity around Rye, which resulted in deposition of slopewash deposits overlying the peat (Long et al 2007), no archaeological evidence for Roman activity is known from the Site and doubt must be placed on the evidence for cultivation from HHWS-107. A more likely explanation is that the cereal type pollen grains represent large grass grains of species growing in the wetland, or cereal pollen deposited via animal agencies (including birds), for example, in their faeces.

7 CONCLUSION AND RECOMMENDATIONS

7.1.1 A program of palaeoenvironmental assessment was undertaken on retained samples, comprising XRF core scanning, OSL and radiocarbon dating and assessment of diatom, foraminifera, ostracods and pollen.

7.1.2 The following overarching aims and objectives and specific research questions were addressed, with consideration provided on the archaeological/geoarchaeological significance of the samples and recommendations for further analysis, where appropriate.

Determine the level of preservation and concentration of palaeoenvironmental remains (pollen, foraminifera, ostracods and diatoms) within the deposits

7.1.3 Foraminifera, ostracods and diatoms were found to be poorly preserved or absent in almost all samples, with only one sample from monolith 111 (TP11) producing a rich foraminifera assemblage. No further analysis is recommended.

7.1.4 Though sufficient pollen was present for assessment from HHWS-107, preservation and concentrations were variable, though largely moderate to poor. Indications of local and extra-local environment are suggested, but there is likely to be some bias in assemblages resulting from differential preservation. No further analysis is recommended.

Interpret the results to inform reconstructions of past environment and landscape change

7.1.5 Limited conclusions can be drawn about past environments and landscape from the microfaunal evidence apart from indications of a marine-brackish environment from a single foraminifera assemblage in monolith 111 (TP11).

7.1.6 The pollen data provided evidence for possible woodland clearance and local agricultural activity. However, evidence for the latter in the form of cereal-type pollen grains should be treated cautiously and may instead reflect large pollen grains of wild grass species or cereal pollen carried via animal vectors. The radiocarbon dating evidence suggests peat formation during the Romano-British period, comparable with evidence from the wider Walland and Romney Marshes.

OSL dating of sediments infilling tidal inlets

7.1.7 Eight samples were OSL dated, four from each of boreholes C01/WA-S03 and G01/WA-SO1. These dates act as initial range-finders and indicate that there was limited datable material present in the samples, with the results likely affected by some partial resetting of grains, resulting in an over-estimate of their age. Over-estimation of OSL ages was apparent in cases where dates could be assessed against closely related radiocarbon dates. No further analysis is recommended.

Sediment provenance and land-ocean interaction

7.1.8 Limited data was provided by the microfaunal assessment. Although XRF core scanning produced variable results there may be some merit in undertaking targeted bulk geochemistry in order to calibrate relative element abundances recorded in C01/WA-S03, G01/WA-S01 and HHWS-107. However, the need for this work is likely reduced by the overall poor preservation of other proxy remains from samples.

BIBLIOGRAPHY

Athersuch J, Horne D J, Whittaker J E 1989 Marine and brackish water ostracods. In: Kermack D M, Barnes, R S K. (eds), *Synopsis of the British Fauna (New Series), no. 43*. E.J. Brill, Leiden (for the Linnean Society of London and The Estuarine and Brackish-water Sciences Association), 359pp

Battarbee R W, Jones V J, Flower R J, Cameron N G, Bennion H B, Carvalho L and Juggins S 2001 Diatoms. In (J.P. Smol and H.J.B. Birks eds.), *Tracking Environmental Change Using Lake Sediments Volume 3: Terrestrial, Algal, and Siliceous Indicators*, 155-202. Dordrecht: Kluwer Academic Publishers

Bayliss A and Marshall P 2022 *Radiocarbon Dating and Chronological Modelling - Guidelines and Best Practice*. Historic England

Bennett K D 1984 The post-glacial history of Pinus sylvestris in the British Isles. *Quaternary Science Reviews* 3, 133–55

Bennett K D Whittington G and Edwards K J 1994 Recent plant nomenclature changes and pollen morphology in the British Isles. *Quaternary Newsletter* 73, 1–6

Bronk Ramsey C 2008 Deposition models for chronological records, *Quaternary Science Reviews*, 27(1-2), 42–60

Bronk Ramsey C 2009 Bayesian analysis of radiocarbon dates, *Radiocarbon* 51, 337–360.

^{14}Chrono 2019 '14Chrono Centre laboratory 14C pre-treatment protocols', http://14chrono.org/site/wp-content/uploads/2020/03/Lab_protocols.pdf (accessed 15.11.2022).

Cushing E J 1967 Evidence for differential pollen preservation in late Quaternary sediments in Minnesota. *Review of Palaeobotany and Palynology* 4, 87–101

Gebregiorgis D, Glosan L, Hathorn E C, Anand P, Nilsson-Kerr, K, Plass A, Luckge A, Clemens S C and Frank M 2020 Normalizing XRF-scanner data: A cautionary note on the interpretation of high-resolution records from organic-rich lakes. *Geochemistry, Geophysics, Geosystems* 21, https://doi.org/10.1029/2019GC008414

Hartley B H G, Barber J R, Carter and P A. Sims. 1996 *An Atlas of British Diatoms*. Biopress Limited. Bristol. pp. 601

Havinga A J 1984 A 20 year experimental investigation into the differential corrosion susceptibility of pollen and spores. *Pollen et Spores* 26, 541–58

Hendey N I 1964 *An Introductory Account of the Smaller Algae of British Coastal Waters*. Part V. Bacillariophyceae (Diatoms). Ministry of Agriculture Fisheries and Food, Series IV. pp. 317

Hustedt F 1953 Die Systematik der Diatomeen in ihren Beziehungen zur Geologie und Okologie nebst einer. *Revision des Halobien-systems. Sv. Bot. Tidskr*., 47, 509–519

Hustedt F 1957 *Die Diatomeenflora des Fluss-systems der Weser im Gebiet der Hansestadt Bremen. Ab. naturw*. Ver. Bremen 34, 181–440

Jacobs 2020 *Lydd Ranges, Folkstone to Cliff End Strategy assessment of Holocene geology and geoarchaeology*. Report ref.: S1 P06

Kirby J, Clarke D, Shaw T and Toole E 2010 The mid to late Holocene evolution of southern Walland Marsh and the origin of the 'Midley Sand'. In: M. Waller, E. Edwards and L. Barber (Eds.) *Romney Marsh: Persistence and Change in a Coastal Lowland 2. The Evolution of Southern Walland Marsh and the Origin of the 'Midley Sand' 23*, Romney Marsh Research Trust, 2010, 23–51

Krammer K and Lange-Bertalot H 1986-1991 *Bacillariophyceae*. Gustav Fisher Verlag, Stuttgart

Long A, Waller M, Hughes P and Spencer C 1998 The Holocene deposition history of Romney Marsh Proper. In Eddison J, Gardiner M and Long A (Eds) *Romney Marsh: Environmental Change and Human Occupation of a coastal lowland*. OUCA Monograph 46, 43–63

Long A J, Waller M P and Plater A J 2006 Coastal resilience and late Holocene tidal inlet history: the evolution of Dungeness Foreland and the Romney Marsh depositional complex (U.K.). *Geomorphology* 82, 309–330

Long A J, Waller M P and Plater A J 2007 *Dungeness and Romney Marsh: barrier dynamics and marshland evolution*. Oxbow Books, Oxford

Long A J. and Hughes P 1995 Evolution of the Dungeness Foreland during the last 4000 years. *Marine Geology* 124, 253–271

Meisch C 2000 *Freshwater Ostracoda of Western and Central Europe*. Spektrum Akademischer Verlag. Heidelberg. ISBN 3 8274 1001 0.

Murray J W 2006 *Ecology and Applications of Benthic Foraminifera*. Cambridge University

Opus 2014 *Folkestone PAR's – Lydd MoD Range: ground investigation of the Environment Agency*. Unpublished Client report

Plater A J, Stupples P, Shaw J and Hemetsberger, S 2006 *Dungeness, SE England, UK: palaeomagnetic secular variation (PSV) dating and environmental magnetic properties of late Holocene marsh sediments*. English Heritage, Research Department Reports 48/2006

Plater A, Stupples P and Roberts H M 2007 hThe deposition history of the Dungeness Foreland. In Long A J, Waller M P and Plater A J (Eds) *Dungeness and Romney Marsh: Barrier dynamics and marshland evolution*. Oxford, Oxbow, 108–154

Plater A J, Stupples P and Roberts H M 2009 Evidence of episodic coastal change during the late Holocene: the Dungeness barrier complex, SE England. *Geomorphology* 104, 47–58

Reimer P J, Austin, W E N, Bard E, Bayliss A, Blackwell P G, Bronk Ramsey C, Butzin M, Cheng H, Edwards R L, Friedrich M, Grootes P M, Guilderson T P, Hajdas I, Heaton T J, Hogg A G, Hughen K A, Kromer B, Manning S W, Muscheler R, Palmer J G, Pearson C, van der Plicht J, Reimer R W, Richards D A, Scott E M, Southon J R, Turney C S M, Wacker L, Adolphi F, Büntgen U, Capano M, Fahrni S M, Fogtmann-Schulz A, Friedrich R, Köhler P, Kudsk S, Miyake F, Olsen J, Reinig F, Sakamoto M, Sookdeo A and Talamo S 2020 The IntCal20 Northern Hemisphere Radiocarbon Age Calibration Curve (0–55 cal kBP), *Radiocarbon* 62(4), 725–757

Rippon S 2021 Battling the tides: the Severn Estuary wetlands during the prehistoric, Roman and medieval periods. In *Martin's Environment: Archaeology and Landscapes. Papers in honour of Professor Martin Bell on the occasion of his retirement and 68th birthday*, Oxford, Archaeopress, 9–17

Roberts, H M and Plater A J 2007 Reconstruction of Holocene foreland progradation using optically stimulated luminescence (OSL) dating: an example from Dungeness, UK. *The Holocene* 17, 495–505

Spencer C D and Woodland W 2002 Palaeoenvironmental changes during the last 4000 years at Scotney Marsh, Romney Marsh, UK. In Long A J, Hipkins S and Clarke H (Eds) *Romney Marsh: coastal and landscape change through the ages*. Oxford, Oxford University Committee for Archaeology Monograph No. 56, 58–74

Spencer C D, Plater A J, Long A J 1998 Rapid coastal change during the mid- to late-Holocene: the record of barrier estuary sedimentation in the Romney Marsh region, south-east England. *The Holocene* 8, 143–163

Stace C 1997 *New Flora of the British Isles* (2nd edition). Cambridge: Cambridge University Press

Van de Noort R and Ellis S (Eds) 2000 *Wetland Heritage of the Hull Valley*. Humber Wetlands Project, University of Hull

Waller M P, Burrin P J and Marlow A 1988. Flandrian sedimentation and palaeoenvironments in Pett Level, the Brede and Lower Rother valleys and Walland Marsh. In: Eddison J, Green C. (Eds.) *Romney Marsh: evolution, occupation, reclamation*. Oxford University Committee for Archaeology, Oxford, No. 24, pp. 3–30

Waller M P and Schofield J E 2007 Mid to late Holocene vegetation and land-use history in the Weald of south-eastern England: multiple pollen profiles from the Rye area*. Vegetation History and Archaeobotany* 16, 367–84

Waller M P and Long A J 2003. Holocene coastal evolution and sea-level change on the southern coast of England: a review. *Journal of Quaternary Science* 18, 251–359

Waller M P, Schofield J E and Long A J 2007 The chrono and biostratigraphy of the natural pits on Dungeness Foreland; implications for foreland evolution and vegetation history. In Long A, Waller M and Plater A (Eds) *The late-Holocene evolution of the Romney Marsh/Dungeness Foreland depositional complex, UK*. English Heritage Monograph Series, Oxbow, 155–188

Werff A Van Der and Huls H 1957-1974 *Diatomeenflora van Nederland*, 10 volumes

Wessex Archaeology 2018 *Lydd Ranges, Folkstone to Cliff End Strategy: desk-based review of geoarchaeological and palaeoenvironmental potential*. Report Ref.: 203181.01

Wessex Archaeology 2021 *Lydd Ranges Sea Defence Scheme: written scheme of investigation for geoarchaeological works*. Report Ref.: 241350.01

Wessex Archaeology 2022 *Lydd Ranges Sea Defence Scheme: Geoarchaeological Survey*. Report Ref.: 241532.01

Witkowski A Lange-Bertalot H and Metzeltin D 2000 Diatom Flora of Marine Coasts I. Iconographia Diatomologica. *Annotated Diatom Micrographs* Ed. by H. Lange-Bertalot Vol. 7. A.R.G. Gantner Verlag. Koeltz Scientific Books. Königstein, Germany pp 92

APPENDIX 1: SPECIALIST REPORTS

University of Gloucestershire

Luminescence dating laboratory

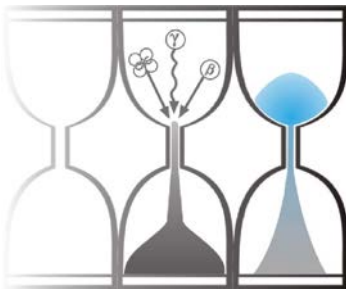

Optical dating of sediments: Lydd Ranges, IK

to

Dr Alex Brown

Wessex Archaeology

Analysis & Reporting, Prof. P.S. Toms
Sample Preparation & Measurement, Dr J.C. Wood
02 December 2022

Contents

Scope of Report

This is a standard report of the Luminescence dating laboratory, University of Gloucestershire. In large part, the document summarises the processes, diagnostics and data drawn upon to deliver Table 1. A conclusion on the analytical validity of each sample's optical age estimate is expressed in Table 2; where there are caveats, the reader is directed to the relevant section of the report that explains the issue further in general terms.

Copyright Notice

Field Code	Lab Code	Overburden (m)	Grain size (μm)	Moisture content (%)	Ge γ-spectrometry (*ex situ*)			α D_r ($Gy.ka^{-1}$)	β D_r ($Gy.ka^{-1}$)	γ D_r ($Gy.ka^{-1}$)	Cosmic D_r ($Gy.ka^{-1}$)	Preheat (ºC for 10s)	Low Dose Repeat Ratio	High Dose Repeat Ratio	Post-IR OSL Ratio
					K (%)	Th (ppm)	U (ppm)								
BHC01 - 4.92-5.02 m	GL22003	4.95	5-15	29	2.00 ± 0.12	10.65 ± 0.63	1.60 ± 0.13	0.31 ± 0.03	1.38 ± 0.10	0.80 ± 0.05	0.10 ± 0.01	220	1.01 ± 0.19	0.98 ± 0.13	0.89 ± 0.17
BHC01 - 6.10-6.20 m	GL22004	6.15	5-15	29	1.25 ± 0.09	7.85 ± 0.51	1.59 ± 0.13	0.26 ± 0.02	0.94 ± 0.07	0.59 ± 0.04	0.08 ± 0.01	220	1.12 ± 0.24	1.08 ± 0.17	0.95 ± 0.20
BHC01 - 6.85-6.95 m	GL22005	6.90	5-15	30	1.52 ± 0.10	9.61 ± 0.59	1.77 ± 0.14	0.30 ± 0.02	1.11 ± 0.08	0.69 ± 0.04	0.07 ± 0.01	260	0.93 ± 0.16	0.96 ± 0.13	1.01 ± 0.18
BHC01 - 7.02-7.12 m	GL22006	7.08	5-15	29	1.26 ± 0.09	8.61 ± 0.55	1.55 ± 0.12	0.27 ± 0.02	0.96 ± 00.07	0.61 ± 0.04	0.07 ± 0.01	240	0.97 ± 0.18	0.96 ± 0.13	0.96 ± 0.18
BHG01 - 4.65-4.75 m	GL22007	4.69	5-15	29	1.47 ± 0.10	8.97 ± 0.56	1.55 ± 0.13	0.27 ± 0.02	1.07 ± 0.08	0.65 ± 0.04	0.10 ± 0.01	240	0.93 ± 0.17	1.07 ± 0.14	1.00 ± 0.17
BHG01 - 5.20-5.30 m	GL22008	5.25	5-15	29	1.28 ± 0.10	9.30 ± 0.57	1.53 ± 0.13	0.28 ± 0.02	0.98 ± 0.07	0.63 ± 0.04	0.09 ± 0.01	220	1.01 ± 0.13	0.99 ± 0.10	0.96 ± 0.12
BHG01 - 5.80-5.90 m	GL22009	5.76	180-250	21	1.07 ± 0.08	6.13 ± 0.44	1.18 ± 0.12	-	0.79 ± 0.09	0.53 ± 0.07	0.08 ± 0.01	220	0.96 ± 0.05	1.00 ± 0.04	0.95 ± 0.05
BHG01 - 6.45-6.55 m	GL22010	6.48	5-15	30	1.45 ± 0.10	8.95 ± 0.55	1.60 ± 0.13	0.27 ± 0.02	1.05 ± 0.08	0.65 ± 0.04	0.08 ± 0.01	240	0.89 ± 0.11	1.01 ± 0.10	0.90 ± 0.12

Field Code	Lab Code	Total D_r ($Gy.ka^{-1}$)	D_e (Gy)	Age (ka)	Date
BHC01 - 4.92-5.02 m	GL22003	2.59 ± 0.12	1.20 ± 0.09	0.46 ± 0.04 (0.04)	AD 1520 – AD 1600
BHC01 - 6.10-6.20 m	GL22004	1.87 ± 0.08	5.59 ± 0.34	2.99 ± 0.23 (0.19)	1200 BC – 740 BC
BHC01 - 6.85-6.95 m	GL22005	2.17 ± 0.10	7.32 ± 0.41	3.37 ± 0.24 (0.20)	1580 BC – 1100 BC
BHC01 - 7.02-7.12 m	GL22006	1.90 ± 0.09	5.48 ± 0.30	2.88 ± 0.20 (0.16)	1060 BC – 660 BC
BHG01 - 4.65-4.75 m	GL22007	2.10 ± 0.09	4.43 ± 0.30	2.11 ± 0.17 (0.15)	260 BC – AD 80
BHG01 - 5.20-5.30 m	GL22008	1.98 ± 0.09	4.99 ± 0.23	2.52 ± 0.16 (0.13)	660 BC – 340 BC
BHG01 - 5.80-5.90 m	GL22009	1.40 ± 0.10	3.48 ± 0.14	2.48 ± 0.20 (0.16)	650 BC – 260 BC
BHG01 - 6.45-6.55 m	GL22010	2.05 ± 0.09	4.91 ± 0.25	2.40 ± 0.16 (0.13)	540 BC – 220 BC

Table 1 D_r, D_e and Age data of submitted samples located at c. 51°N, 1°E, 5m. Age estimates expressed relative to year of sampling. Uncertainties in age are quoted at 1σ confidence, are based on analytical errors and reflect combined systematic and experimental variability and (in parenthesis) experimental variability alone (see 6.0). **Blue** indicates samples with accepted age estimates, **red**, age estimates with caveats (see Table 2).

Generic considerations	Field Code	Lab Code	Sample specific considerations
Absence of *in situ* γ spectrometry data (see section 4.0)	BHC01 - 4.92-5.02 m	GL22003	None
	BHC01 - 6.10-6.20 m	GL22004	None
	BHC01 - 6.85-6.95 m	GL22005	None
	BHC01 - 7.02-7.12 m	GL22006	None
	BHG01 - 4.65-4.75 m	GL22007	None
	BHG01 - 5.20-5.30 m	GL22008	None
	BHG01 - 5.80-5.90 m	GL22009	None
	BHG01 - 6.45-6.55 m	GL22010	None

Table 2 Analytical validity of sample suite age estimates and caveats for consideration

1.0 Mechanisms and principles

Upon exposure to ionising radiation, electrons within the crystal lattice of insulating minerals are displaced from their atomic orbits. Whilst this dislocation is momentary for most electrons, a portion of charge is redistributed to meta-stable sites (traps) within the crystal lattice. In the absence of significant optical and thermal stimuli, this charge can be stored for extensive periods. The quantity of charge relocation and storage relates to the magnitude and period of irradiation. When the lattice is optically or thermally stimulated, charge is evicted from traps and may return to a vacant orbit position (hole). Upon recombination with a hole, an electron's energy can be dissipated in the form of light generating crystal luminescence providing a measure of dose absorption.

Herein, quartz is segregated for dating. The utility of this minerogenic dosimeter lies in the stability of its datable signal over the mid to late Quaternary period, predicted through isothermal decay studies (e.g. Smith *et al.*, 1990; retention lifetime 630 Ma at 20°C) and evidenced by optical age estimates concordant with independent chronological controls (e.g. Murray and Olley, 2002). This stability is in contrast to the anomalous fading of comparable signals commonly observed for other ubiquitous sedimentary minerals such as feldspar and zircon (Wintle, 1973; Templer, 1985; Spooner, 1993)

Optical age estimates of sedimentation (Huntley *et al.*, 1985) are premised upon reduction of the minerogenic time dependent signal (Optically Stimulated Luminescence, OSL) to zero through exposure to sunlight and, once buried, signal reformulation by absorption of litho- and cosmogenic radiation. The signal accumulated post burial acts as a dosimeter recording total dose absorption, converting to a chronometer by estimating the rate of dose absorption quantified through the assay of radioactivity in the surrounding lithology and streaming from the cosmos.

$$\text{Age} = \frac{\text{Mean Equivalent Dose } (D_e, \text{ Gy})}{\text{Mean Dose Rate } (D_r, \text{ Gy.ka}^{-1})}$$

Aitken (1998) and Bøtter-Jensen *et al*. (2003) offer a detailed review of optical dating.

2.0 Sample Preparation

Eight sediment samples were collected within cores and submitted as core lengths for Optical dating. To preclude optical erosion of the datable signal prior to measurement, all samples were opened and prepared under controlled laboratory illumination provided by Encapsulite RB-10 (red) filters. To isolate that material potentially exposed to daylight during sampling, sediment located within 10 mm of each core face was removed.

The remaining sample was dried and then sieved. The fine sand and fine silt fractions were segregated and subjected to acid and alkaline digestion (10% HCl, 15% H_2O_2) to attain removal of carbonate and organic components respectively. For fine sand fractions, a further acid digestion in HF (40%, 60 mins) was used to etch the outer 10-15 μm layer affected by α radiation and degrade each samples' feldspar content. During HF treatment, continuous magnetic stirring was used to effect isotropic etching of grains. 10% HCl was then added to remove acid soluble fluorides. Each sample was dried, resieved and quartz isolated from the remaining heavy mineral fraction using a sodium polytungstate density separation at 2.68g.cm^{-3}. Twelve 8 mm multi-grain aliquots (*c*. 3-6 mg) of quartz from each sample were then mounted on aluminium discs for determination of D_e values.

Fine silt sized quartz, along with other mineral grains of varying density and size, was extracted by sample sedimentation in acetone (<15 μm in 2 min 20 s, >5 μm in 21 mins at 20ºC). Feldspars and amorphous silica were then removed from this fraction through acid digestion (35% H_2SiF_6 for 2 weeks, Jackson *et al*., 1976; Berger *et al*., 1980). Following

addition of 10% HCl to remove acid soluble fluorides, grains degraded to <5 μm as a result of acid treatment were removed by acetone sedimentation. Twelve multi-grain aliquots (ca. 1.5 mg) were then mounted on aluminium discs for D_e evaluation.

All drying was conducted at 40°C to prevent thermal erosion of the signal. All acids and alkalis were Analar grade. All dilutions (removing toxic-corrosive and non-minerogenic luminescence-bearing substances) were conducted with distilled water to prevent signal contamination by extraneous particles.

3.0 Acquisition and accuracy of D_e value

All minerals naturally exhibit marked inter-sample variability in luminescence per unit dose (sensitivity). Therefore, the estimation of D_e acquired since burial requires calibration of the natural signal using known amounts of laboratory dose. D_e values were quantified using a single-aliquot regenerative-dose (SAR) protocol (Murray and Wintle 2000; 2003) facilitated by a Risø TL-DA-15 irradiation-stimulation-detection system (Markey *et al*., 1997; Bøtter-Jensen *et al*., 1999). Within this apparatus, optical signal stimulation is provided by an assembly of blue diodes (5 packs of 6 Nichia NSPB500S), filtered to 470±80 nm conveying 15 $mW.cm^{-2}$ using a 3 mm Schott GG420 positioned in front of each diode pack. Infrared (IR) stimulation, provided by 6 IR diodes (Telefunken TSHA 6203) stimulating at 875±80nm delivering ~40 $mW.cm^{-2}$, was used to indicate the presence of contaminant feldspars (Hütt *et al*., 1988). Stimulated photon emissions from quartz aliquots are in the ultraviolet (UV) range and were filtered from stimulating photons by 7.5 mm HOYA U-340 glass and detected by an EMI 9235QA photomultiplier fitted with a blue-green sensitive bialkali photocathode. Aliquot irradiation was conducted using a 1.48 GBq $^{90}Sr/^{90}Y$ β source calibrated for multi-grain aliquots of 5-15 and 180-250 μm quartz against the 'Hotspot 800' ^{60}Co γ source located at the National Physical Laboratory (NPL), UK.

SAR by definition evaluates D_e through measuring the natural signal (Fig. 1) of a single aliquot and then regenerating that aliquot's signal by using known laboratory doses to enable calibration. For each aliquot, five different regenerative-doses were administered so as to image dose response. D_e values for each aliquot were then interpolated, and associated counting and fitting errors calculated, by way of exponential plus linear regression (Fig. 1). Weighted (geometric) mean D_e values were calculated, given sufficient mass, from 12 aliquots using the central age model outlined by Galbraith *et al*. (1999) and are quoted at 1σ confidence (Table 1). The accuracy with which D_e equates to total absorbed dose and that dose absorbed since burial was assessed. The former can be considered a function of laboratory factors, the latter, one of environmental issues. Diagnostics were deployed to estimate the influence of these factors and criteria instituted to optimise the accuracy of D_e values.

3.1 Laboratory Factors

3.1.1 Feldspar contamination

The propensity of feldspar signals to fade and underestimate age, coupled with their higher sensitivity relative to quartz makes it imperative to quantify feldspar contamination. At room temperature, feldspars generate a signal (IRSL; Fig. 1) upon exposure to IR whereas quartz does not. The signal from feldspars contributing to OSL can be depleted by prior exposure to IR. For all aliquots the contribution of any remaining feldspars was estimated from the OSL IR depletion ratio (Duller, 2003). The influence of IR depletion on the OSL signal can be illustrated by comparing the regenerated post-IR OSL D_e with the applied regenerative-dose. If the addition to OSL by feldspars is insignificant, then the repeat dose ratio of OSL to post-IR OSL should be statistically consistent with unity (Table 1). If any aliquots do not fulfil this criterion, then the sample age estimate should be accepted tentatively. The source of feldspar contamination is rarely rooted in sample preparation; it predominantly results from the occurrence of feldspars as inclusions within quartz.

3.1.2 Preheating

Preheating aliquots between irradiation and optical stimulation is necessary to ensure comparability between natural and laboratory-induced signals. However, the multiple irradiation and preheating steps that are required to define single-aliquot regenerative-dose response leads to signal sensitisation, rendering calibration of the natural signal inaccurate. The SAR protocol (Murray and Wintle, 2000; 2003) enables this sensitisation to be monitored and corrected using a test dose, here set at 5 Gy preheated to 220°C for 10s, to track signal sensitivity between irradiation-preheat steps. However, the accuracy of sensitisation correction for both natural and laboratory signals can be preheat dependent.

The Dose Recovery test was used to assess the optimal preheat temperature for accurate correction and calibration of the time dependent signal. Dose Recovery (Fig. 2) attempts to quantify the combined effects of thermal transfer and sensitisation on the natural signal, using a precise lab dose to simulate natural dose. The ratio between the applied dose and recovered D_e value should be statistically concordant with unity. For this diagnostic, 6 aliquots were each assigned a 10 s preheat between 180°C and 280°C.

That preheat treatment fulfilling the criterion of accuracy within the Dose Recovery test was selected to generate the final D_e value from a further 12 aliquots. Further thermal treatments, prescribed by Murray and Wintle (2000; 2003), were applied to optimise accuracy and precision. Optical stimulation occurred at 125ºC in order to minimise effects associated with photo-transferred thermoluminescence and maximise signal to noise ratios. Inter-cycle optical stimulation was conducted at 280ºC to minimise recuperation.

3.1.3 Irradiation

For all samples having D_e values in excess of 100 Gy, matters of signal saturation and laboratory irradiation effects are of concern. With regards the former, the rate of signal accumulation generally adheres to a saturating exponential form and it is this that limits the precision and accuracy of D_e values for samples having absorbed large doses. For such samples, the functional range of D_e interpolation by SAR has been verified up to 600 Gy by Pawley *et al*. (2010). Age estimates based on D_e values exceeding this value should be accepted tentatively.

3.1.4 Internal consistency

Abanico plots (Dietze *et al*., 2016) are used to illustrate inter-aliquot D_e variability (Fig. 3). D_e values are standardised relative to the central D_e value for natural signals and are described as overdispersed when >5% lie beyond $\pm 2\sigma$ of the standardising value; resulting from a heterogeneous absorption of burial dose and/or response to the SAR protocol. For multi-grain aliquots, overdispersion of natural signals does not necessarily imply inaccuracy. However where overdispersion is observed for regenerated signals, the efficacy of sensitivity correction may be problematic. Murray and Wintle (2000; 2003) suggest repeat dose ratios (Table 1) offer a measure of SAR protocol success, whereby ratios ranging across 0.9-1.1 represent effective sensitivity correction. However, this variation of repeat dose ratios in the high-dose region can have a significant impact on D_e interpolation.

3.2 Environmental factors

3.2.1 Incomplete zeroing

Post-burial OSL signals residual of pre-burial dose absorption can result where pre-burial sunlight exposure is limited in spectrum, intensity and/or period, leading to age overestimation. This effect is particularly acute for material eroded and redeposited sub-aqueously (Olley *et al*., 1998, 1999; Wallinga, 2002) and exposed to a burial dose of <20 Gy (e.g. Olley *et al*., 2004), has some influence in sub-aerial contexts but is rarely of consequence where aerial transport has occurred. Within single-aliquot regenerative-dose optical dating there are two diagnostics of partial resetting (or bleaching); signal analysis (Agersnap-Larsen *et al*., 2000; Bailey *et al*., 2003) and inter-aliquot D_e distribution studies (Murray *et al*., 1995).

Within this study, signal analysis was used to quantify the change in D_e value with respect to optical stimulation time for multi-grain aliquots. This exploits the existence of traps within minerogenic dosimeters that bleach with different efficiency for a given wavelength of light to verify partial bleaching. D_e (t) plots (Fig. 4; Bailey *et al*., 2003) are constructed from separate integrals of signal decay as laboratory optical stimulation progresses. A statistically significant increase in natural D_e (t) is indicative of partial bleaching assuming three conditions are fulfilled. Firstly, that a statistically significant increase in D_e (t) is observed when partial bleaching is simulated within the laboratory. Secondly, that there is no significant rise in D_e (t) when full bleaching is simulated. Finally, there should be no significant augmentation in D_e (t) when zero dose is simulated. Where partial bleaching is detected, the age derived from the sample should be considered a maximum estimate only. However, the utility of signal analysis is strongly dependent upon a samples pre-burial experience of sunlight's spectrum and its residual to post-burial signal ratio. Given in the majority of cases, the spectral exposure history of a deposit is uncertain, the absence of an increase in natural D_e (t) does not necessarily testify to the absence of partial bleaching.

Where requested and feasible, the insensitivities of multi-grain single-aliquot signal analysis may be circumvented by inter-aliquot D_e distribution studies. This analysis uses aliquots of single sand grains to quantify inter-grain D_e distribution. At present, it is contended that asymmetric inter-grain D_e distributions are symptomatic of partial bleaching and/or pedoturbation (Murray *et al*., 1995; Olley *et al*., 1999; Olley *et al*., 2004; Bateman *et al*., 2003). For partial bleaching at least, it is further contended that the D_e acquired during burial is located in the minimum region of such ranges. The mean and breadth of this minimum region is the subject of current debate, as it is additionally influenced by heterogeneity in microdosimetry, variable inter-grain response to SAR and residual to post-burial signal ratios.

3.2.2 Turbation

As noted in section 3.1.1, the accuracy of sedimentation ages can further be controlled by post-burial trans-strata grain movements forced by pedo- or cryoturbation. Berger (2003) contends pedogenesis prompts a reduction in the apparent sedimentation age of parent material through bioturbation and illuviation of younger material from above and/or by biological recycling and resetting of the datable signal of surface material. Berger (2003) proposes that the chronological products of this remobilisation are A-horizon age estimates reflecting the cessation of pedogenic activity, Bc/C-horizon ages delimiting the maximum age for the initiation of pedogenesis with estimates obtained from Bt-horizons providing an intermediate age 'close to the age of cessation of soil development'. Singhvi et al. (2001), in contrast, suggest that B and C-horizons closely approximate the age of the parent material, the A-horizon, that of the 'soil forming episode'. Recent analyses of inter-aliquot D_e distributions have reinforced this complexity of interpreting burial age from pedoturbated deposits (Lombard *et al*., 2011; Gliganic *et al*., 2015; Jacobs *et al*., 2008; Bateman *et al*., 2007; Gliganic *et al*., 2016). At present there is no definitive post-sampling mechanism for the direct detection of and correction for post-burial sediment remobilisation. However, intervals of palaeosol evolution can be delimited by a maximum age derived from parent material and a minimum age obtained from a unit overlying the palaeosol. Inaccuracy forced by cryoturbation may be bidirectional, heaving older material upwards or drawing younger material downwards into the level to be dated. Cryogenic deformation of matrix-supported material is, typically, visible; sampling of such cryogenically-disturbed sediments can be avoided.

4.0 Acquisition and accuracy of D_r value

Lithogenic D_r values were defined through measurement of U, Th and K radionuclide concentration and conversion of these quantities into α, β and γ D_r values (Table 1). α and β contributions were estimated from sub-samples by laboratory-based γ spectrometry using an Ortec GEM-S high purity Ge coaxial detector system, calibrated using certified reference materials supplied by CANMET. γ dose rates can be estimated from *in situ* NaI gamma spectrometry or, where direct measurements are unavailable as in the present case, from laboratory-based Ge γ spectrometry. *In situ*

measurements reduce uncertainty relating to potential heterogeneity in the γ dose field surrounding each sample. The level of U disequilibrium was estimated by laboratory-based Ge γ spectrometry. Estimates of radionuclide concentration were converted into D_r values (Adamiec and Aitken, 1998), accounting for D_r modulation forced by grain size (Mejdahl, 1979), present moisture content (Zimmerman, 1971) and, where D_e values were generated from 5-15 μm quartz, reduced signal sensitivity to α radiation (a-value 0.050 $\pm$ 0.002). Cosmogenic D_r values were calculated on the basis of sample depth, geographical position and matrix density (Prescott and Hutton, 1994).

The spatiotemporal validity of D_r values can be considered a function of five variables. Firstly, age estimates devoid of *in situ* γ spectrometry data should be accepted tentatively if the sampled unit is heterogeneous in texture or if the sample is located within 300 mm of strata consisting of differing texture and/or mineralogy. However, where samples are obtained throughout a vertical profile, consistent values of γ D_r based solely on laboratory measurements may evidence the homogeneity of the γ field and hence accuracy of γ D_r values. Secondly, disequilibrium can force temporal instability in U and Th emissions. The impact of this infrequent phenomenon (Olley *et al*., 1996) upon age estimates is usually insignificant given their associated margins of error. However, for samples where this effect is pronounced (>50% disequilibrium between ^{238}U and ^{226}Ra; Fig. 5), the resulting age estimates should be accepted tentatively. Thirdly, pedogenically-induced variations in matrix composition of B and C-horizons, such as radionuclide and/or mineral remobilisation, may alter the rate of energy emission and/or absorption. If D_r is invariant through a dated profile and samples encompass primary parent material, then element mobility is likely limited in effect. Fourthly, spatiotemporal detractions from present moisture content are difficult to assess directly, requiring knowledge of the magnitude and timing of differing contents. However, the maximum influence of moisture content variations can be delimited by recalculating D_r for minimum (zero) and maximum (saturation) content. Finally, temporal alteration in the thickness of overburden alters cosmic D_r values. Cosmic D_r often forms a negligible portion of total D_r. It is possible to quantify the maximum influence of overburden flux by recalculating D_r for minimum (zero) and maximum (surface sample) cosmic D_r.

5.0 Estimation of Age

Ages reported in Table 1 provide an estimate of sediment burial period based on mean D_e and D_r values and their associated analytical uncertainties. Uncertainty in age estimates is reported as a product of systematic and experimental errors, with the magnitude of experimental errors alone shown in parenthesis (Table 1). Cumulative frequency plots indicate the inter-aliquot variability in age (Fig. 6). The maximum influence of temporal variations in D_r forced by minima-maxima in moisture content and overburden thickness is also illustrated in Fig. 6. Where uncertainty in these parameters exists this age range may prove instructive, however the combined extremes represented should not be construed as preferred age estimates. The analytical validity of each sample is presented in Table 2.

6.0 Analytical uncertainty

All errors are based upon analytical uncertainty and quoted at 1σ confidence. Error calculations account for the propagation of systematic and/or experimental (random) errors associated with D_e and D_r values.

For D_e values, systematic errors are confined to laboratory β source calibration. Uncertainty in this respect is that combined from the delivery of the calibrating γ dose (1.2%; NPL, pers. comm.), the conversion of this dose for SiO_2 using the respective mass energy-absorption coefficient (2%; Hubbell, 1982) and experimental error, totalling 3.5%. Mass attenuation and bremsstrahlung losses during γ dose delivery are considered negligible. Experimental errors relate to D_e interpolation using sensitisation corrected dose responses. Natural and regenerated sensitisation corrected dose points (S_i) were quantified by,

$$S_i = (D_i - x.L_i) / (d_i - x.L_i) \quad \textbf{Eq.1}$$

where D_i = Natural or regenerated OSL, initial 0.2 s

L_i = Background natural or regenerated OSL, final 5 s

d_i = Test dose OSL, initial 0.2 s

x = Scaling factor, 0.08

The error on each signal parameter is based on counting statistics, reflected by the square-root of measured values. The propagation of these errors within Eq. 1 generating σS_i follows the general formula given in Eq. 2. σS_i were then used to define fitting and interpolation errors within exponential plus linear regressions.

For D_r values, systematic errors accommodate uncertainty in radionuclide conversion factors (5%), β attenuation coefficients (5%), a-value (4%; derived from a systematic α source uncertainty of 3.5% and experimental error), matrix density (0.20 $g.cm^{-3}$), vertical thickness of sampled section (specific to sample collection device), saturation moisture content (3%), moisture content attenuation (2%) and burial moisture content (2.5%, unless direct evidence exists of the magnitude and period of differing content). Experimental errors are associated with radionuclide quantification for each sample by Ge gamma spectrometry.

The propagation of these errors through to age calculation was quantified using the expression,

$$\sigma y\,(\delta y/\delta x) = (\Sigma\,((\delta y/\delta x_n).\sigma x_n)^2)^{1/2} \quad \textbf{Eq. 2}$$

where y is a value equivalent to that function comprising terms x_n and where σy and σx_n are associated uncertainties.

Errors on age estimates are presented as combined systematic and experimental errors and experimental errors alone. The former (combined) error should be considered when comparing luminescence ages herein with independent chronometric controls. The latter assumes systematic errors are common to luminescence age estimates generated by means identical to those detailed herein and enable direct comparison with those estimates.

Fig. 1 Signal Calibration

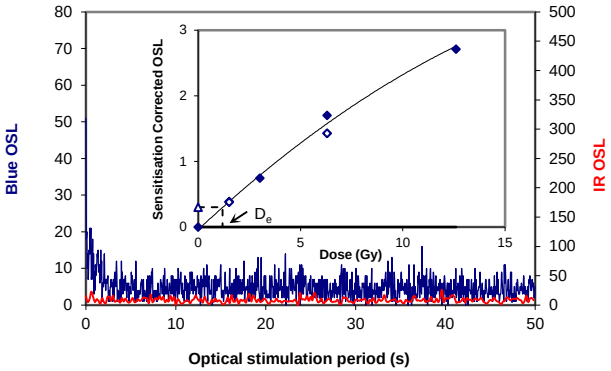

Fig. 2 Dose Recovery

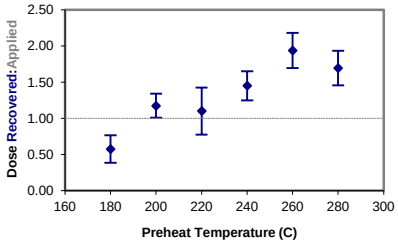

Fig. 4 Signal Analysis

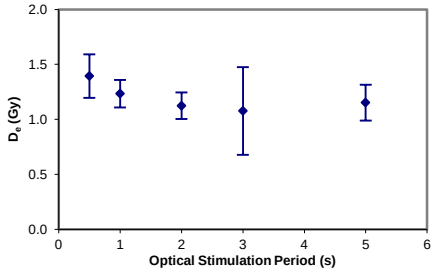

Fig. 3 Inter-aliquot D_e distribution

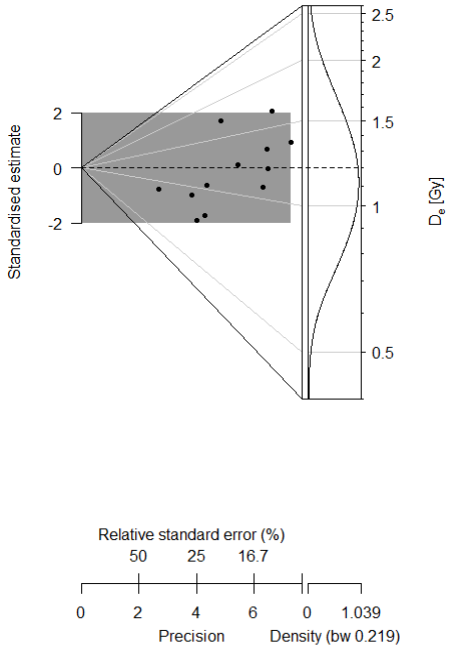

Fig. 5 U Decay Activity

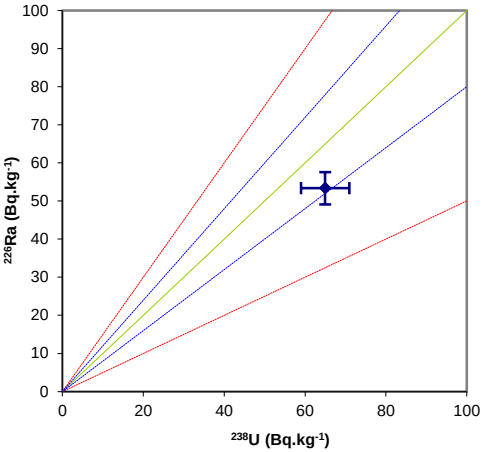

Fig. 6 Age Range

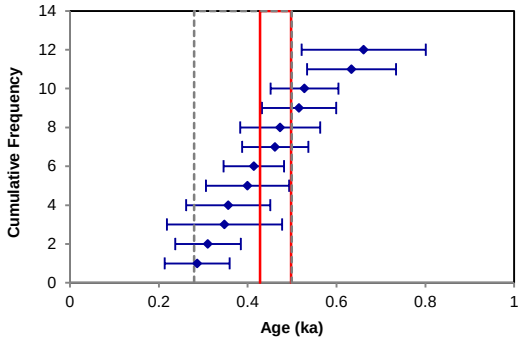

Fig. 1 Signal Calibration Natural blue and laboratory-induced infrared (IR) OSL signals. Detectable IR signal decays are diagnostic of feldspar contamination. Inset, the natural blue OSL signal (open triangle) of each aliquot is calibrated against known laboratory doses to yield equivalent dose (D_e) values. Repeats of low and high doses (open diamonds) illustrate the success of sensitivity correction.

Fig. 2 Dose Recovery The acquisition of D_e values is necessarily predicated upon thermal treatment of aliquots succeeding environmental and laboratory irradiation. The Dose Recovery test quantifies the combined effects of thermal transfer and sensitisation on the natural signal using a precise lab dose to simulate natural dose. Based on this an appropriate thermal treatment is selected to generate the final D_e value.

Fig. 3 Inter-aliquot D_e distribution Abanico plot of inter-aliquot statistical concordance in D_e values derived from **natural** irradiation. Discordant data (those points lying beyond ±2 standardised ln D_e) reflect heterogeneous dose absorption and/or inaccuracies in calibration.

Fig. 4 Signal Analysis Statistically significant increase in **natural** D_e value with signal stimulation period is indicative of a partially-bleached signal, provided a significant increase in D_e results from **simulated partial bleaching** followed by insignificant adjustment in D_e for simulated **zero** and **full bleach** conditions. Ages from such samples are considered maximum estimates. In the absence of a significant rise in D_e with stimulation time, simulated partial bleaching and zero/full bleach tests are not assessed.

Fig. 5 U Activity Statistical concordance (equilibrium) in the activities of the daughter radioisotope ^{226}Ra with its parent ^{238}U may signify the temporal stability of D_r emissions from these chains. Significant differences (disequilibrium; >50%) in activity indicate addition or removal of isotopes creating a time-dependent shift in D_r values and increased uncertainty in the accuracy of age estimates. A 20% disequilibrium marker is also shown.

Fig. 6 Age Range The Cumulative frequency plot indicates the inter-aliquot variability in age. It also shows the **mean age range**; an estimate of sediment burial period based on mean D_e and D_r values with associated analytical uncertainties. The **maximum influence** of temporal variations in D_r forced by minima-maxima variation in moisture content and overburden thickness is outlined and may prove instructive where there is uncertainty in these parameters. However the combined extremes represented should not be construed as preferred age estimates.

Sample: GL22003

Fig. 1 Signal Calibration

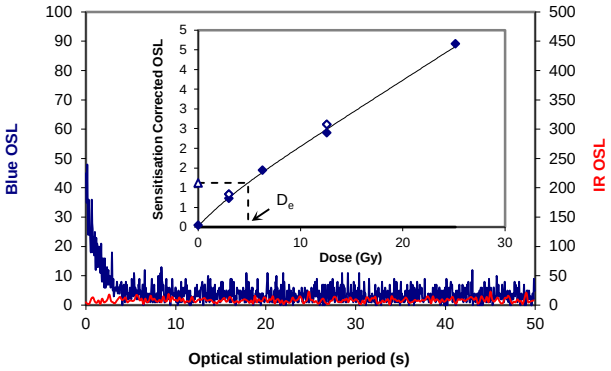

Fig. 1 Signal Calibration Natural blue and laboratory-induced infrared (IR) OSL signals. Detectable IR signal decays are diagnostic of feldspar contamination. Inset, the natural blue OSL signal (open triangle) of each aliquot is calibrated against known laboratory doses to yield equivalent dose (D_e) values. Repeats of low and high doses (open diamonds) illustrate the success of sensitivity correction.

Fig. 2 Dose Recovery The acquisition of D_e values is necessarily predicated upon thermal treatment of aliquots succeeding environmental and laboratory irradiation. The Dose Recovery test quantifies the combined effects of thermal transfer and sensitisation on the natural signal using a precise lab dose to simulate natural dose. Based on this an appropriate thermal treatment is selected to generate the final D_e value.

Fig. 3 Inter-aliquot D_e distribution Abanico plot of inter-aliquot statistical concordance in D_e values derived from **natural** irradiation. Discordant data (those points lying beyond ±2 standardised ln D_e) reflect heterogeneous dose absorption and/or inaccuracies in calibration.

Fig. 4 Signal Analysis Statistically significant increase in **natural** D_e value with signal stimulation period is indicative of a partially-bleached signal, provided a significant increase in D_e results from **simulated partial bleaching** followed by insignificant adjustment in D_e for simulated **zero** and **full bleach** conditions. Ages from such samples are considered maximum estimates. In the absence of a significant rise in D_e with stimulation time, simulated partial bleaching and zero/full bleach tests are not assessed.

Fig. 5 U Activity Statistical concordance (equilibrium) in the activities of the daughter radioisotope ^{226}Ra with its parent ^{238}U may signify the temporal stability of D_r emissions from these chains. Significant differences (disequilibrium; >50%) in activity indicate addition or removal of isotopes creating a time-dependent shift in D_r values and increased uncertainty in the accuracy of age estimates. A 20% disequilibrium marker is also shown.

Fig. 6 Age Range The Cumulative frequency plot indicates the inter-aliquot variability in age. It also shows the **mean age range**; an estimate of sediment burial period based on mean D_e and D_r values with associated analytical uncertainties. The **maximum influence** of temporal variations in D_r forced by minima-maxima variation in moisture content and overburden thickness is outlined and may prove instructive where there is uncertainty in these parameters. However the combined extremes represented should not be construed as preferred age estimates.

Fig. 2 Dose Recovery

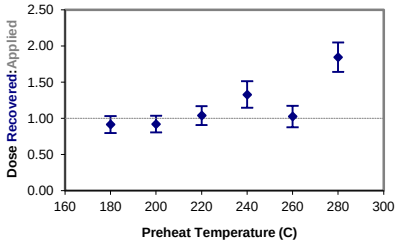

Fig. 3 Inter-aliquot D_e distribution

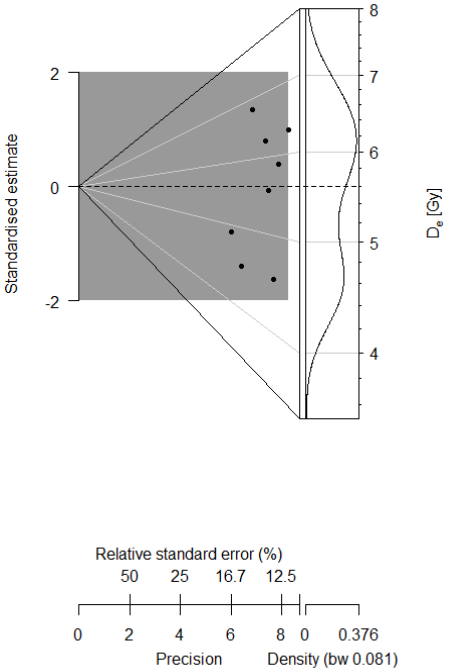

Fig. 4 Signal Analysis

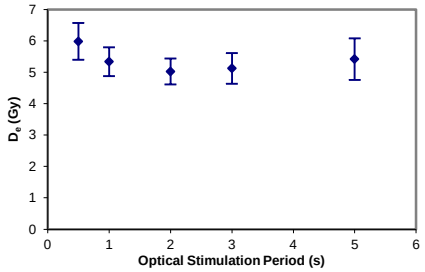

Fig. 5 U Decay Activity

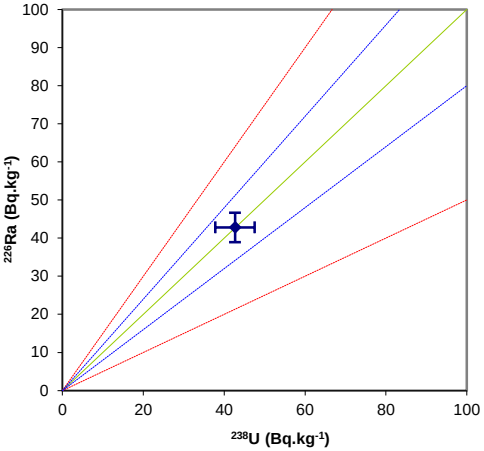

Fig. 6 Age Range

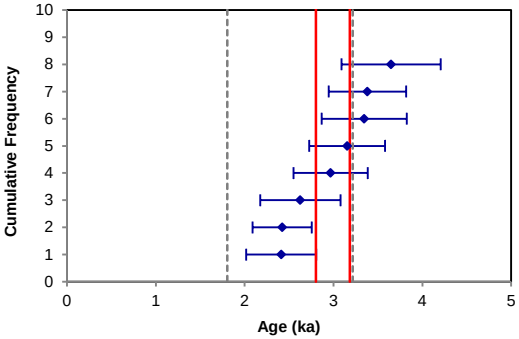

Fig. 1 Signal Calibration

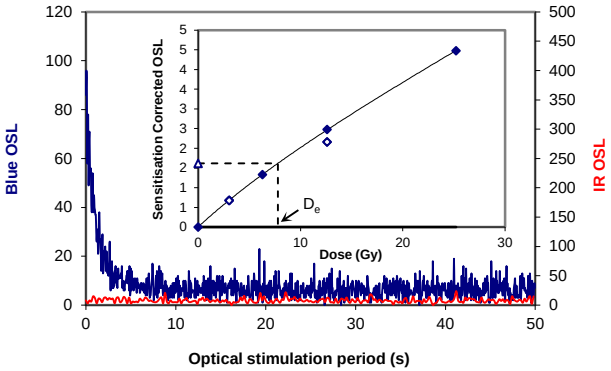

Fig. 1 Signal Calibration Natural blue and laboratory-induced infrared (IR) OSL signals. Detectable IR signal decays are diagnostic of feldspar contamination. Inset, the natural blue OSL signal (open triangle) of each aliquot is calibrated against known laboratory doses to yield equivalent dose (D_e) values. Repeats of low and high doses (open diamonds) illustrate the success of sensitivity correction.

Fig. 2 Dose Recovery The acquisition of D_e values is necessarily predicated upon thermal treatment of aliquots succeeding environmental and laboratory irradiation. The Dose Recovery test quantifies the combined effects of thermal transfer and sensitisation on the natural signal using a precise lab dose to simulate natural dose. Based on this an appropriate thermal treatment is selected to generate the final D_e value.

Fig. 3 Inter-aliquot D_e distribution Abanico plot of inter-aliquot statistical concordance in D_e values derived from **natural** irradiation. Discordant data (those points lying beyond ±2 standardised ln D_e) reflect heterogeneous dose absorption and/or inaccuracies in calibration.

Fig. 4 Signal Analysis Statistically significant increase in **natural** D_e value with signal stimulation period is indicative of a partially-bleached signal, provided a significant increase in D_e results from **simulated partial bleaching** followed by insignificant adjustment in D_e for simulated **zero** and **full bleach** conditions. Ages from such samples are considered maximum estimates. In the absence of a significant rise in D_e with stimulation time, simulated partial bleaching and zero/full bleach tests are not assessed.

Fig. 5 U Activity Statistical concordance (equilibrium) in the activities of the daughter radioisotope ^{226}Ra with its parent ^{238}U may signify the temporal stability of D_r emissions from these chains. Significant differences (disequilibrium; >50%) in activity indicate addition or removal of isotopes creating a time-dependent shift in D_r values and increased uncertainty in the accuracy of age estimates. A 20% disequilibrium marker is also shown.

Fig. 6 Age Range The Cumulative frequency plot indicates the inter-aliquot variability in age. It also shows the **mean age range**; an estimate of sediment burial period based on mean D_e and D_r values with associated analytical uncertainties. The **maximum influence** of temporal variations in D_r forced by minima-maxima variation in moisture content and overburden thickness is outlined and may prove instructive where there is uncertainty in these parameters. However the combined extremes represented should not be construed as preferred age estimates.

Fig. 2 Dose Recovery

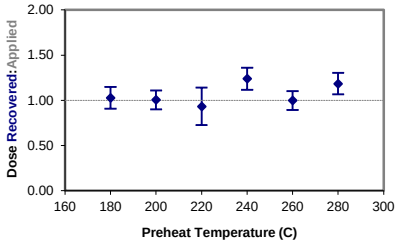

Fig. 3 Inter-aliquot D_e distribution

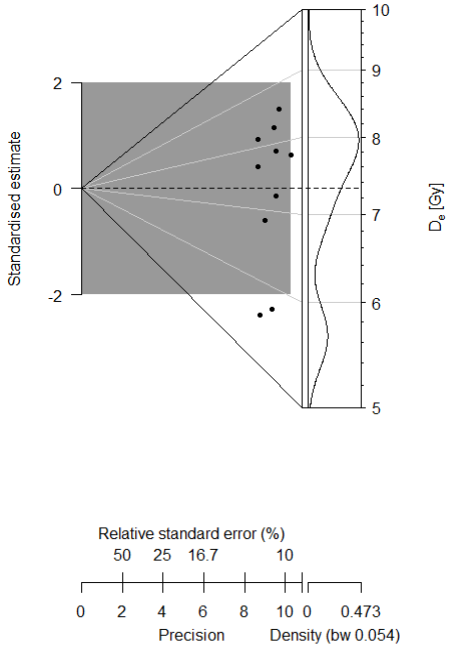

Fig. 4 Signal Analysis

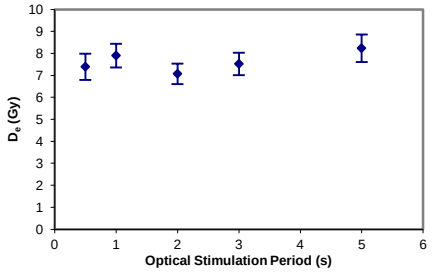

Fig. 5 U Decay Activity

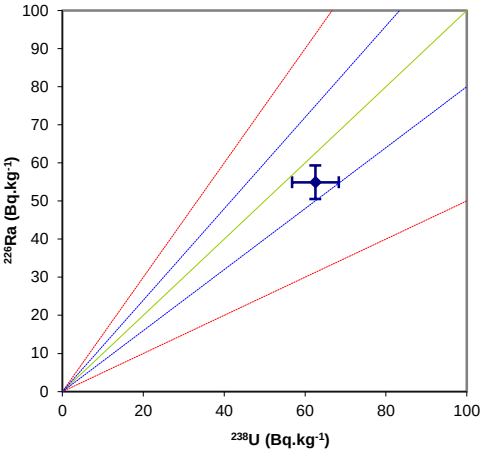

Fig. 6 Age Range

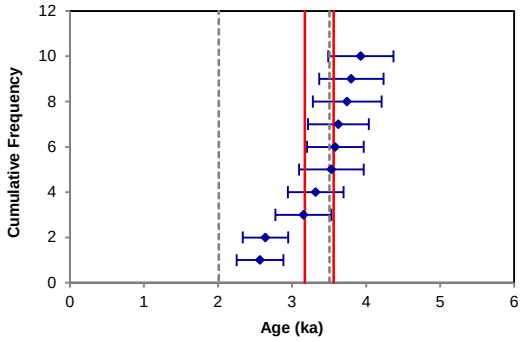

Fig. 1 Signal Calibration

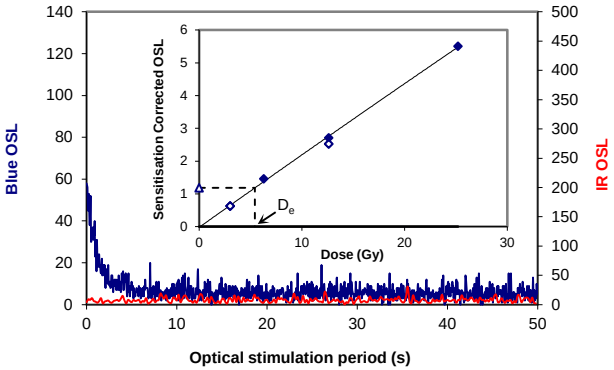

Fig. 2 Dose Recovery

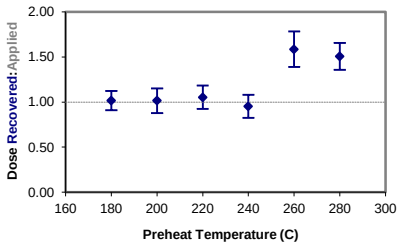

Fig. 4 Signal Analysis

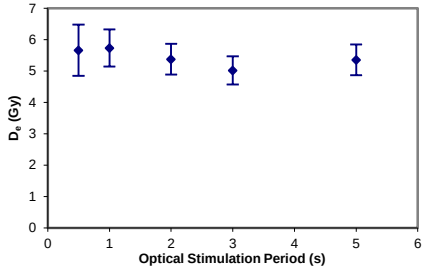

Fig. 3 Inter-aliquot D_e distribution

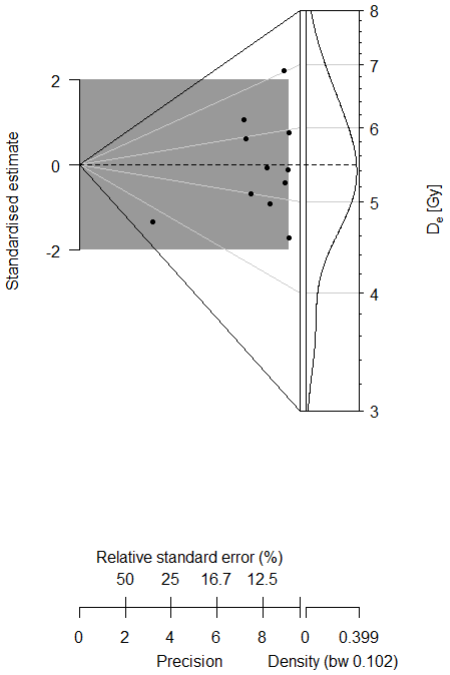

Fig. 5 U Decay Activity

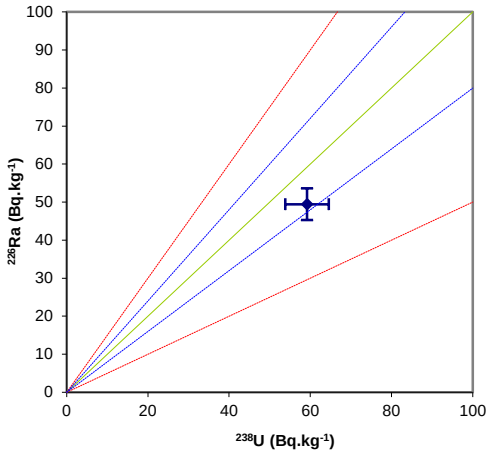

Fig. 6 Age Range

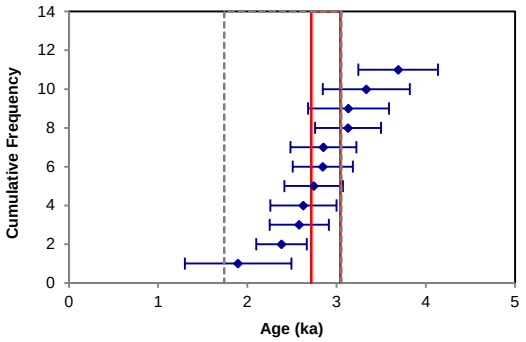

Fig. 1 Signal Calibration Natural blue and laboratory-induced infrared (IR) OSL signals. Detectable IR signal decays are diagnostic of feldspar contamination. Inset, the natural blue OSL signal (open triangle) of each aliquot is calibrated against known laboratory doses to yield equivalent dose (D_e) values. Repeats of low and high doses (open diamonds) illustrate the success of sensitivity correction.

Fig. 2 Dose Recovery The acquisition of D_e values is necessarily predicated upon thermal treatment of aliquots succeeding environmental and laboratory irradiation. The Dose Recovery test quantifies the combined effects of thermal transfer and sensitisation on the natural signal using a precise lab dose to simulate natural dose. Based on this an appropriate thermal treatment is selected to generate the final D_e value.

Fig. 3 Inter-aliquot D_e distribution Abanico plot of inter-aliquot statistical concordance in D_e values derived from **natural** irradiation. Discordant data (those points lying beyond ±2 standardised ln D_e) reflect heterogeneous dose absorption and/or inaccuracies in calibration.

Fig. 4 Signal Analysis Statistically significant increase in **natural** D_e value with signal stimulation period is indicative of a partially-bleached signal, provided a significant increase in D_e results from **simulated partial bleaching** followed by insignificant adjustment in D_e for simulated **zero** and **full bleach** conditions. Ages from such samples are considered maximum estimates. In the absence of a significant rise in D_e with stimulation time, simulated partial bleaching and zero/full bleach tests are not assessed.

Fig. 5 U Activity Statistical concordance (equilibrium) in the activities of the daughter radioisotope ^{226}Ra with its parent ^{238}U may signify the temporal stability of D_r emissions from these chains. Significant differences (disequilibrium; >50%) in activity indicate addition or removal of isotopes creating a time-dependent shift in D_r values and increased uncertainty in the accuracy of age estimates. A 20% disequilibrium marker is also shown.

Fig. 6 Age Range The Cumulative frequency plot indicates the inter-aliquot variability in age. It also shows the **mean age range**; an estimate of sediment burial period based on mean D_e and D_r values with associated analytical uncertainties. The **maximum influence** of temporal variations in D_r forced by minima-maxima variation in moisture content and overburden thickness is outlined and may prove instructive where there is uncertainty in these parameters. However the combined extremes represented should not be construed as preferred age estimates.

Sample: GL22006

Fig. 1 Signal Calibration

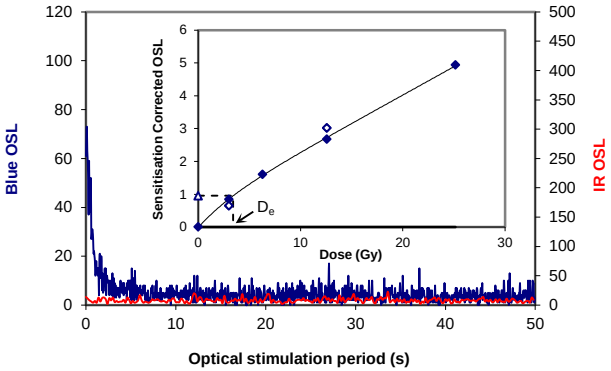

Fig. 2 Dose Recovery

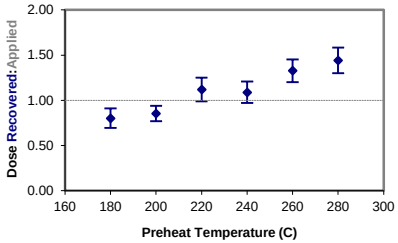

Fig. 4 Signal Analysis

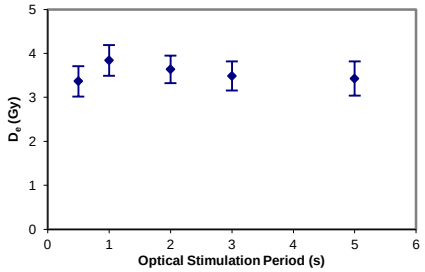

Fig. 3 Inter-aliquot D_e distribution

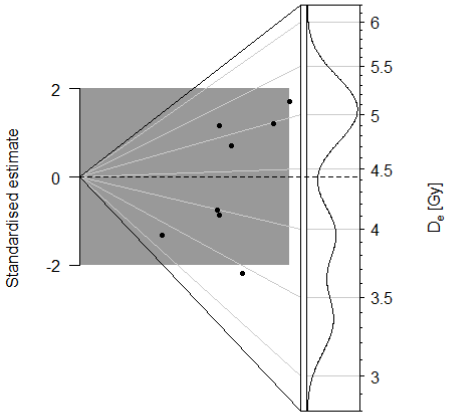

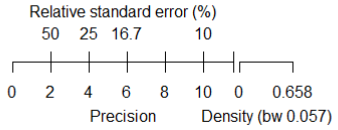

Fig. 5 U Decay Activity

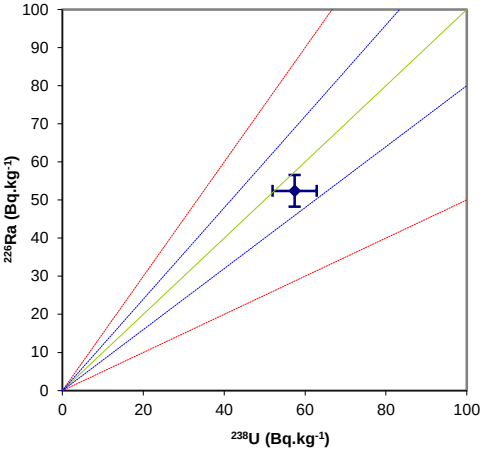

Fig. 6 Age Range

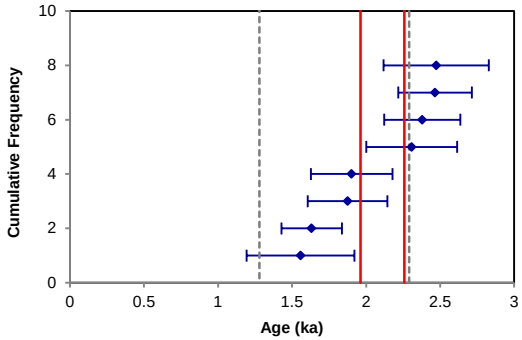

Fig. 1 Signal Calibration Natural blue and laboratory-induced infrared (IR) OSL signals. Detectable IR signal decays are diagnostic of feldspar contamination. Inset, the natural blue OSL signal (open triangle) of each aliquot is calibrated against known laboratory doses to yield equivalent dose (D_e) values. Repeats of low and high doses (open diamonds) illustrate the success of sensitivity correction.

Fig. 2 Dose Recovery The acquisition of D_e values is necessarily predicated upon thermal treatment of aliquots succeeding environmental and laboratory irradiation. The Dose Recovery test quantifies the combined effects of thermal transfer and sensitisation on the natural signal using a precise lab dose to simulate natural dose. Based on this an appropriate thermal treatment is selected to generate the final D_e value.

Fig. 3 Inter-aliquot D_e distribution Abanico plot of inter-aliquot statistical concordance in D_e values derived from **natural** irradiation. Discordant data (those points lying beyond ±2 standardised ln D_e) reflect heterogeneous dose absorption and/or inaccuracies in calibration.

Fig. 4 Signal Analysis Statistically significant increase in **natural** D_e value with signal stimulation period is indicative of a partially-bleached signal, provided a significant increase in D_e results from **simulated partial bleaching** followed by insignificant adjustment in D_e for simulated **zero** and **full bleach** conditions. Ages from such samples are considered maximum estimates. In the absence of a significant rise in D_e with stimulation time, simulated partial bleaching and zero/full bleach tests are not assessed.

Fig. 5 U Activity Statistical concordance (equilibrium) in the activities of the daughter radioisotope ^{226}Ra with its parent ^{238}U may signify the temporal stability of D_r emissions from these chains. Significant differences (disequilibrium; >50%) in activity indicate addition or removal of isotopes creating a time-dependent shift in D_r values and increased uncertainty in the accuracy of age estimates. A 20% disequilibrium marker is also shown.

Fig. 6 Age Range The Cumulative frequency plot indicates the inter-aliquot variability in age. It also shows the **mean age range**; an estimate of sediment burial period based on mean D_e and D_r values with associated analytical uncertainties. The **maximum influence** of temporal variations in D_r forced by minima-maxima variation in moisture content and overburden thickness is outlined and may prove instructive where there is uncertainty in these parameters. However the combined extremes represented should not be construed as preferred age estimates.

Sample: GL22007

Fig. 1 Signal Calibration

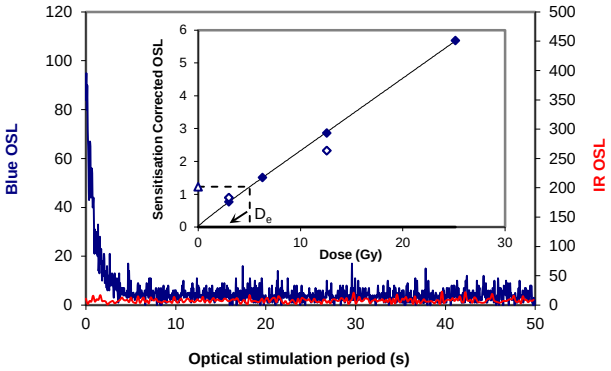

Fig. 2 Dose Recovery

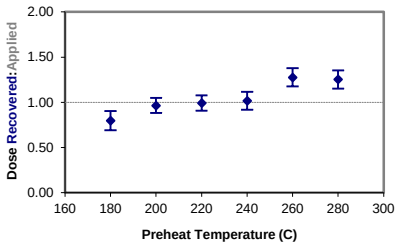

Fig. 4 Signal Analysis

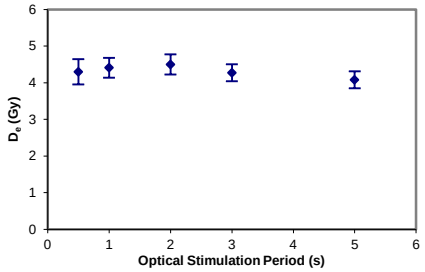

Fig. 3 Inter-aliquot D_e distribution

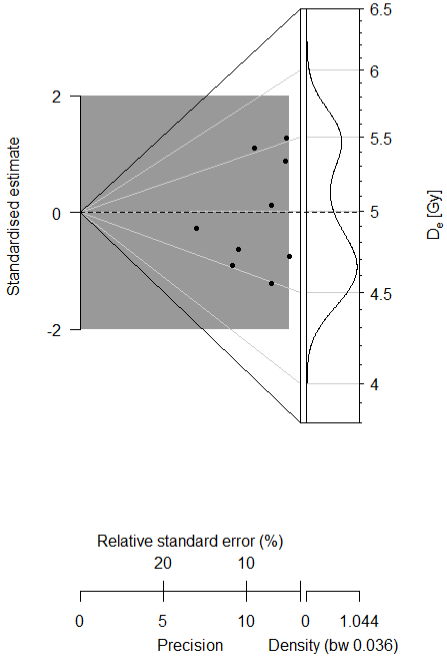

Fig. 5 U Decay Activity

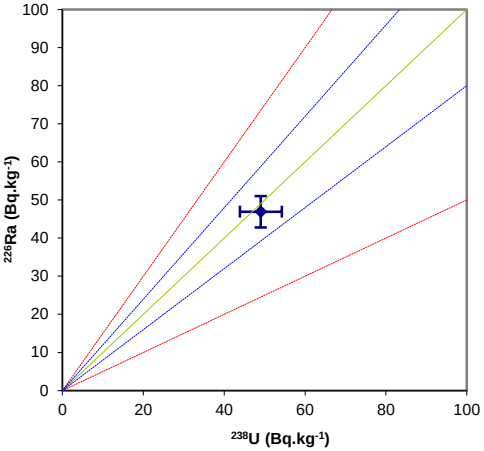

Fig. 6 Age Range

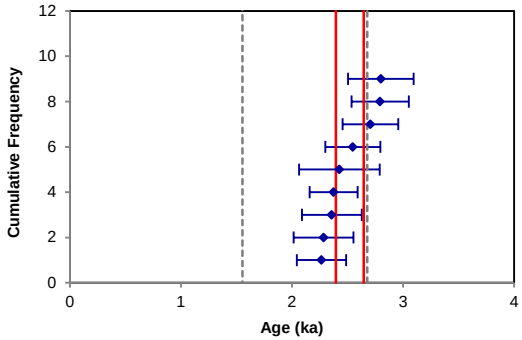

Fig. 1 Signal Calibration Natural blue and laboratory-induced infrared (IR) OSL signals. Detectable IR signal decays are diagnostic of feldspar contamination. Inset, the natural blue OSL signal (open triangle) of each aliquot is calibrated against known laboratory doses to yield equivalent dose (D_e) values. Repeats of low and high doses (open diamonds) illustrate the success of sensitivity correction.

Fig. 2 Dose Recovery The acquisition of D_e values is necessarily predicated upon thermal treatment of aliquots succeeding environmental and laboratory irradiation. The Dose Recovery test quantifies the combined effects of thermal transfer and sensitisation on the natural signal using a precise lab dose to simulate natural dose. Based on this an appropriate thermal treatment is selected to generate the final D_e value.

Fig. 3 Inter-aliquot D_e distribution Abanico plot of inter-aliquot statistical concordance in D_e values derived from **natural** irradiation. Discordant data (those points lying beyond **±2 standardised ln D_e**) reflect heterogeneous dose absorption and/or inaccuracies in calibration.

Fig. 4 Signal Analysis Statistically significant increase in **natural** D_e value with signal stimulation period is indicative of a partially-bleached signal, provided a significant increase in D_e results from **simulated partial bleaching** followed by insignificant adjustment in D_e for simulated **zero** and **full bleach** conditions. Ages from such samples are considered maximum estimates. In the absence of a significant rise in D_e with stimulation time, simulated partial bleaching and zero/full bleach tests are not assessed.

Fig. 5 U Activity Statistical concordance (equilibrium) in the activities of the daughter radioisotope ^{226}Ra with its parent ^{238}U may signify the temporal stability of D_r emissions from these chains. Significant differences (disequilibrium; >50%) in activity indicate addition or removal of isotopes creating a time-dependent shift in D_r values and increased uncertainty in the accuracy of age estimates. A 20% disequilibrium marker is also shown.

Fig. 6 Age Range The Cumulative frequency plot indicates the inter-aliquot variability in age. It also shows the **mean age range**; an estimate of sediment burial period based on mean D_e and D_r values with associated analytical uncertainties. The **maximum influence** of temporal variations in D_r forced by minima-maxima variation in moisture content and overburden thickness is outlined and may prove instructive where there is uncertainty in these parameters. However the combined extremes represented should not be construed as preferred age estimates.

Fig. 1 Signal Calibration

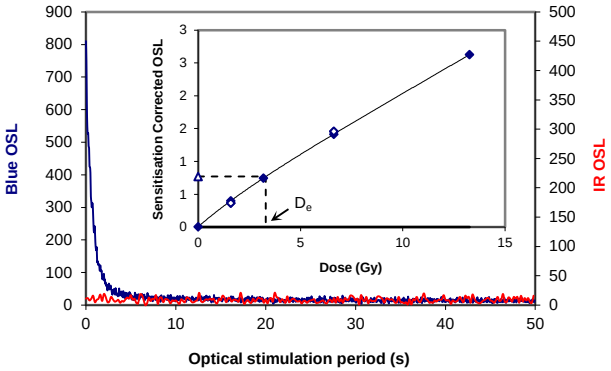

Fig. 2 Dose Recovery

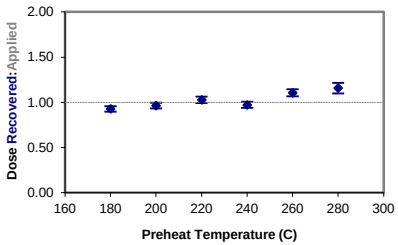

Fig. 4 Signal Analysis

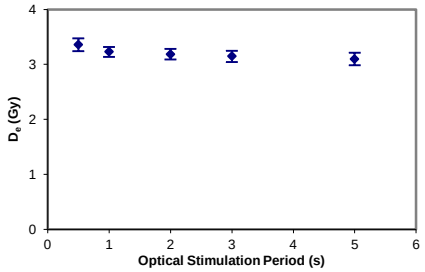

Fig. 3 Inter-aliquot D_e distribution

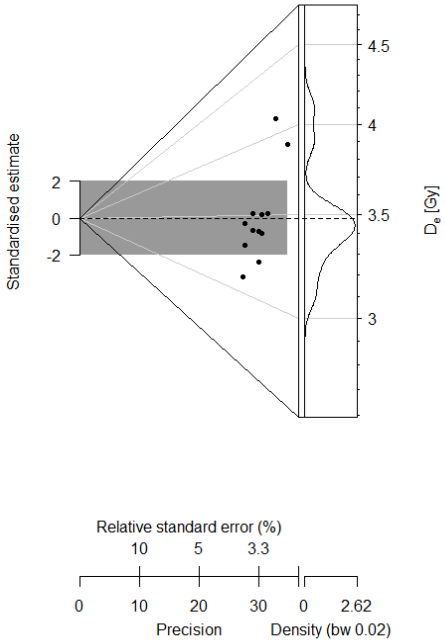

Fig. 5 U Decay Activity

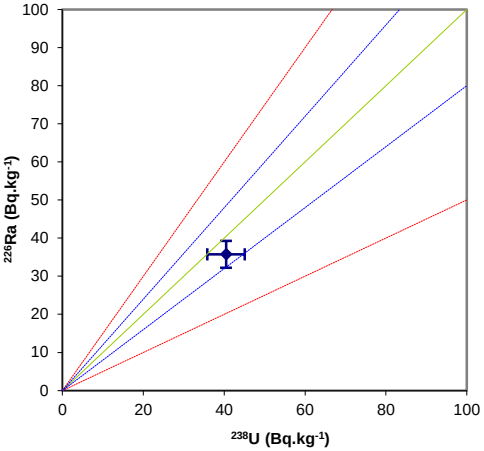

Fig. 6 Age Range

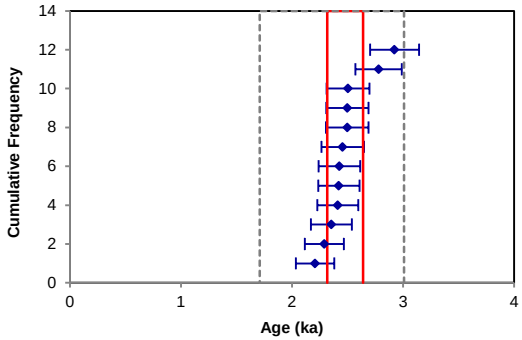

Fig. 1 Signal Calibration Natural blue and laboratory-induced infrared (IR) OSL signals. Detectable IR signal decays are diagnostic of feldspar contamination. Inset, the natural blue OSL signal (open triangle) of each aliquot is calibrated against known laboratory doses to yield equivalent dose (D_e) values. Repeats of low and high doses (open diamonds) illustrate the success of sensitivity correction.

Fig. 2 Dose Recovery The acquisition of D_e values is necessarily predicated upon thermal treatment of aliquots succeeding environmental and laboratory irradiation. The Dose Recovery test quantifies the combined effects of thermal transfer and sensitisation on the natural signal using a precise lab dose to simulate natural dose. Based on this an appropriate thermal treatment is selected to generate the final D_e value.

Fig. 3 Inter-aliquot D_e distribution Abanico plot of inter-aliquot statistical concordance in D_e values derived from **natural** irradiation. Discordant data (those points lying beyond **±2 standardised ln D_e**) reflect heterogeneous dose absorption and/or inaccuracies in calibration.

Fig. 4 Signal Analysis Statistically significant increase in **natural** D_e value with signal stimulation period is indicative of a partially-bleached signal, provided a significant increase in D_e results from **simulated partial bleaching** followed by insignificant adjustment in D_e for simulated **zero** and **full bleach** conditions. Ages from such samples are considered maximum estimates. In the absence of a significant rise in D_e with stimulation time, simulated partial bleaching and zero/full bleach tests are not assessed.

Fig. 5 U Activity Statistical concordance (equilibrium) in the activities of the daughter radioisotope ^{226}Ra with its parent ^{238}U may signify the temporal stability of D_r emissions from these chains. Significant differences (disequilibrium; >50%) in activity indicate addition or removal of isotopes creating a time-dependent shift in D_r values and increased uncertainty in the accuracy of age estimates. A 20% disequilibrium marker is also shown.

Fig. 6 Age Range The Cumulative frequency plot indicates the inter-aliquot variability in age. It also shows the **mean age range**; an estimate of sediment burial period based on mean D_e and D_r values with associated analytical uncertainties. The **maximum influence** of temporal variations in D_r forced by minima-maxima variation in moisture content and overburden thickness is outlined and may prove instructive where there is uncertainty in these parameters. However the combined extremes represented should not be construed as preferred age estimates.

Sample: GL22009

Fig. 1 Signal Calibration

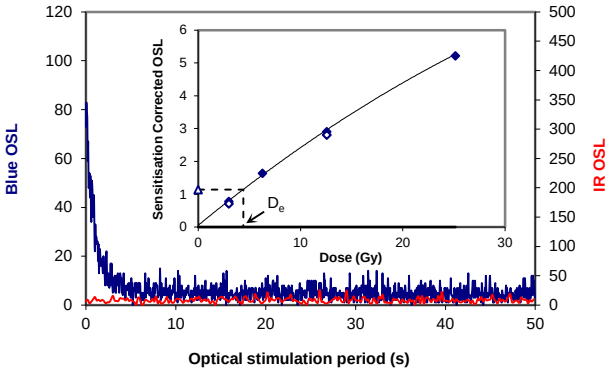

Fig. 2 Dose Recovery

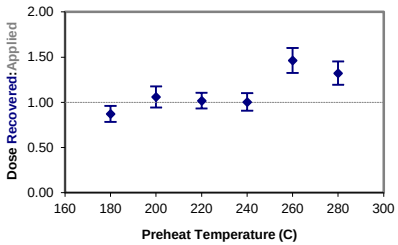

Fig. 4 Signal Analysis

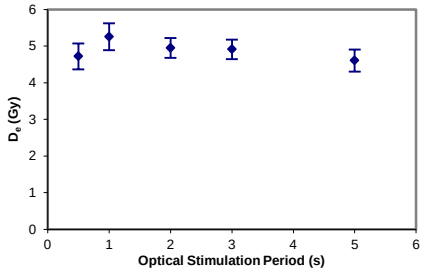

Fig. 3 Inter-aliquot D_e distribution

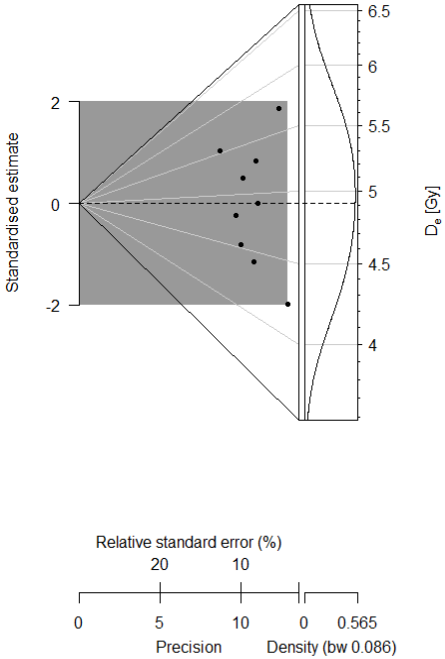

Fig. 5 U Decay Activity

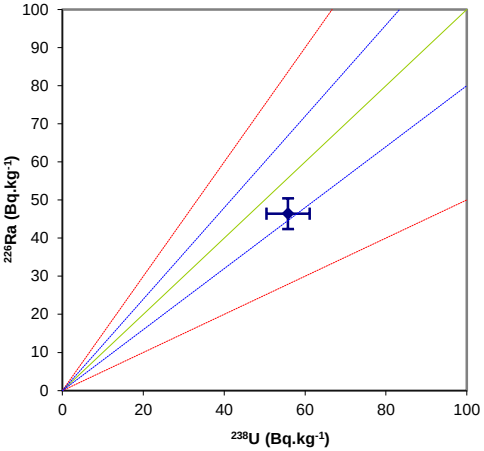

Fig. 6 Age Range

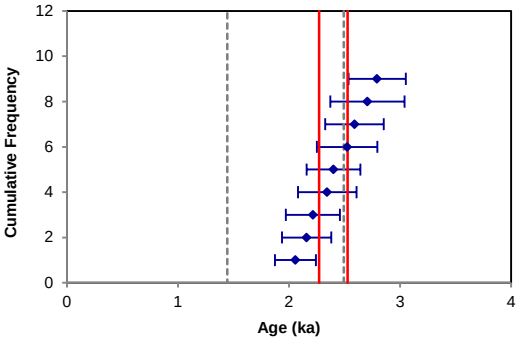

Fig. 1 Signal Calibration Natural blue and laboratory-induced infrared (IR) OSL signals. Detectable IR signal decays are diagnostic of feldspar contamination. Inset, the natural blue OSL signal (open triangle) of each aliquot is calibrated against known laboratory doses to yield equivalent dose (D_e) values. Repeats of low and high doses (open diamonds) illustrate the success of sensitivity correction.

Fig. 2 Dose Recovery The acquisition of D_e values is necessarily predicated upon thermal treatment of aliquots succeeding environmental and laboratory irradiation. The Dose Recovery test quantifies the combined effects of thermal transfer and sensitisation on the natural signal using a precise lab dose to simulate natural dose. Based on this an appropriate thermal treatment is selected to generate the final D_e value.

Fig. 3 Inter-aliquot D_e distribution Abanico plot of inter-aliquot statistical concordance in D_e values derived from **natural** irradiation. Discordant data (those points lying beyond ±2 standardised ln D_e) reflect heterogeneous dose absorption and/or inaccuracies in calibration.

Fig. 4 Signal Analysis Statistically significant increase in **natural** D_e value with signal stimulation period is indicative of a partially-bleached signal, provided a significant increase in D_e results from **simulated partial bleaching** followed by insignificant adjustment in D_e for simulated **zero** and **full bleach** conditions. Ages from such samples are considered maximum estimates. In the absence of a significant rise in D_e with stimulation time, simulated partial bleaching and zero/full bleach tests are not assessed.

Fig. 5 U Activity Statistical concordance (equilibrium) in the activities of the daughter radioisotope ^{226}Ra with its parent ^{238}U may signify the temporal stability of D_r emissions from these chains. Significant differences (disequilibrium; >50%) in activity indicate addition or removal of isotopes creating a time-dependent shift in D_r values and increased uncertainty in the accuracy of age estimates. A 20% disequilibrium marker is also shown.

Fig. 6 Age Range The Cumulative frequency plot indicates the inter-aliquot variability in age. It also shows the **mean age range**; an estimate of sediment burial period based on mean D_e and D_r values with associated analytical uncertainties. The **maximum influence** of temporal variations in D_r forced by minima-maxima variation in moisture content and overburden thickness is outlined and may prove instructive where there is uncertainty in these parameters. However the combined extremes represented should not be construed as preferred age estimates.

Sample: GL22010

References

Adamiec, G. and Aitken, M.J. (1998) Dose-rate conversion factors: new data. *Ancient TL*, 16, 37-50.

Agersnap-Larsen, N., Bulur, E., Bøtter-Jensen, L. and McKeever, S.W.S. (2000) Use of the LM-OSL technique for the detection of partial bleaching in quartz. *Radiation Measurements*, 32, 419-425.

Aitken, M. J. (1998) An introduction to optical dating: the dating of Quaternary sediments by the use of photon-stimulated luminescence. Oxford University Press.

Bailey, R.M., Singarayer, J.S. , Ward, S. and Stokes, S. (2003) Identification of partial resetting using D_e as a function of illumination time. *Radiation Measurements*, 37, 511-518.

Bateman, M.D., Frederick, C.D., Jaiswal, M.K., Singhvi, A.K. (2003) Investigations into the potential effects of pedoturbation on luminescence dating. *Quaternary Science Reviews*, 22, 1169-1176.

Bateman, M.D., Boulter, C.H., Carr, A.S., Frederick, C.D., Peter, D. and Wilder, M. (2007) Detecting post-depositional sediment disturbance in sandy deposits using optical luminescence. *Quaternary Geochronology*, 2, 57-64.

Berger, G.W. (2003). Luminescence chronology of late Pleistocene loess-paleosol and tephra sequences near Fairbanks, Alaska. *Quaternary Research*, 60, 70-83.

Berger, G.W., Mulhern, P.J. and Huntley, D.J. (1980). Isolation of silt-sized quartz from sediments. *Ancient TL*, 11, 147-152.

Bøtter-Jensen, L., Mejdahl, V. and Murray, A.S. (1999) New light on OSL. *Quaternary Science Reviews*, 18, 303-310.

Bøtter-Jensen, L., McKeever, S.W.S. and Wintle, A.G. (2003) Optically Stimulated Luminescence Dosimetry. Elsevier, Amsterdam.

Dietze, M., Kreutzer, S., Burow, C., Fuchs, M.C., Fischer, M., Schmidt, C. (2016) The abanico plot: visualising chronometric data with individual standard errors. *Quaternary Geochronology*, 31, 1-7.

Duller, G.A.T (2003) Distinguishing quartz and feldspar in single grain luminescence measurements. *Radiation Measurements*, 37, 161-165.

Galbraith, R. F., Roberts, R. G., Laslett, G. M., Yoshida, H. and Olley, J. M. (1999) Optical dating of single and multiple grains of quartz from Jinmium rock shelter (northern Australia): Part I, Experimental design and statistical models. *Archaeometry*, 41, 339-364.

Gliganic, L.A., May, J.-H. and Cohen, T.J. (2015). All mixed up: using single-grain equivalent dose distributions to identify phases of pedogenic mixing on a dryland alluvial fan. *Quaternary International*, 362, 23-33.

Gliganic, L.A., Cohen, T.J., Slack, M. and Feathers, J.K. (2016) Sediment mixing in Aeolian sandsheets identified and quantified using single-grain optically stimulated luminescence. *Quaternary Geochronology*, 32, 53-66.

Huntley, D.J., Godfrey-Smith, D.I. and Thewalt, M.L.W. (1985) Optical dating of sediments. *Nature*, 313, 105-107.

Hubbell, J.H. (1982) Photon mass attenuation and energy-absorption coefficients from 1keV to 20MeV. *International Journal of Applied Radioisotopes*, 33, 1269-1290.

Hütt, G., Jaek, I. and Tchonka, J. (1988) Optical dating: K-feldspars optical response stimulation spectra. *Quaternary Science Reviews*, 7, 381-386.

Jackson, M.L., Sayin, M. and Clayton, R.N. (1976). Hexafluorosilicic acid regent modification for quartz isolation. *Soil Science Society of America Journal*, 40, 958-960.

Jacobs, A., Wintle, A.G., Duller, G.A.T, Roberts, R.G. and Wadley, L. (2008) New ages for the post-Howiesons Poort, late and finale middle stone age at Sibdu, South Africa. *Journal of Archaeological Science*, 35, 1790-1807.

Lombard, M., Wadley, L., Jacobs, Z., Mohapi, M. and Roberts, R.G. (2011) Still Bay and serrated points from the Umhlatuzana rock shelter, Kwazulu-Natal, South Africa. *Journal of Archaeological Science*, 37, 1773-1784.

Markey, B.G., Bøtter-Jensen, L., and Duller, G.A.T. (1997) A new flexible system for measuring thermally and optically stimulated luminescence. *Radiation Measurements*, 27, 83-89.

Mejdahl, V. (1979) Thermoluminescence dating: beta-dose attenuation in quartz grains. *Archaeometry*, 21, 61-72.

Murray, A.S. and Olley, J.M. (2002) Precision and accuracy in the Optically Stimulated Luminescence dating of sedimentary quartz: a status review. *Geochronometria*, 21, 1-16.

Murray, A.S. and Wintle, A.G. (2000) Luminescence dating of quartz using an improved single-aliquot regenerative-dose protocol. *Radiation Measurements*, 32, 57-73.

Murray, A.S. and Wintle, A.G. (2003) The single aliquot regenerative dose protocol: potential for improvements in reliability*. Radiation Measurements*, 37, 377-381.

Murray, A.S., Olley, J.M. and Caitcheon, G.G. (1995) Measurement of equivalent doses in quartz from contemporary water-lain sediments using optically stimulated luminescence*. Quaternary Science Reviews*, 14, 365-371.

Olley, J.M., Murray, A.S. and Roberts, R.G. (1996) The effects of disequilibria in the Uranium and Thorium decay chains on burial dose rates in fluvial sediments. *Quaternary Science Reviews*, 15, 751-760.

Olley, J.M., Caitcheon, G.G. and Murray, A.S. (1998) The distribution of apparent dose as determined by optically stimulated luminescence in small aliquots of fluvial quartz: implications for dating young sediments. *Quaternary Science Reviews*, 17, 1033-1040.

Olley, J.M., Caitcheon, G.G. and Roberts R.G. (1999) The origin of dose distributions in fluvial sediments, and the prospect of dating single grains from fluvial deposits using -optically stimulated luminescence. *Radiation Measurements,* 30**,** 207-217.

Olley, J.M., Pietsch, T. and Roberts, R.G. (2004) Optical dating of Holocene sediments from a variety of geomorphic settings using single grains of quartz. *Geomorphology*, 60, 337-358.

Pawley, S.M., Toms, P.S., Armitage, S.J., Rose, J. (2010) Quartz luminescence dating of Anglian Stage fluvial sediments: Comparison of SAR age estimates to the terrace chronology of the Middle Thames valley, UK. *Quaternary Geochronology*, 5, 569-582.

Prescott, J.R. and Hutton, J.T. (1994) Cosmic ray contributions to dose rates for luminescence and ESR dating: large depths and long-term time variations. *Radiation Measurements*, 23, 497-500.

Singhvi, A.K., Bluszcz, A.., Bateman, M.D., Someshwar Rao, M. (2001). Luminescence dating of loess-palaeosol sequences and coversands: methodological aspects and palaeoclimatic implications. *Earth Science Reviews*, 54, 193-211.

Smith, B.W., Rhodes, E.J., Stokes, S., Spooner, N.A. (1990) The optical dating of sediments using quartz. *Radiation Protection Dosimetry*, 34, 75-78.

Spooner, N.A. (1993) The validity of optical dating based on feldspar. Unpublished D.Phil. thesis, Oxford University.

Templer, R.H. (1985) The removal of anomalous fading in zircons*. Nuclear Tracks and Radiation Measurements*, 10, 531-537.

Wallinga, J. (2002) Optically stimulated luminescence dating of fluvial deposits: a review. *Boreas* 31, 303-322.

Wintle, A.G. (1973) Anomalous fading of thermoluminescence in mineral samples. *Nature*, 245, 143-144.

Zimmerman, D. W. (1971) Thermoluminescent dating using fine grains from pottery. *Archaeometry*, 13, 29-52.

UBANo	Sample ID	Material Type	^{14}C Age	±	F14C	±	mg Graphite
UBA-49060	241533_C01_5.83-5.85	Rubus sp. (Brambles) seed x 3	1905	25	0.7889	0.0024	0.821
UBA-49061	241533_HHWS-107_0.62-0.64	Salicaceae (willow/poplar) twig with bark on outer edge	1701	25	0.8091	0.0025	1.005
UBA-49062	241533_HHWS-107_0.77-0.79	Salicaceae - twig with bark and pith	1868	21	0.7925	0.0021	0.952

Inez Lopez-Doriga
Wessex Archaeology
Portway House
Old Sarum Park
Salisbury, Wiltshire SP4 6EB
England

^{14}CHRONO Centre
Queens University Belfast
42 Fitzwilliam Street
Belfast BT9 6AX
Northern Ireland

Radiocarbon Date Certificate

Laboratory Identification:	UBA-49060
Date of Measurement:	2022-11-16
Site:	Lydd Ranges
Sample ID:	241533_C01_5.83-5.85
Material Dated:	seed or nutshell
Pretreatment:	AAA
mg Graphite:	0.821
Submitted by:	Ines Lopez Doriga

Conventional ^{14}C Age:	1905±25 BP
Fraction corrected	using AMS $\delta^{13}C$

Inez Lopez-Doriga
Wessex Archaeology
Portway House
Old Sarum Park
Salisbury, Wiltshire SP4 6EB
England

^{14}CHRONO Centre
Queens University Belfast
42 Fitzwilliam Street
Belfast BT9 6AX
Northern Ireland

Radiocarbon Date Certificate

Laboratory Identification:	UBA-49061
Date of Measurement:	2022-11-16
Site:	Lydd Ranges
Sample ID:	241533_HHWS-107_0.62-0.64
Material Dated:	wood
Pretreatment:	AAA
mg Graphite:	1.005
Submitted by:	Ines Lopez Doriga

Conventional ^{14}C Age:	1701±25 BP
Fraction corrected	using AMS $\delta^{13}C$

Inez Lopez-Doriga
Wessex Archaeology
Portway House
Old Sarum Park
Salisbury, Wiltshire SP4 6EB
England

^{14}CHRONO Centre
Queens University Belfast
42 Fitzwilliam Street
Belfast BT9 6AX
Northern Ireland

Radiocarbon Date Certificate

Laboratory Identification:	UBA-49062
Date of Measurement:	2022-11-17
Site:	Lydd Ranges
Sample ID:	241533_HHWS-107_0.77-0.79
Material Dated:	wood
Pretreatment:	AAA
mg Graphite:	0.952
Submitted by:	Ines Lopez Doriga

Conventional ^{14}C Age:	1868±21 BP
Fraction corrected	using AMS $\delta^{13}C$

Marine samples will require re-calibration with the marine calibration curve

3

RADIOCARBON CALIBRATION PROGRAM*
CALIB REV8.2

*To be used in conjunction with:
Stuiver, M., and Reimer, P.J., 1993, Radiocarbon, 35, 215-230.

UBA-49060
49060
Radiocarbon Age BP 1905 +/- 25
Calibration data set: intcal20.14c # Reimer et al. 2020

% area enclosed	cal AD age ranges	relative area under probability distribution
68.3 (1 sigma)	cal AD 84- 95	0.140
	116- 169	0.648
	185- 203	0.212
95.4 (2 sigma)	cal AD 66- 212	1.000

Median Probability: 142

UBA-49061
49061
Radiocarbon Age BP 1701 +/- 25
Calibration data set: intcal20.14c # Reimer et al. 2020

% area enclosed	cal AD age ranges	relative area under probability distribution
68.3 (1 sigma)	cal AD 264- 273	0.135
	349- 404	0.865
95.4 (2 sigma)	cal AD 257- 282	0.191
	328- 415	0.809

Median Probability: 364

UBA-49062
49062
Radiocarbon Age BP 1868 +/- 21
Calibration data set: intcal20.14c # Reimer et al. 2020

% area enclosed	cal AD age ranges	relative area under probability distribution
68.3 (1 sigma)	cal AD 129- 144	0.205
	154- 194	0.584
	199- 213	0.212
95.4 (2 sigma)	cal AD 125- 230	1.000

Median Probability: 174

References for calibration datasets:
Reimer P, Austin WEN, Bard E, Bayliss A, Blackwell PG, Bronk Ramsey C, Butzin M
Edwards RL, Friedrich M, Grootes PM, Guilderson TP, Hajdas I, Heaton TJ, Hogg A
Kromer B, Manning SW, Muscheler R, Palmer JG, Pearson C, van der Plicht J, Reim
Richards DA, Scott EM, Southon JR, Turney CSM, Wacker L, Adolphi F, BÃ¼ntgen U,
Fahrni S, Fogtmann-Schulz A, Friedrich R, KÃ¶hler P, Kudsk S, Miyake F, Olsen J
Sakamoto M, Sookdeo A, Talamo S. 2020.
The IntCal20 Northern Hemisphere radiocarbon age calibration curve (0-55 cal kB
Radiocarbon 62. doi: 10.1017/RDC.2020.41.

Comments:
* This standard deviation (error) includes a lab error multiplier.
** 1 sigma = square root of (sample std. dev.^2 + curve std. dev.^2)
** 2 sigma = 2 x square root of (sample std. dev.^2 + curve std. dev.^2)
where ^2 = quantity squared.
[ ] = calibrated range impinges on end of calibration data set
0* represents a "negative" age BP
1955* or 1960* denote influence of nuclear testing C-14

NOTE: Cal ages and ranges are rounded to the nearest year which
may be too precise in many instances. Users are advised to

round results to the nearest 10 yr for samples with standard deviation in the radiocarbon age greater than 50 yr.

Posterior Probability Distributions

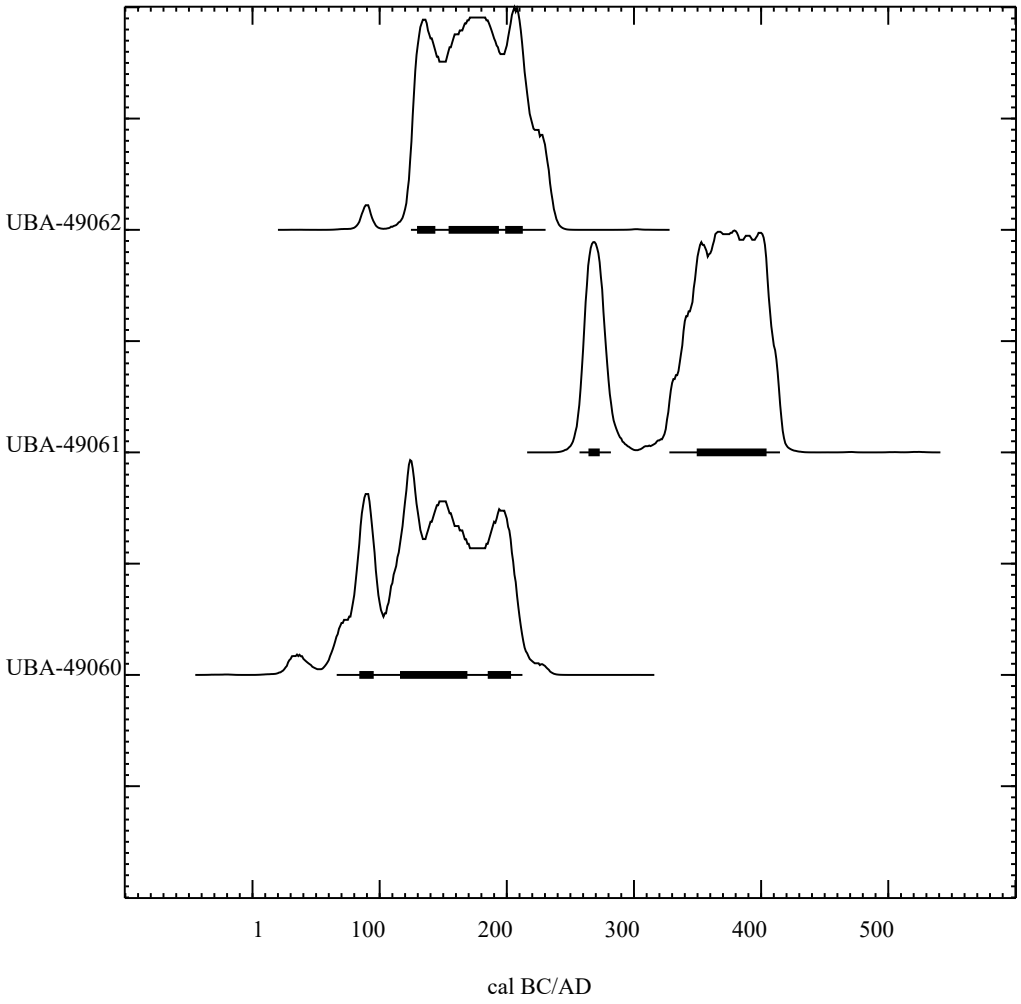

<>

1.1 Appendix 1: Environmental Data

Table 1: Assessment of the macrofossil evidence.

Borehole	Depth (mgbl)	Bulk volume (ml)	Sample composition
C01	5.83-5.85	100	Predominantly *Phragmites australis* rhizomes (some leaves) A**, degraded wood fragments C, plant macroremains A*: *Rubus* sp. C, *Cirsium* sp., Asteraceae, Chenopodiaceae, Apiaceae, *Ranunculus* subg. *Batrachium* C, *Carex* spp. B, *Juncus* sp. C, other - Foraminifera A, insects/beetles A
HHWS-107	0.62-0.64	70	Predominantly wood fragments inc. some twigs, *Phragmites australis* rhizomes and leaves A, moss stems with leaflets, plant macroremains A**: *Juncus* sp., *Carex* sp., Cyperaceae, *Rubus fruticosus, Sambucus nigra*, Lamiaceae (small-seeded), *Lemna* sp., *Eupatorium cannabinum, Ranunculus* cf. *flammula*, other - *Daphnia* sp. egg cases A, insects/beetles B, Bryozoa A
HHWS-107	0.77-0.79	60	Wood fragments inc. some twigs, *Phragmites australis* rhizomes and leaves A, monocot/herbaceous stems, moss stems with leaflets, plant macroremains: indet. seed

Key: C = 1–4, B = 9–5, A = 10–29, A* = 30–99, A** = 100–500.

Table 2: Radiocarbon dating results.

Lab. Ref	Core	Sample reference	Material	Radiocarbon Age (BP)	Calibrated date	Modelled date
					95% probability	
UBA-49060	C01	241533_C01_5.83-5.85	Waterlogged plant remains: *Rubus* sp. (brambles) seed x 3	1905±25	cal. AD 70–210	-
UBA-49061	HHWS-107	241533_HHWS-107_0.62-0.64	Wood (waterlogged): Salicaceae (willow/poplar) twig with bark on outer edge	1701±25	cal. AD 260–420	*cal. AD 255–415*
UBA-49062	HHWS-107	241533_HHWS-107_0.77-0.79	Wood (waterlogged): Salicaceae - twig with bark and pith (2/3 growth rings)	1868±21	cal. AD 130–230	*cal. AD 120–235*

Diatom assessment of samples from Lydd Ranges, Dungeness

Nigel Cameron, Environmental Change Research Centre,
Department of Geography, University College London,
Pearson Building, Gower Street, London WC1E 6BT

Introduction

Wessex Archaeology was commissioned to undertake a palaeoenvironmental assessment of a coastal defence site at Lydd Ranges on the Dungeness Foreland.

Eight samples, from two cores, have been selected for diatom assessment. One core is from clay exposures on the beach and a second core is from landward of the current sea defences containing deposits within one of the inter-ridge depressions.

Based on the results of diatom and other palaeoenvironmental assessments, it is intended to carry out OSL and radiocarbon dating.

The core through the inter-ridge depression includes a peat that may not be *in-situ*, but this could be elucidated by pollen analysis. Further, it is not clear whether these depressions are channels that were open to the sea or connected to the marshes to landward (Alex Brown pers. comm.). The diatom assessment may assist in answering this question.

The 8 sub-samples for diatom assessment, selected from 2 cores, have been prepared and assessed for diatoms.

The diatom assessment considers the numbers of diatoms, the state of preservation of the diatom assemblages, species diversity, diatom species environmental preferences and the potential of the sediments for further diatom analysis.

Methods

Diatom preparation followed standard techniques (Battarbee *et al.* 2001). Two coverslips were made from each sample and fixed in Naphrax for diatom microscopy. A large area of the coverslips on each slide was scanned for diatoms at magnifications of x400 and x1000 under phase contrast illumination.

Diatom floras and taxonomic publications were consulted to assist with diatom identification; these include Hendey (1964), Werff & Huls (1957-1974), Hartley et al. (1996), Krammer & Lange-Bertalot (1986-1991) and Witkowski *et al.* (2000). Diatom species' salinity preferences are indicated using the halobian groups of Hustedt (1953, 1957: 199), these salinity groups are summarised as follows:

1. Polyhalobian: >30 g l-1

2. Mesohalobian: 0.2-30 g l-1

3. Oligohalobian - Halophilous: optimum in slightly brackish water

4. Oligohalobian - Indifferent: optimum in freshwater but tolerant of slightly brackish water

5. Halophobous: exclusively freshwater

6. Unknown: taxa of unknown salinity preference.

Results & Discussion

Diatom sample depths and Monolith numbers are shown in Table 1.

Table 1. Lydd Ranges Diatom assessment samples (HHWS – hand-held window sampler) *depths on sample bag shown (depths given in document supplied were 0.94-0.97m)

Monolith & Lab No.	Top depth (m)	Bottom Depth (m)	Sediment type
<111>			
1	0.81	083	-
2 *	0.95	0.98	-
3	1.04	1.07	Sandy mud
4	1.16	1.19	Sandy mud
HHWS-107			
5	0.34	-	Stiff Fe mottled grey silty clay (Inter-ridge marsh deposit)
6	0.46	-	ditto
7	0.58	-	Stiff dark grey silty clay, evidence of lamination (Inter-ridge marsh deposit)
8	0.98	-	ditto

A summary of the results of the diatom evaluation is shown in Table 2. The records of diatom taxa and their salinity classifications are shown in Table 3 (Excel file attached): 1 – present; 2 – common; 3 – more common.

Table 2. Summary of diatom evaluation results for Monolith <111> and HHWS-107 (fw – freshwater; bk – brackish; mar – marine; mar-bk – marine-brackish; aero – aerophilous; mod – moderate; ex – extremely; indet – indeterminate diatom; non-pk – non-planktonic)

Core & Diatom Sample Number	Diatoms	Diatom Numbers	Quality of Preservation	Diversity	Assemblage type	Potential for % count
<111>						
1	present	mod	mod	mod	mar, mar-bk	good
2	present	mod	mod to poor	mod	mar, mar-bk	good
3	present	mod	poor to mod	mod	mar, mar-bk	good
4	trace	ex low	ex poor	centric sp.	unknown	none
HHWS-107						
5	present	ex low	ex poor	-	indet fragments	none
6	present	ex low	ex poor	-	? fw	none
7	present	v low	v poor	low	fw non-pk, aero	v low
8	present	mod	mod	mod	mar, mar-bk	good

Monolith <111> (Samples 1 to 4)

Diatoms are present in extremely low numbers and are extremely poorly preserved in sample 4 from Monolith <111>. The dissolved and broken valve of an indeterminate centric diatom species was recorded. There is no further potential for diatom analysis of this sample.

Diatoms are present in moderately high numbers in the top three samples from the sequence. The quality of valve preservation varies from moderately good to poor and all three samples have moderate diversity. The diatom assemblages of samples 1, 2 and 3 are composed of marine and marine-brackish diatom taxa. All three samples have good potential for percentage diatom analysis.

The most common species in samples 1 to 3 is the marine planktonic diatom *Paralia sulcata*. Other marine taxa that are common in one or more of these samples are *Cymatosira belgica, Rhaphoneis surirella and Rhaphoneis amphiceros*. Polyhalobous diatoms that are present these samples are *Anorthoneis* sp., *Grammatophora* sp., *Nitzschia panduriformis, Rhaphoneis minutissima, Thalassionema nitzschiodes, Trachyneis aspera* and *Surirella comis.*

The marine-brackish and brackish-marine diatoms present in samples 1 to 3 are *Actinoptychus undulatus, Cocconeis scutellum, Pseudopodosira westii, Thalassiosira decipiens, Diploneis aestuari, Diploneis didyma* and *Melosira moniliformis*.

The halophilous, aerophile *Navicula cincta* is relatively common in sample 1. Freshwater diatoms are absent from all three samples. The diatom assemblages of samples 1 to 3 represent coastal marine habitats.

HHWS-107 (Samples 5 to 8)

Diatoms are present in all 4 samples from this sequence.

The bottom sample from HHWS-107 has a moderately high number of diatoms that are moderately well-preserved and the assemblage is of moderate diversity. There is good potential for percentage diatom analysis of sample 8. The diatom assemblage is composed entirely of marine, marine-brackish and brackish water diatoms that indicate a tidal depositional environment. The dominant marine taxa include *Cymatosira belgica, Paralia sulcata, Rhaphoneis minutissima, Rhaphoneis surirella, Thalassionema nitzschiodes* and *Trachyneis aspera*. Marine-brackish and brackish water diatoms include *Actinoptychus undulatus, Thalassiosira decipiens, Diploneis aestuari, Melosira moniliforms* and *Actinocyclus normanii*. Freshwater diatoms were not recorded in sample 8.

Sample 7 contains a very low number of diatoms; the quality of diatom preservation is very poor and species diversity is low. There is very low potential for further analysis, however, the diatom taxa present in sample 7 are informative. Except for a fragment of the marine planktonic species *Paralia sulcata*, the diatom assemblage is composed of non-planktonic freshwater taxa. These diatoms include *Craticula cuspidata, Epithemia adnata, Pinnularia divergens* and *Synedra ulna*. The *Epithemia* spp. present suggest the presence of aquatic macrophytes. Freshwater aerophilous diatoms include *Hantzschia amphioxys* and *Pinnularia major*. Chrysophyte stomatocysts are also relatively common in sample 7. The presence of both aerophilous diatoms and chrysophyte cysts suggest an ephemeral freshwater aquatic habitat subject to lower water levels or drying out.

The numbers of diatoms in the top two samples are extremely low and the quality of diatom preservation is extremely poor in the two samples. The diatom fragments in the top sample are indeterminate and at best the diatoms in sample 6 are identifiable only to the generic level. The *Pinnularia* sp. fragments are probably derived from a freshwater species. There is no further potential for analysis of samples 5 and 6.

Conclusions

- The environment represented by the assemblage in the bottom sample from Monolith <111> is not clear (possibly a marine centric diatom is present). There is no further potential for diatom analysis of the extremely poorly preserved diatoms in sample 4 from Monolith <111>.
- Diatoms are present in moderately high numbers, with some good preservation and moderate diversity in the top three samples from Monolith <111>. The diatom assemblages of samples 1, 2 and 3 are composed of marine and marine-brackish diatom taxa that represent coastal marine habitats. Freshwater diatoms are absent from these samples. All three samples have good potential for percentage diatom analysis.
- The diatom assemblage at the base of the HHWS-107 sequence is composed entirely of marine, marine-brackish and brackish water diatoms that indicate a tidal depositional environment. There is good potential for analysis of sample 8.
- The diatom assemblage of HHWS-107 sample 7 is composed mainly of non-planktonic freshwater taxa. Epiphytic freshwater diatoms were recorded. The presence of both aerophilous diatoms and chrysophyte cysts suggest an ephemeral freshwater aquatic habitat, subject to lower water levels or drying out. There is very low potential for further analysis of sample 7.
- The top two samples of HHWS-107 have very poorly preserved diatoms. There may be fragments of a freshwater genus in sample 6. There is no further potential for analysis of samples 5 and 6.

Acknowledgements

Thanks to Alex Brown of Wessex Archaeology for providing the samples for diatom assessment.

References

Battarbee, R.W., Jones, V.J., Flower, R.J., Cameron, N.G., Bennion, H.B., Carvalho, L. & Juggins, S. 2001. Diatoms. In (J.P. Smol and H.J.B. Birks eds.), Tracking Environmental Change Using Lake Sediments Volume 3: Terrestrial, Algal, and Siliceous Indicators, 155-202. Dordrecht: Kluwer Academic Publishers.

Hartley, B., H.G. Barber, J.R. Carter & P.A. Sims. 1996. *An Atlas of British Diatoms.* Biopress Limited. Bristol. pp. 601.

Hendey, N.I. 1964 An Introductory Account of the Smaller Algae of British Coastal Waters. Part V. Bacillariophyceae (Diatoms). Ministry of Agriculture Fisheries and Food, Series IV. pp. 317.

Hustedt, F. 1953. Die Systematik der Diatomeen in ihren Beziehungen zur Geologie und Okologie nebst einer Revision des Halobien-systems. *Sv. Bot. Tidskr.*, 47: 509-519.

Hustedt, F. 1957. Die Diatomeenflora des Fluss-systems der Weser im Gebiet der Hansestadt Bremen. *Ab. naturw. Ver. Bremen* 34, 181-440.

Krammer, K. & H. Lange-Bertalot, 1986-1991. *Bacillariophyceae.* Gustav Fisher Verlag, Stuttgart.

Vos, P.C. & H. de Wolf 1988. Methodological aspects of palaeoecological diatom research in coastal areas of the Netherlands. *Geologie en Mijnbouw* 67: 31-40

Vos, P.C. & H. de Wolf 1993. Diatoms as a tool for reconstructing sedimentary environments in coastal wetlands; methodological aspects. *Hydrobiologia* 269/270: 285-296

Werff, A. Van Der & H. Huls. 1957-1974 *Diatomeenflora van Nederland*, 10 volumes

Witkowski, A, H. Lange-Bertalot & D. Metzeltin 2000. *Diatom Flora of Marine Coasts I.* Iconographia Diatomologica. Annotated Diatom Micrographs Ed. by H. Lange-Bertalot Vol. 7. A.R.G. Gantner Verlag. Koeltz Scientific Books. Königstein, Germany pp 92

BioChron

Biostratigraphy
Geochronology
Project management

Report No: 06/22 **26 February 2023**

Microfaunal assessment of eight samples from Lydd Ranges

by

John Athersuch

for

Wessex Archaeology

Introduction

Eight samples were submitted by Wessex Archaeology for microfaunal assessment in two batches, one from WA241532 and the other from HHWS–107. The samples were subject to the usual preparation procedure, i.e. sieved in water at 125µm, the resulting residue dried and then examined under a binocular microscope. The samples from HHWS–107 were rather small and produced extremely small residues so microfaunal recovery was poor.

Results

WA241532, 0.81 – 0.83m

This sample differs from the others in this batch in having low numbers of ostracods and foraminifera but high species richness. Most specimens were either species or juveniles which made identification difficult in some cases.

The following ostracods were recovered: *Palmoconcha laevata* (3v), *Propontocypris trigonella* (2v), *Aurila convexa* (3v) are all shallow marine species. *Pontocythere elongata* (3v) is often found in outer estuaries. *Hirschmannia viridis* (3v) is a marine to brackish indicator while *Cytherura gibba* is prefers brackish environments. All of these species prefer a weed rich environment. Other taxa recovered include *Leptocythere* sp.(1v), two species of *Semicytherura* sp.(3v) and an indeterminate form.

The following foraminifera included: miliolids (13), *Ammonia ?tepida* (5), *Haynesina germanica* (5), *Elphidium williamsoni* (2). This assemblage indicates a marine to brackish environment.

A single specimen of a circular centric diatom resembling *Coskinodiscus* was also recovered.

Sponge spicules and echinoid spines were also present indicating marine influence.

Overall a strongly marine influence depositional environment is suggested for this sample, possibly an outer estuary setting.

WA241532, 0.95 – 0.98m

Ostracods and foraminifera were found infrequently in this sample.

Ostracods recovered were *Hemicythere villosa* (1v), *Aurila convexa* (1v) and *?Schlerochilus* sp. 1v)

Foraminifer included *Ammonia batava* (3), *Ammonia ?tepida* (9), *Haynesina germanica* (2) and Oolina sp. (1)

Shell fragments and sponge spicules were rare.

This assemblage suggests a strongly marine influence brackish water environment, possibly in an outer estuary setting.

WA241532, 1.04 – 1.07

Foraminifera were rare and ostracods absent from this sample. The foraminiferal species include *Ammonia batava* (1), *Ammonia* sp. with umbilical plug (10) and a reworked miliolid.

In addition shell fragments (mainly bivalves) were common and echinoderm fragments were rare**.**

This assemblage suggests a marginal marine environment.

WA241532, 1.16 – 1.19m

A low diversity assemblage of foraminifera and ostracods was recovered from this sample.

Foraminifera comprised *Ammonia* sp. with umbilical plug (22) and a single reworked miliolid.

Ostracods were *Pontocythere elongata* (1v), *Hemicythere villosa* (1v) and *Aurila convexa* (1c).

Shell fragments and echinoid spines were rare.

This assemblage suggests a marginal marine environment.

HHWS – 107, 34m

No microfauna.

HHWS – 107, 0.46m

Rare unidentified seeds and a single charophyte oogonium were recovered. No microfauna.

The charophyte gives a suggestion of a freshwater to very low salinity environment.

HHWS – 107, 0.58m

No microfauna

HHWS – 107, 0.98m

A single charophyte oogonium was recovered. No microfauna.

The charophyte gives a suggestion of a freshwater to very low salinity environment.

Note: abbreviations relating to ostracods: v = valves, c = carapace

John Athersuch

X:\Projects\241533\Graphics_Office\Rep figs\Geoarch\2023_02_24\241533_ArcPro\241533_ArcPro.aprx

599500 600000 600500 601000

118000 117500

Midrips

Lydd Ranges

Denge Marsh

Geomorphological Character Zone C

Geomorphological Character Zone E

Geomorphological Character Zone G

HHWS130 HHWS129 HHWS128 HHWS127 HHWS126 HHWS125 HHWS124 HHWS123 HHWS122 HHWS121 E01 TP1

HHWS112 HHWS111 HHWS113 HHWS114 HHWS115 HHWS119 HHWS120 HHWS116 HHWS117 HHWS118 G01

TP14 TP13 TP4 TP2 TP3

HHWS110 HHWS109 HHWS108 HHWS107 HHWS106 HHWS105 HHWS104 HHWS101 HHWS102 HHWS103 C01 BH03-2013

TP8 TP7 TP12 TP6 TP11 TP5 TP10 TP9

- Borehole location
- Transect C (North to South)
- Transect C (West to East)
- Transect E (North to South)
- Transect E (West to East)
- Transect G (North to South)
- Transect G (West to East)
- Transect C to G
- Intertidal clay exposure (point)
- Intertidal clay exposure
- Geomorphological Character Zone
- Green Wall

0 250 m

Coordinate system: OSGB 1936 British National Grid

Date: 24/02/2023	Created by: KJF	
Scale: 1:5,000 at A3	Revision: 0	

Figure 1: Site plan showing borehole and transect locations

X:\Projects\241533\Graphics_Office\Rep figs\Geoarch\2023_02_24

W

E

Zone C

Zone E

Zone G

C01/WA-S03

E01/WA-S02

G01/WA-S01

HHWS129
HHWS128
HHWS127
HHWS126
HHWS125
HHWS124
HHWS123
HHWS113
HHWS114
HHWS115
HHWS116
HHWS117
HHWS118
HHWS107
HHWS108
HHWS106
HHWS105
HHWS104
HHWS103
HHWS102

Intertidal marsh sediments

Storm beach gravels

Shoreface sand and gravel

Nearshore sands

Depth (m OD)

7.0
6.0
5.0
4.0
3.0
2.0
1.0
0.0
-1.0
-2.0
-3.0
-4.0
-5.0
-6.0
-7.0
-8.0

0
100
200
300
400
500
600
700
800
900
1,000
1,100
1,200

Distance (m)

Stratigraphy

- No recovery
- Topsoil
- Redeposited silty clay - sea wall
- Silty clay - marsh deposits
- Silty clay gravels - marsh deposits
- Peat
- Sandy gravels - contemporary erosion
- Gravels - storm beach
- Sands and gravels - spit/barrier complex
- Pre-barrier near shore sands
- Laminated fine sand
- Sand

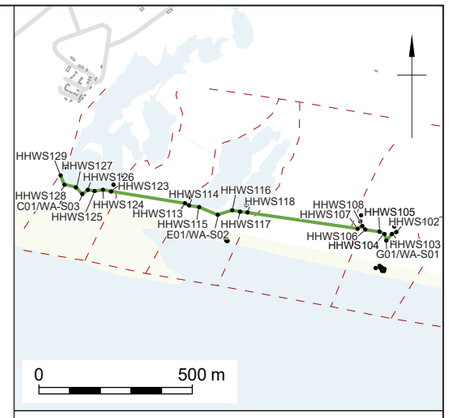

- Borehole location
- Transect C to G
- Geomorphological Character Zone

Coordinate system: OSGB 1936 British National Grid

Created by: KJF	Date: 27/02/2023	
Scale: Inset 1:20,000 at A3	Revision: 0	

Figure 2: Transect Zones C-G

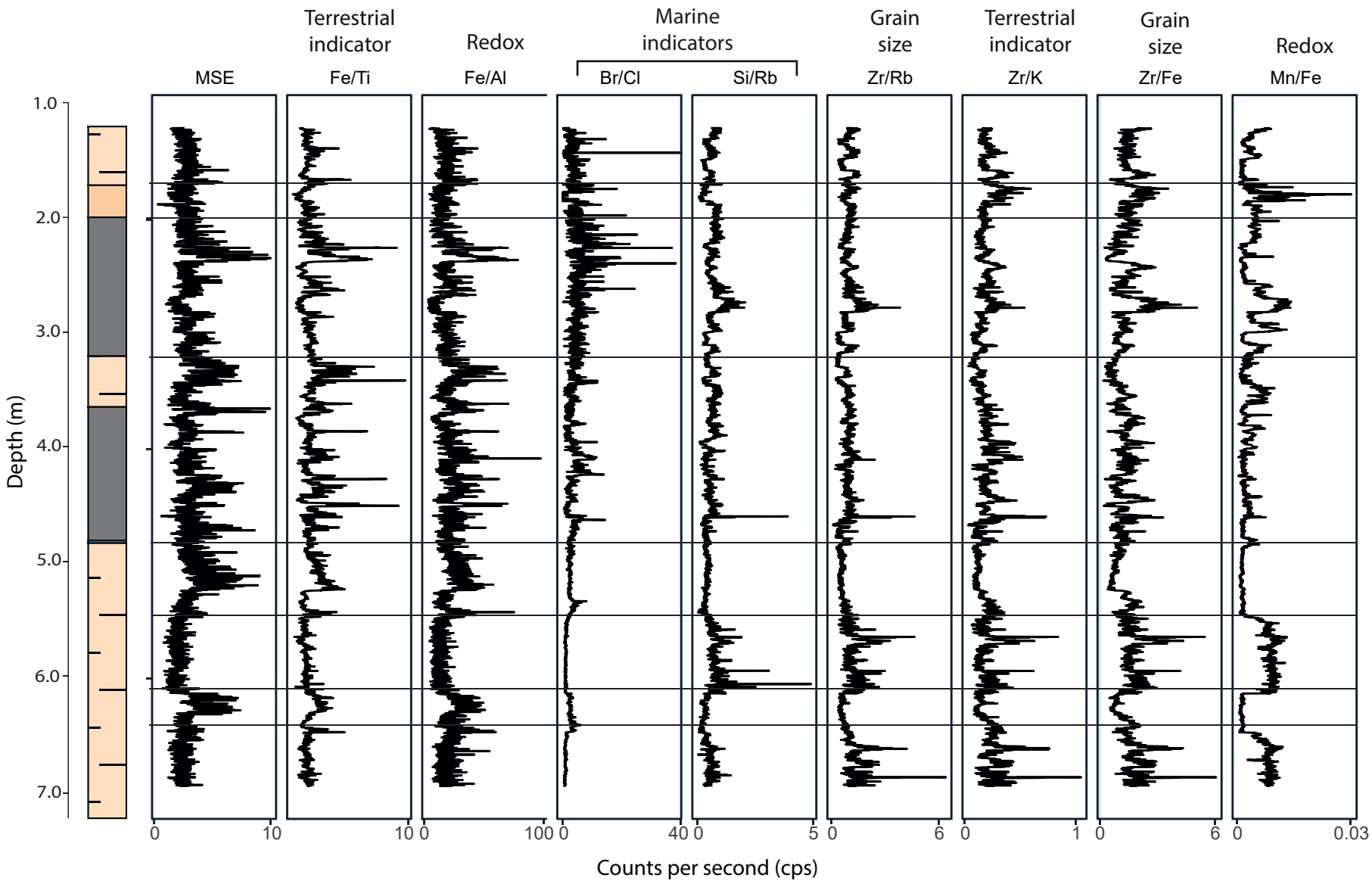

Date: 27/02/2023	Created by: KJF	Revision: 0	Scale: NTS at A4

Figure 3: XRF chemical ratios for C01/WA-S03

X:\Projects\241533\Graphics_Office\Rep figs\Geoarch\2023_02_24

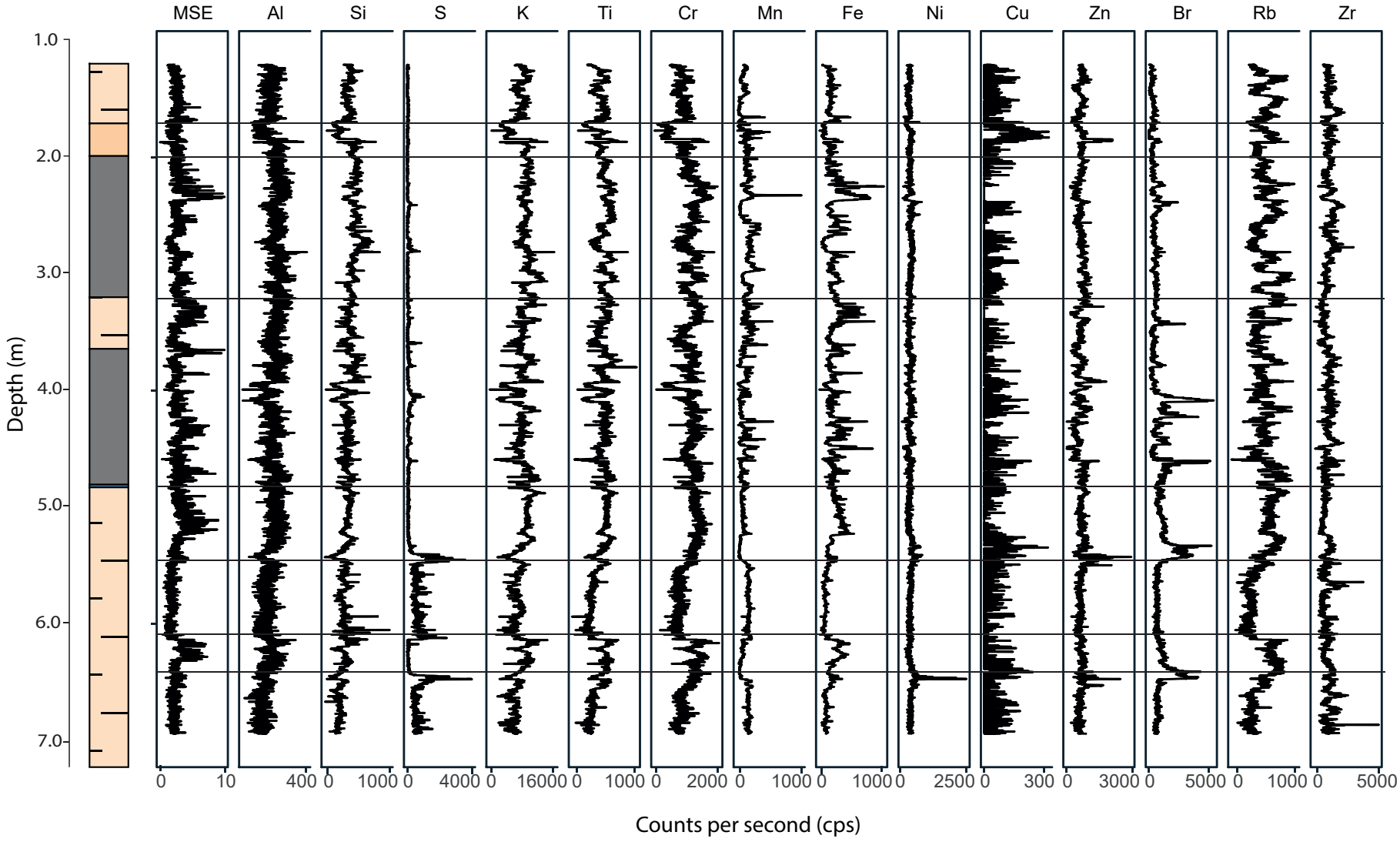

Date: 27/02/2023	Created by: KJF	Revision: 0	Scale: NTS at A4

Figure 4: XRF elements for C01/WA-S03

X:\Projects\241533\Graphics_Office\Rep figs\Geoarch\2023_02_24

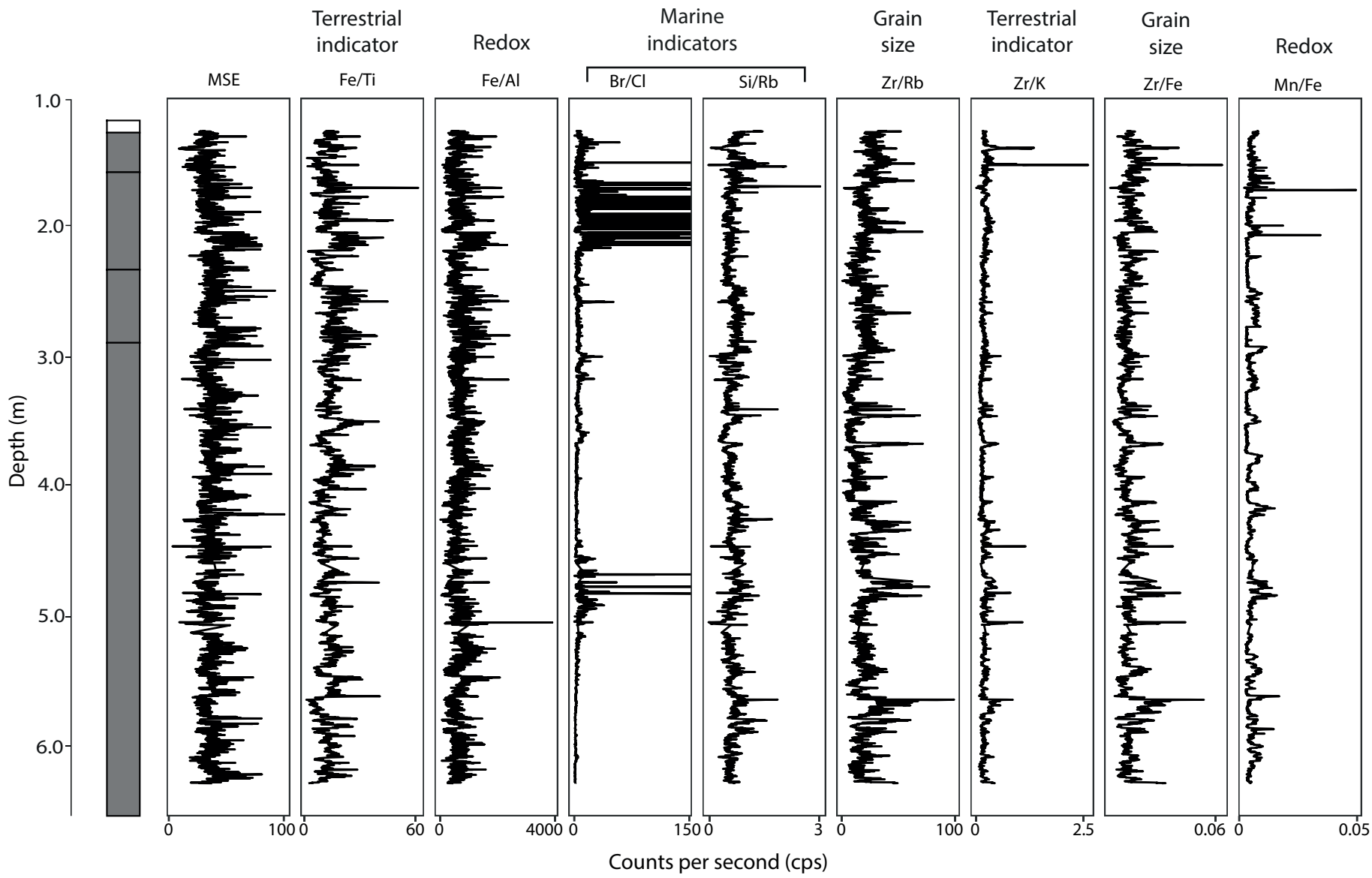

Date: 27/02/2023	Created by: KJF	Revision: 0	Scale: NTS at A4

Figure 5: XRF chemical ratios for E01/WA-S02

X:\Projects\241533\Graphics_Office\Rep figs\Geoarch\2023_02_24

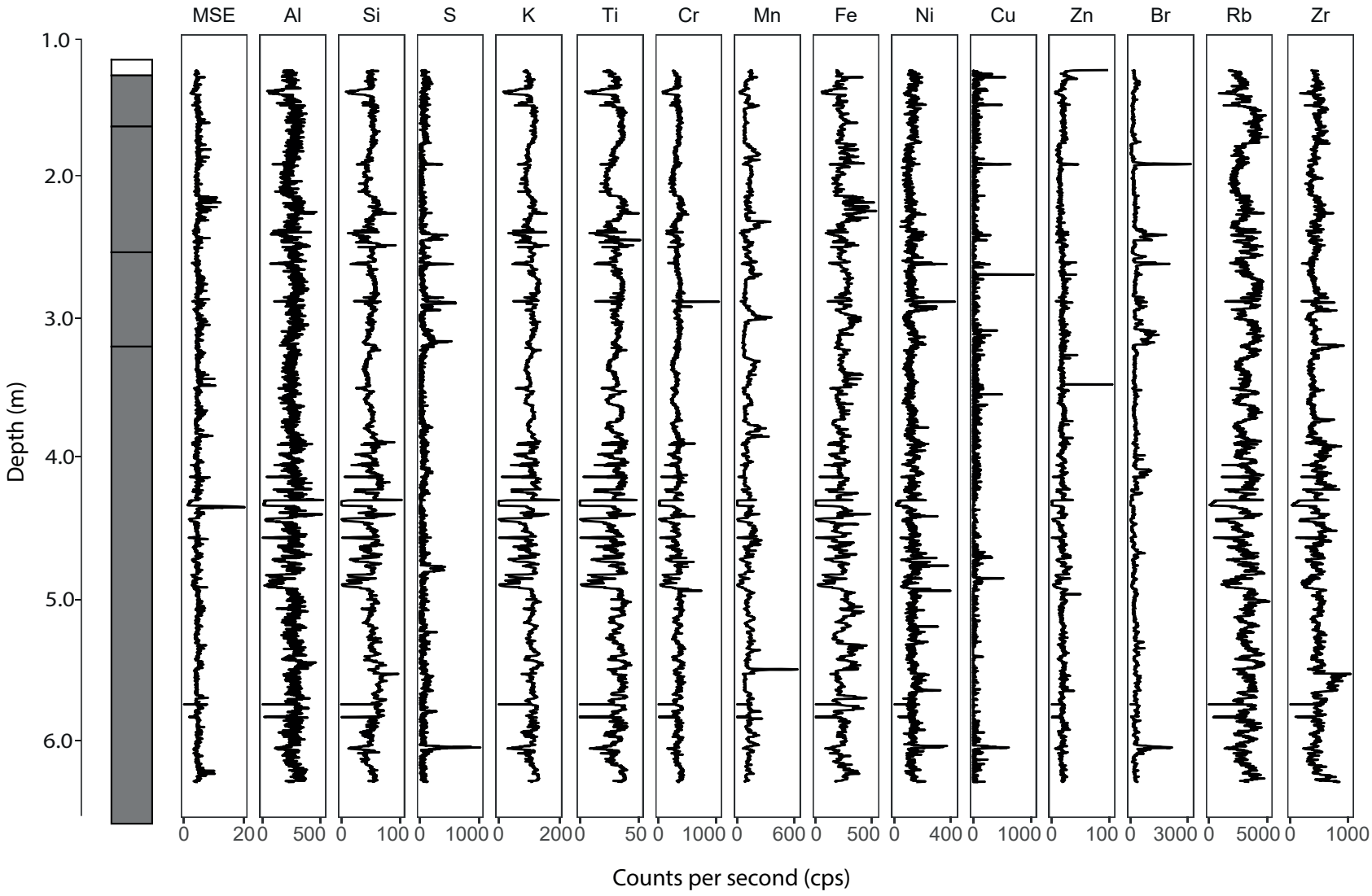

Date: 27/02/2023	Created by: KJF	Revision: 0	Scale: NTS at A4

Figure 6: XRF elements for E01/WA-S02

X:\Projects\241533\Graphics_Office\Rep figs\Geoarch\2023_02_24

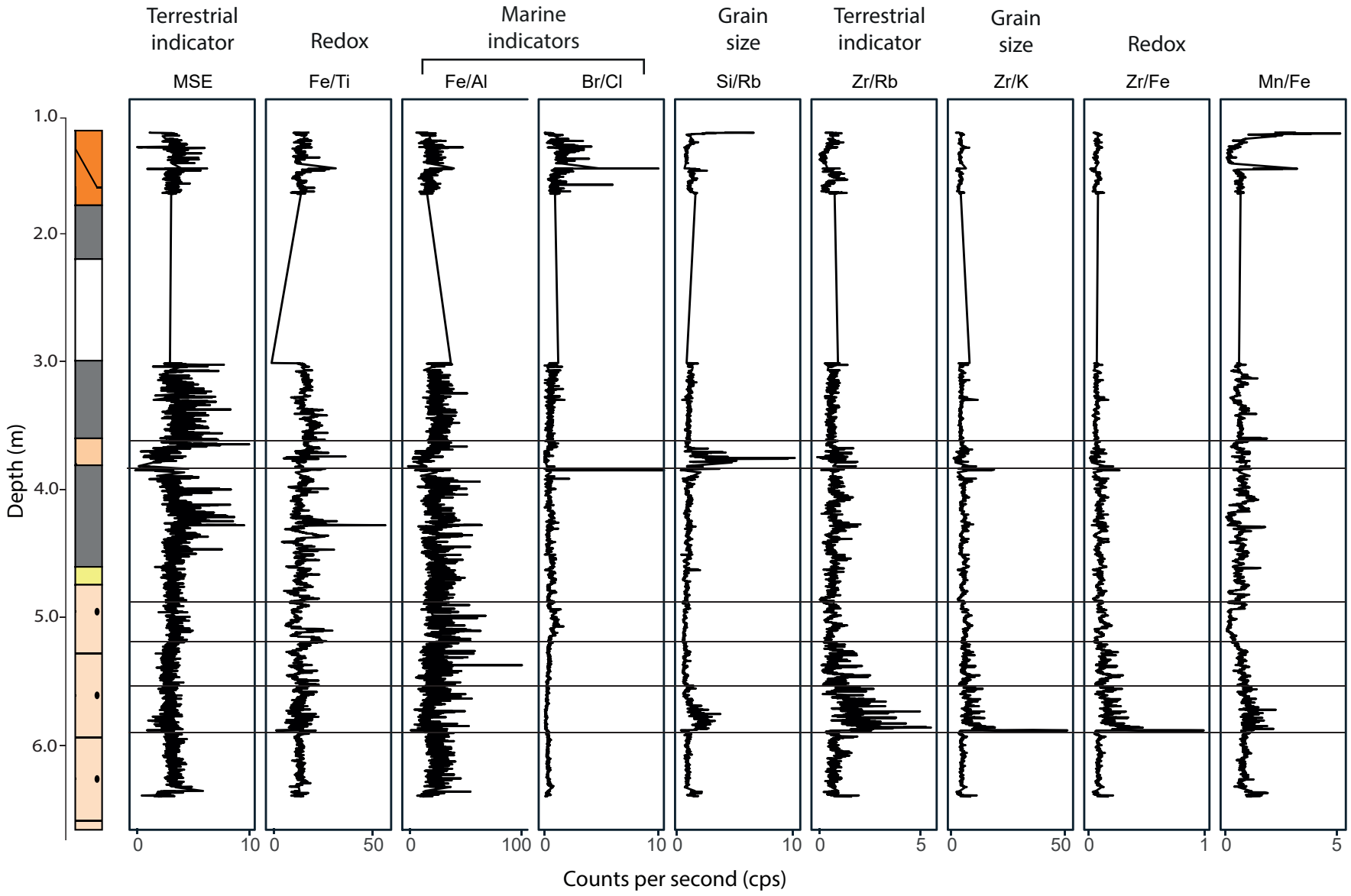

Date: 27/02/2023	Created by: KJF	Revision: 0	Scale: NTS at A4

Figure 7: XRF chemical ratios for G01/WA-S01

X:\Projects\241533\Graphics_Office\Rep figs\Geoarch\2023_02_24

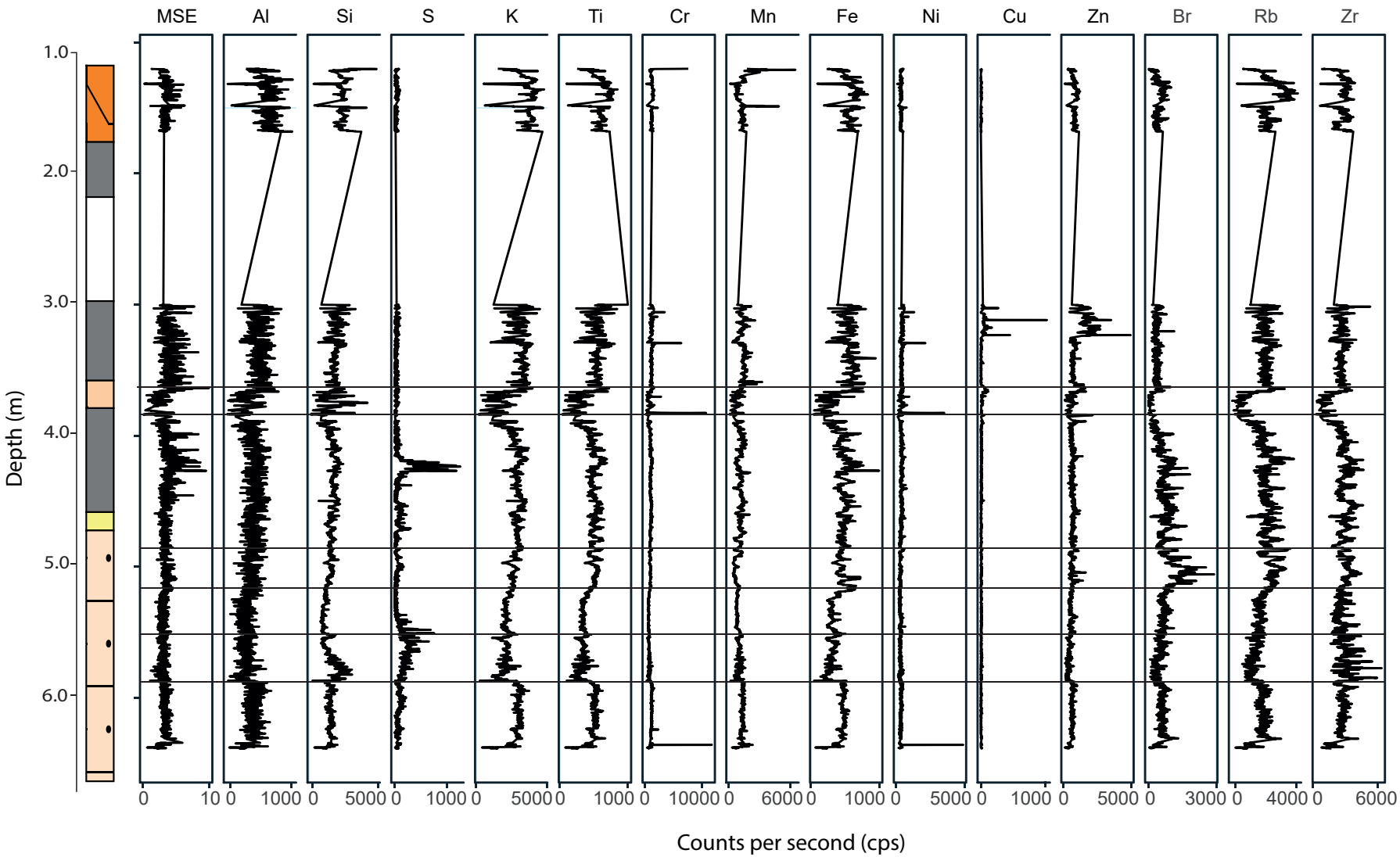

Date: 27/02/2023	Created by: KJF	Revision: 0	Scale: NTS at A4

Figure 8: XRF elements for G01/WA-S01

X:\Projects\241533\Graphics_Office\Rep figs\Geoarch\2023_02_24

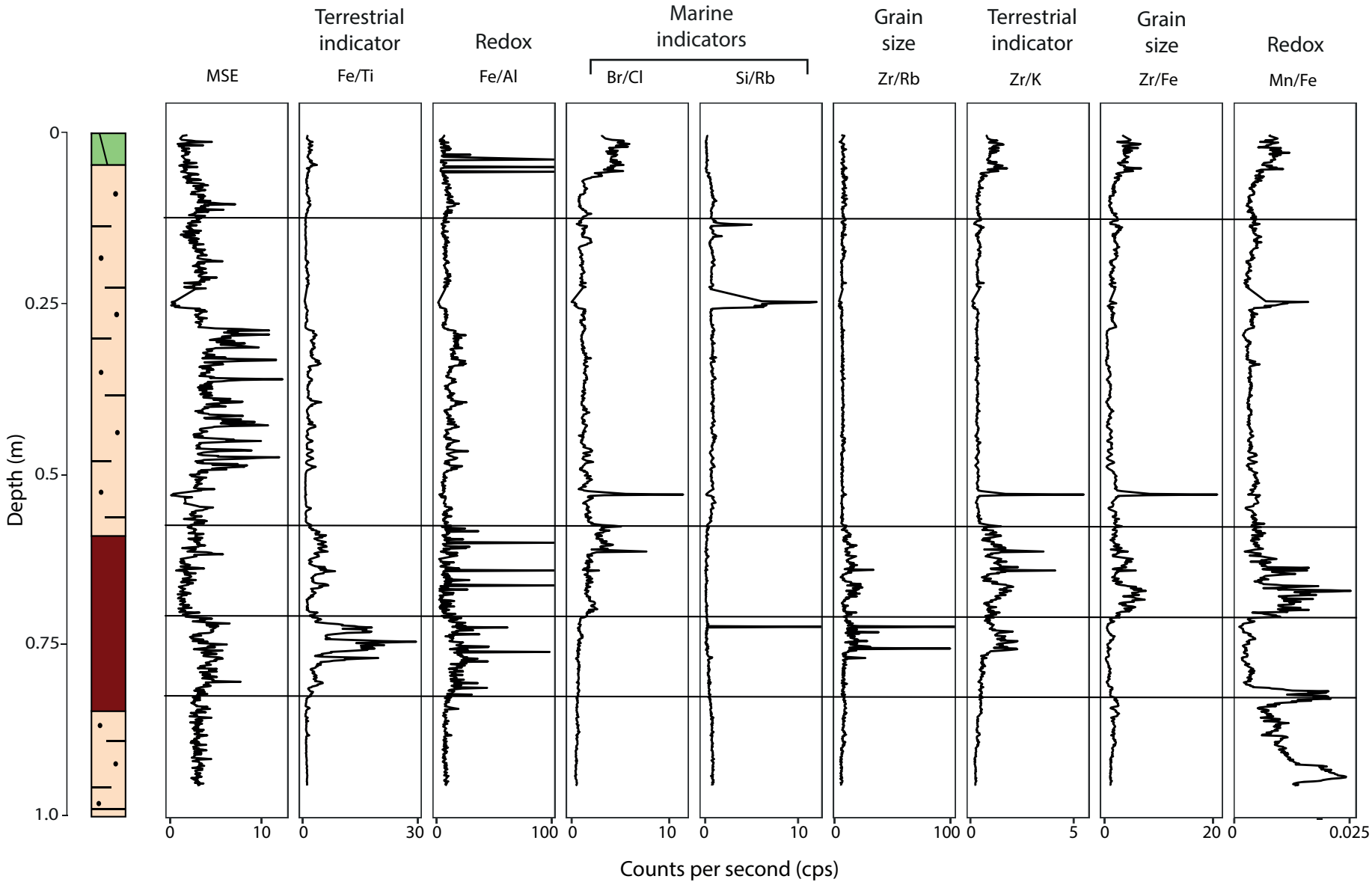

Date: 27/02/2023	Created by: KJF	Revision: 0	Scale: NTS at A4

Figure 9: XRF chemical ratios for HHWS-107

X:\Projects\241533\Graphics_Office\Rep figs\Geoarch\2023_02_24

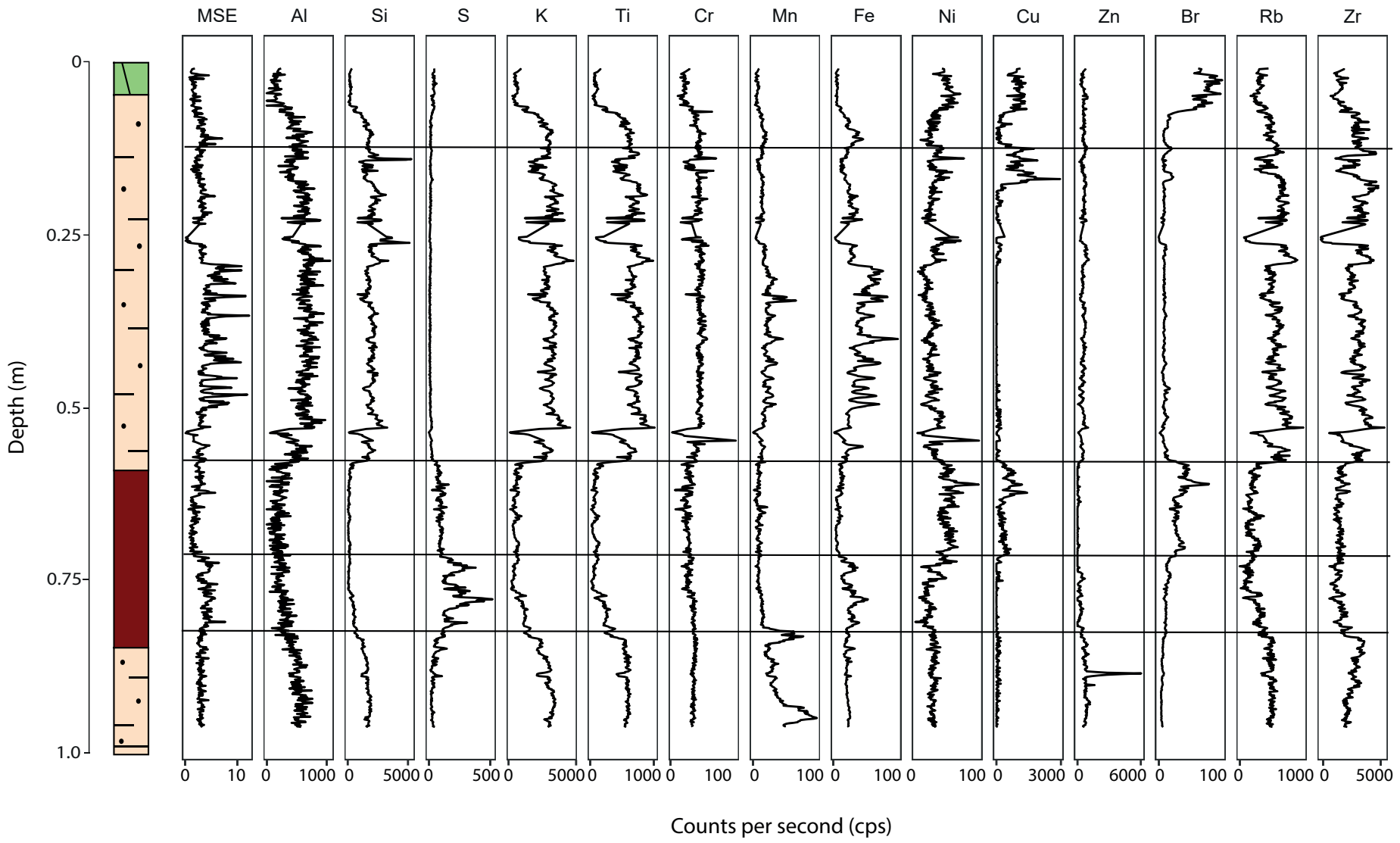

Date: 27/02/2023	Created by: KJF	Revision: 0	Scale: NTS at A4

Figure 10: XRF elements for HHWS-107

X:\Projects\241533\Graphics_Office\Rep figs\Geoarch\2023_02_24

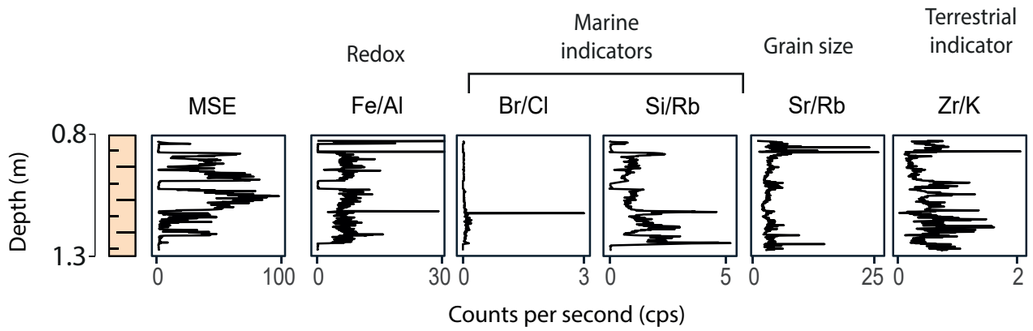

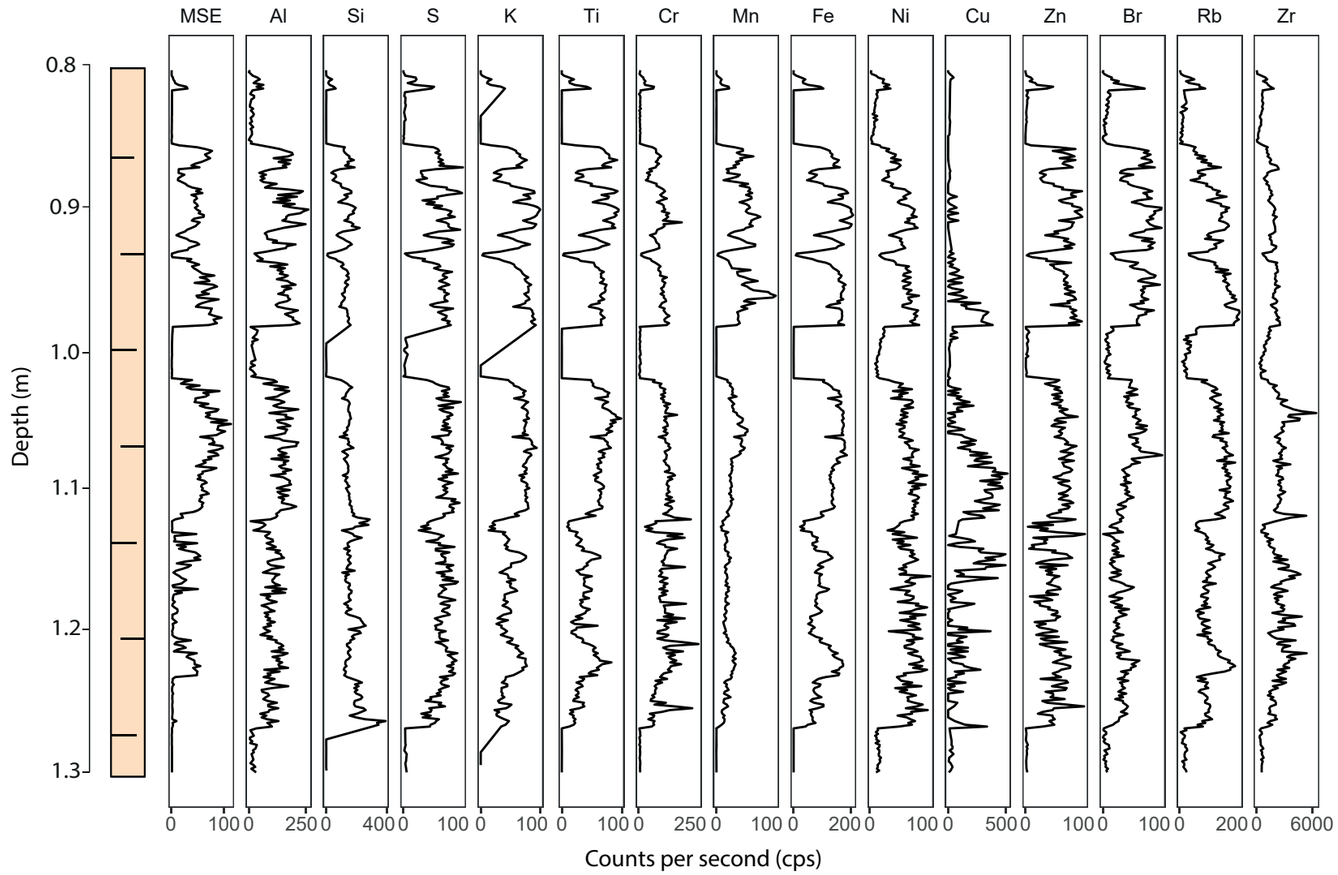

Created by: KJF	Date: 27/02/2023	
Scale: NTS at A3	Revision: 0	

Figure 11: XRF chemical ratios and elements for Monolith 111

X:\Projects\241533\Graphics_Office\Rep figs\Geoarch\2023_02_24

W

E

Zone C

Zone E

Zone G

C01/WA-S03

E01/WA-S02

G01/WA-S01

HHWS129
HHWS128
HHWS127
HHWS126
HHWS125
HHWS124
HHWS123
HHWS113
HHWS114
HHWS115
HHWS116
HHWS117
HHWS118
HHWS107
HHWS108
HHWS106
HHWS105
HHWS104
HHWS103
HHWS102

AD 1520-1600
AD 66-212
1200-740 BC
1580-1100 BC
1060-660 BC
Intertidal marsh sediments

260 BC-AD 80
660-240 BC
AD 129-230
AD 257-415
650-260 BC
540-220 BC

Storm beach gravels

Shoreface sand and gravel

Nearshore sands

Depth (m OD)

7.0
6.0
5.0
4.0
3.0
2.0
1.0
0.0
-1.0
-2.0
-3.0
-4.0
-5.0
-6.0
-7.0
-8.0

0
100
200
300
400
500
600
700
800
900
1,000
1,100
1,200

Distance (m)

Stratigraphy

- No recovery
- Topsoil
- Redeposited silty clay - sea wall
- Silty clay - marsh deposits
- Silty clay gravels - marsh deposits
- Peat
- Sandy gravels - contemporary erosion
- Gravels - storm beach
- Sands and gravels - spit/barrier complex
- Pre-barrier near shore sands
- Laminated fine sand
- Sand

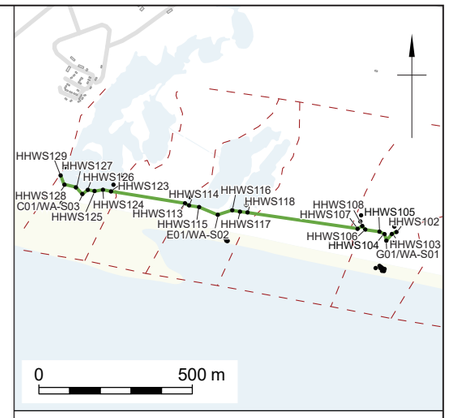

- Borehole location
- Transect C to G
- Geomorphological Character Zone

Coordinate system: OSGB 1936 British National Grid

Created by: KJF	Date: 27/02/2023	
Scale: Inset 1:20,000 at A3	Revision: 0	

Figure 12: Transect Zones C-G, showing results of the scientific dating

Wessex Archaeology Ltd registered office Portway House, Old Sarum Park, Salisbury, Wiltshire SP4 6EB
Tel: 01722 326867 Fax: 01722 337562 info@wessexarch.co.uk www. wessexarch.co.uk

FS 606559